# NAVAL POSTGRADUATE SCHOOL
## Monterey, California


# THESIS

**DESIGN, CHARACTERIZATION, AND PERFORMANCE OF A VALVELESS PULSE DETONATION ENGINE**

by

Robert G. Johnson

June 2000

Thesis Advisor: Christopher Brophy
Second Reader: David W. Netzer

**Approved for public release; distribution is unlimited.**

| REPORT DOCUMENTATION PAGE | | Form Approved OMB No. 0704-0188 |
|---|---|---|

Public reporting burden for this collection of information is estimated to average 1 hour per response, including the time for reviewing instruction, searching existing data sources, gathering and maintaining the data needed, and completing and reviewing the collection of information. Send comments regarding this burden estimate or any other aspect of this collection of information, including suggestions for reducing this burden, to Washington headquarters Services, Directorate for Information Operations and Reports, 1215 Jefferson Davis Highway, Suite 1204, Arlington, VA 22202-4302, and to the Office of Management and Budget, Paperwork Reduction Project (0704-0188) Washington DC 20503.

| 1. AGENCY USE ONLY *(Leave blank)* | 2. REPORT DATE June 2000 | 3. REPORT TYPE AND DATES COVERED Master's Thesis |
|---|---|---|
| **TITLE AND SUBTITLE : Design, Characterization, and Performance of a Valveless Pulse Detonation Engine** | | 5. FUNDING NUMBERS ContractNumber: N0001499WR20085 |
| 6. AUTHOR(S) Johnson, Robert G. | | |
| 7. PERFORMING ORGANIZATION NAME(S) AND ADDRESS(ES) Naval Postgraduate School Monterey, CA 93943-5000 | | 8. PERFORMING ORGANIZATION REPORT NUMBER |
| 9. SPONSORING / MONITORING AGENCY NAME(S) AND ADDRESS(ES) Office of Naval Research Ballston Tower One 800 N. Quincy Street Arlington, VA 22217-5660 | | 10. SPONSORING / MONITORING AGENCY REPORT NUMBER |

**11. SUPPLEMENTARY NOTES** The views expressed in this thesis are those of the author and do not reflect the official policy or position of the Department of Defense or the U.S. Government.

| 12a. DISTRIBUTION / AVAILABILITY STATEMENT | 12b. DISTRIBUTION CODE |
|---|---|
| Approved for public release; distribution is unlimited. | |

**13. ABSTRACT** ***(maximum 200 words)***

Current interest in developing a low cost, less complex tactical missile propulsion system that operates on readily available liquid fuels and can operate from low subsonic to a flight Mach number of 5 is driving research on pulse detonation engines.

This research program involved the design, construction, and testing of a valveless Pulse Detonation Engine using a JP-10/air mixture as the primary combustible reactants. A small JP-10/oxygen pre-detonation tube was used to initiate the detonation in the JP-10/air mixture in the engine. The engine was tested at various inlet conditions and equivalence ratios in order to determine the detonable regime of the fuel/air mixture. The original area transition from the pre-detonation tube to the main combustion tube appeared to be too extreme, so a tube was added to extend the pre-detonation tube into the throat of a shock focusing device inserted flush with the head end of the main combustion tube to promote more favorable transition conditions.

| 14. SUBJECT TERMS: Pulse Detonation Engine, JP-10, Liquid Fuels, Combustion | | | 15. NUMBER OF PAGES 130 |
|---|---|---|---|
| | | | 16. PRICE CODE |
| 17. SECURITY CLASSIFICATION OF REPORT Unclassified | 18. SECURITY CLASSIFICATION OF THIS PAGE Unclassified | 19. SECURITY CLASSIFICATION OF ABSTRACT Unclassified | 20. LIMITATION OF ABSTRACT UL |

NSN 7540-01-280-5500

Standard Form 298 (Rev. 2-89)
Prescribed by ANSI Std. 239-18

#13 Abstract (Continued)

In addition, the effects of a transient detonation process on the inlet operation and performance of the engine was theoretically predicted, using a two dimensional grid in a viscous grid computational fluid dynamics code, and experimentally evaluated from subsonic to supersonic operation.

**Approved for public release; distribution is unlimited.**

# DESIGN, CHARACTERIZATION, AND PERFORMANCE OF A VALVELESS PULSE DETONATION ENGINE

Robert G. Johnson
Lieutenant, United States Navy
B.S., United States Naval Academy, 1992

Submitted in partial fulfillment of the
requirements for the degree of

**MASTER OF SCIENCE IN ASTRONAUTICAL ENGINEERING**

from the

**NAVAL POSTGRADUATE SCHOOL**
**June 2000**

THIS PAGE INTENTIONALLY LEFT BLANK

# ABSTRACT

Current interest in developing a low cost, less complex tactical missile propulsion system that operates on readily available liquid fuels and can operate from low subsonic to a flight Mach number of 5 is driving research on pulse detonation engines.

This research program involved the design, construction, and testing of a valveless Pulse Detonation Engine using a JP-10/air mixture as the primary combustible reactants. A small JP-10/oxygen pre-detonation tube was used to initiate the detonation in the JP-10/air mixture in the engine. The engine was tested at various inlet conditions and equivalence ratios in order to determine the detonable regime of the fuel/air mixture. The original area transition from the pre-detonation tube to the main combustion tube appeared to be too extreme, so a tube was added to extend the pre-detonation tube into the throat of a shock focusing device inserted flush with the head end of the main combustion tube to promote more favorable transition conditions.

In addition, the effects of a transient detonation process on the inlet operation and performance of the engine was theoretically predicted, using a two dimensional grid in a viscous computational fluid dynamics code, and experimentally evaluated from subsonic to supersonic operation.

THIS PAGE INTENTIONALLY LEFT BLANK

# TABLE OF CONTENTS

# LIST OF FIGURES

THIS PAGE INTENTIONALLY LEFT BLANK

# LIST OF TABLES

THIS PAGE INTENTIONALLY LEFT BLANK

# ACKNOWLEDGEMENTS

The author would like to acknowledge the financial support of the Office of Naval Research under ONR Contract N0001499WR20085.

The author would also like to thank Professor David W. Netzer, Professor Christopher Brophy, and ASEE Postdoctoral researcher Dr. Jose Sinibaldi for the invaluable assistance and education provided me during the development of this thesis. The completion of this work would not have been possible without them.

The author would also like to thank Mr. Harry Conner for his extensive work on testing equipment and test cell development for this thesis. His hard work and dedication directly contributed to the author being able to graduate on time.

In addition, Mr. Glenn Harrell, Mr. Frank Franzen, and Mr. John Moulton need to be thanked for their outstanding machining of the Pulse Detonation Engine components used in this thesis.

THIS PAGE INTENTIONALLY LEFT BLANK

# I. INTRODUCTION

## A. EXISTING PROPULSION SYSTEMS

The current state of the art in missile propulsion technology has been limited within the United States primarily to the use of solid propellants [Ref. 1]. As evidence, Table 1-1 contains a list of mission categories, available U. S. missile systems, and the type of propulsion used by each system. Solid propellant motors have been adopted as the propulsion system of choice because of their simplicity of design, economical cost, and proven reliability. However, an average lower specific Impulse ($I_{sp}$), an inability to throttle or extinguish the motor, propellant cracking and age-related breakdown, and the higher risk of toxicity and munition explosion associated with solid propellants are undesirable characteristics [Ref. 1]. Air breathing missiles such as the Tomahawk and Harpoon missile systems have a much higher $I_{sp}$ (800-900 s) but operate at subsonic velocities. Although extensive research into the feasibility of a long-range supersonic ramjet propulsion system, known as FastHawk, has been completed at China Lake, there are currently no supersonic air breathing missiles, other than targets, being employed in the United States arsenal, primarily because of the cost and complexity of traditional liquid engine designs. The use of liquid fuel pulse detonation engine technology is expected to provide a missile propulsion system capable of long range flight, throttlable from subsonic to supersonic with a loiter capability, while offering the designer an engine that combines the advantages of both liquid and solid propellant engines. While gaseous fuel pulse detonation engines have been demonstrated in the laboratory environment, a liquid fueled engine will be required for practical application because of the higher specific energy density and the reduced volume/storage requirements. Increased

thermodynamic efficiency, lower operational cost, and the reduced complexity inherent in pulse detonation engine systems should allow these systems to be readily adopted for use in multiple propulsion applications and environments.

| Mission Category | Name | Diameter (ft) | Length (ft) | Propulsion | Launch Weight (lb) |
|---|---|---|---|---|---|
| Surface-to-surface (long range) | Minuteman III | 6.2 | 59.8 | 3 stages, solid | 78,000 |
| | Polaris A 3 | 4.5 | 31 | 2 stages, solid | 35,000 |
| | Poseidon | 6.2 | 34 | 2 stages, solid | 65,000 |
| | Titan II | 10 | 103 | 2 stages, liquid | 330,000 |
| Surface-to-air | Chaparral | 0.42 | 9.5 | 1 stage, solid | 185 |
| | Improved Hawk | 1.2 | 16.5 | 1 stage, solid | 1,398 |
| | Standard Missile | 1.13 | 15 or 27 | 2 stage, solid | 1350 2,996 |
| | Redeye | 0.24 | 4 | 1 stage, solid | 18 |
| Air-to-Surface | Maverick | 1.00 | 8.2 | 1 stage, solid | 475 |
| | Shrike | 0.67 | 10 | 1 stage, solid | 400 |
| | SRAM | 1.46 | 14 | 2 staged grains | 2,230 |
| Air-to-air | Falcon | 0.6 | 6.5 | 1 stage, solid | 152 |
| | Phoenix | 1.25 | 13 | 1 stage, solid | 980 |
| | Sidewinder | 0.42 | 9.5 | 1 stage, solid | 191 |
| | Sparrow | 0.67 | 12 | 1 stage, solid | 515 |
| Antisubmarine | Subroc | 1.75 | 22 | 1 stage, solid | 4,000 |
| Battlefield Support (surface-to-surface, short range) | Lance | 1.8 | 20 | 2 stages, liquid | 2,424 |
| | Hellfire (antitank) | 0.58 | 5.67 | 1 stage, solid | 95 |
| | Pershing II | 3.3 | 34.5 | 2 stages, solid | 10,000 |
| | Tow (anti-tank) | 0.5 | 3.84 | 1 stage, solid | 40 |
| Cruise missile (subsonic) | Tomahawk | 1.74 | 21 | solid booster + turbofan | 3,900 |
| Surface-to-missile | Patriot | 1.34 | 17.4 | 1 stage, solid | NA |

Table 1-1. Current Missile Propulsion Technology. From Ref. [1]

## B. PULSE DETONATION ENGINES: PAST AND PRESENT

There has been an ongoing interest in detonation research for at least a hundred years. Gaseous detonations were first discovered by Bertolet in 1881. Chapman (1899) and Jouget (1905) independently determined that the combustion products from a detonation propagate at sonic speed relative to the detonation wave. Early modeling of detonation waves, modeled as a shock wave followed by a combustion process, was done separately by Zeldovich, Von Neumann, and Doring during the early years of the last century. The use of detonations in propulsion applications has its roots in the middle of

the twentieth century when researchers were finally able to rapidly mix fuel and oxidizer at high speeds in a controlled manner in order to initiate and sustain a detonation. Early research focused on both standing (stabilized) and unsteady (intermittent) detonations. Investigations were prompted by the fast energy conversion rate that is characteristic of a detonation process, as well as higher theoretical thermodynamic efficiencies than in a deflagration (constant pressure) process. The first useful studies on the use of detonations in a propulsion system included work performed by Hoffmann, Bitondo, and Nicholls, et. al. Some early applications included a rotating detonation wave rocket motor, Oblique detonation wave engine (ODWE), and a Ram accelerator. [Ref. 2]

Early attempts to understand the physics and aerodynamics of propulsive duct systems, which includes pulse detonation engines, concluded that the concept "...should be capable of any desired level of thrust per unit area, with a corresponding reduction in specific fuel consumption. Valveless operation was also investigated and shown to offer a route to eliminating the dependency on fixed acoustical frequencies tied to a given chamber geometry." [Ref. 3] In addition, the possibility of very high frequency operation beyond the audible range through the use of feedback techniques was predicted, as well as supersonic operation of a propulsive duct. [Ref. 3]

Studies were performed in the 1970's that investigated the use of detonation thrusters and laser supported detonations. Detonative thrusters were considered for use in the dense or high-pressure atmospheres of other planets in our solar system, where a lowering of conventional thruster combustor pressure to ambient would lead to significant inefficiencies. Laser supported detonation was used in two different studies. The first concept was to propel objects to low earth orbit by generating a detonation and a

high kinetic energy jet moving away from the object through the deposition of laser energy on a solid or liquid propellant. The second concept was to sustain a standing oblique detonation wave for supersonic combustion by rapidly adding energy from a pulsed laser to a steady supersonic stream of detonable gases. [Ref. 2]

The current work in detonation propulsion has primarily focused on the use of intermittent detonation in pulse detonation engines. The first known experiments that successfully demonstrated repetitive or pulsed detonation was attainable in a propulsive manner were carried out at the United States Naval Postgraduate School in Monterey, California in 1985 [Ref. 3]. Recent investigations at the school's Rocket Propulsion and Combustion Laboratory involved the generation of ethylene and air detonations to evaluate and qualify the testing facility. An experimental specific impulse ($I_s$) of approximately 1000 to 1400 seconds was estimated using pressure time history and fuel consumption rates. The ethylene/air tests proved to be satisfactory and led to the modification of the facility to study the detonation properties for liquid JP-10 and air/Oxygen [Ref. 4]. Liquid fuels are more desirable than compressed gases because of their higher energy density, considerably better storage properties, and their lack of inherent explosive capability. In particular, JP-10 is being tested because of its current application in military weapons (Harpoon missile) and because it is already approved for shipboard use. Achieving a detonation in a very short length, however, is difficult when using a liquid fuel because of the critical atomization and mixing of the fuel and oxidizer required. Using air as the oxidizer in the combustor eliminates the need for additional tankage, leading to a higher specific impulse and greater flexibility in the missile design.

A valveless pulse detonation engine geometry, in which only the fuel injection is valved, is depicted in Figure 1-1.

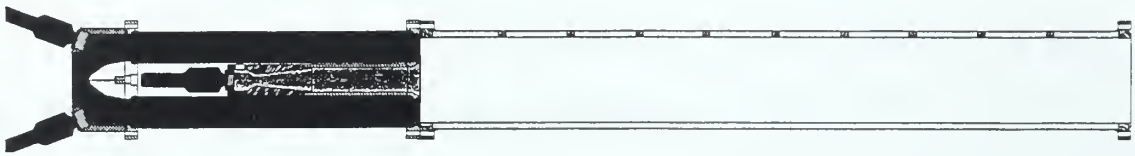

Figure 1-1. Pulse Detonation Engine.

Other agencies have also conducted gaseous pulse detonation engine experiments and/or numerical modeling of these engines, to include the determination of detonation velocities and deflagration to detonation transition (DDT) lengths for given equivalence ratios, rotary injection valve multiple detonation tube experiments, nozzle shaping effects on pulse detonation engine performance, and pulse detonation rocket engines [Ref. 2]. Some conceptual studies that are being investigated include the use of a pulse detonation wave augmentation device for thrust generation and mixing/combustion augmentation in a hybrid engine for a single stage to orbit air breathing hypersonic vehicle to achieve increased thermodynamic efficiencies. [Ref. 2]

THIS PAGE INTENTIONALLY LEFT BLANK

# II. BACKGROUND THEORY

## A. INTRODUCTION

Analysis of a Pulse Detonation Engine requires a thorough understanding of the detonation process and the mechanics of a detonation wave. A detonation wave is defined by the close coupling of a strong shock wave to a heat release region immediately behind the shock where the combustion of the highly compressed combustible reactants occurs.

## B. COMBUSTION PROCESSES

The difference between a detonation and other combustion events is significant enough to warrant clarification. In an explosion, a chemical exothermic reaction occurs in an environment in which the energy loss is less than the energy released. The reaction rate is amplified by the resulting temperature increase, leading to an extremely fast rate of energy generation in the form of pressure and temperature.

A combustion process occurs when reactants and oxidizers are mixed and ignited, resulting in the rapid oxidation of the fuel. There are three types of combustion processes: a) Constant Pressure, also known as a deflagration, in which the entropy rise of the working fluid is maximized for the given heat release, b) Constant Volume, and c) Chapman-Jouget Detonation. The detonation process has a much lower entropy rise for the given energy release relative to a deflagration process. This results in more work available.

The two primary combustion processes to be discussed here are a deflagration and a detonation. A deflagration is a combustion wave that propagates subsonically (slower than the speed of sound) into unburned reactants. The transport of thermal energy and

reactants govern the flame front propagation rate. Deflagration processes include the combustion of a simple candle flame to that inside a jet engine. Detonations release approximately the same amount of energy but at a much faster rate and within a very narrow flame front. Typical combustion wave velocities for a detonation exceed 2,000 m/s, much faster than deflagration combustion waves that typically propagate at 1 to 10 meters per second. The detonation wave, and the deflagration wave, can be modeled as a one-dimensional stationary planar wave, as seen in Figure 2-1. [Ref. 5]

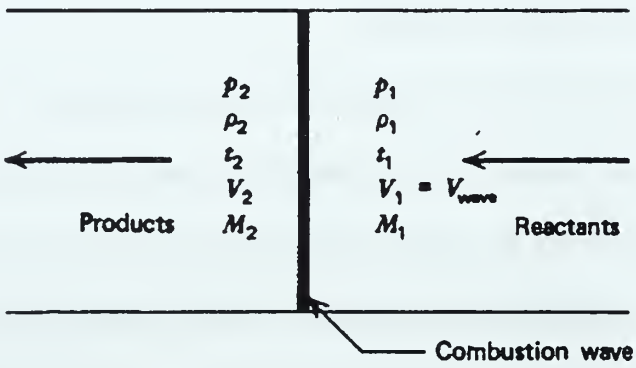


Figure 2-1. Stationary Combustion Wave System. From Ref. [6]

As the reactants "pass through" the combustion wave, the ratio of the product properties to the reactant properties shift to a commensurate value, depending on whether the planar wave is a detonation or deflagration wave. Typical values for these ratios can be found in Table 2-1.

| | Detonation | Deflagration |
|---|---|---|
| $u_1/c_1$ | 5–10 | 0.0001–0.03 |
| $u_2/u_1$ | 0.4–0.7 (deceleration) | 4–6 (acceleration) |
| $p_2/p_1$ | 13–55 (compression) | ≈ 0.98 (slight expansion) |
| $T_2/T_1$ | 8–21 (heat addition) | 4–16 (heat addition) |
| $\rho_2/\rho_1$ | 1.7–2.6 | 0.06–0.25 |

Table 2-1. Differences between Detonation and Deflagration in Gases. From Ref. [5]

For the purposes of this thesis, a detonation process can be said to exist if a near instantaneous pressure rise at the leading edge of the waveform of 300 psig or greater and wave velocities approaching theoretical are measured throughout the length of the engine in which the combustion process takes place.

### 1. JP-10 Deflagration Properties

Deflagration flame speeds are dependent on the temperature of the reaction, but generally are on the order of ten meters per second. A laminar JP-10/Air deflagration flame propagates at an approximate rate of 0.6 meters per second at room temperature, while a turbulent flame propagates at speeds no greater than 10 meters per second. [Ref. 5]

### 2. JP-10 Detonation Properties

Detonation waves have specific velocities, pressures, and temperatures that are a function of the fuel to oxidizer ratio or equivalence ratios ($\phi$), which can be theoretically determined with good accuracy relative to experimental results. There are thermodynamic equilibrium codes that calculate the detonation wave speeds, pressures, and temperatures for a given set of reactants. The Thermo-Chemical Equilibrium Program (TEP), CET89, and CETPC codes are all capable of computing detonation velocities, but individual versions may only be able to compute the detonation properties of particular fuels in their databases that contain detailed information on a particular fuel.

The ideal computation of the post detonation conditions would be to perform a three-dimensional Computational Fluid Dynamic analysis that would include real gas behavior, shifting specific heats, finite-rate chemical kinetics, etc. This method would be exhaustive and is currently unavailable, so a technique that makes a few analytical assumptions and utilizes the Thermo-Chemical equilibrium code was used. The post detonation properties were calculated in the following manner.

First, the initial conditions (including $T_1$, $P_1$, $R_1$, and $C_{v1}$) of the reactants were set. Second, TEP uses the estimated $T_1$ and $P_1$, the conservation equations, and minimizes the entropy gain to obtain $T_2$, $P_2$, $M_2$, and $C_{p2}$ for the combustion products. The results can be seen in Figures 2-2 and 2-3.

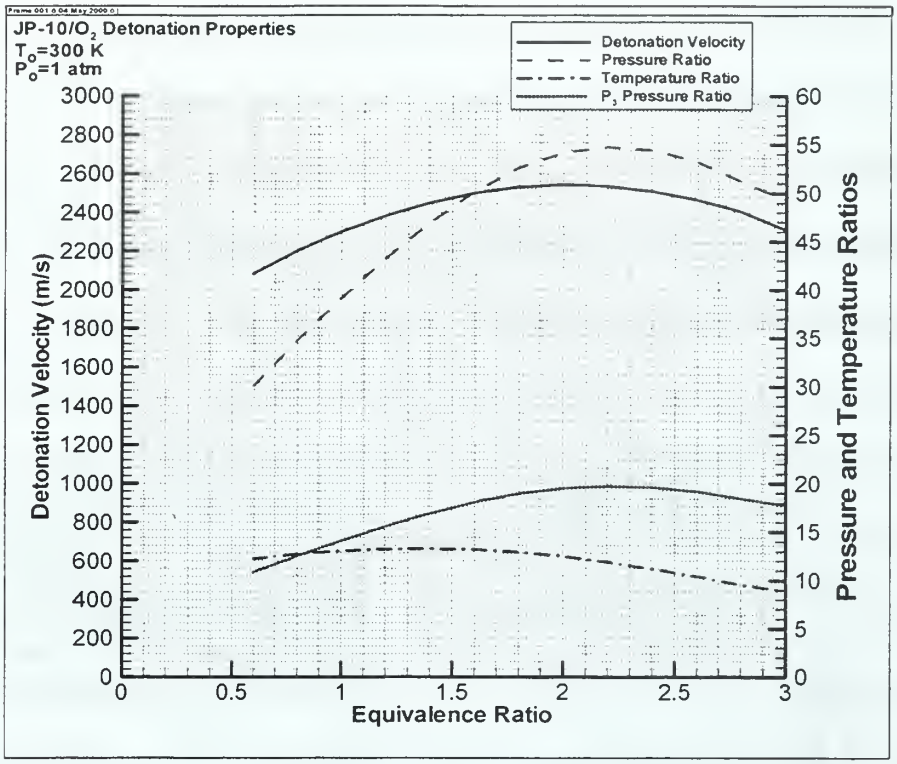


Figure 2-2. JP-10/$O_2$ Detonation Properties.

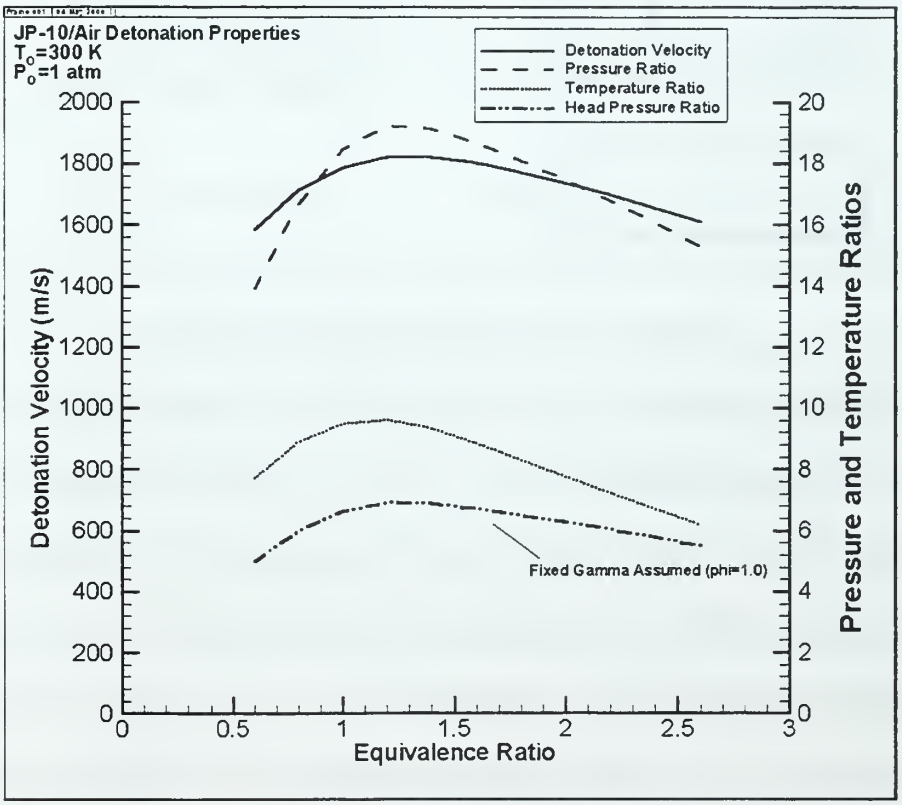


Figure 2-3. JP-10/Air Detonation Properties.

## C. PULSE DETONATION ENGINE OPERATION THEORY

### 1. Detonation Kinematics

The combustion cycle of a pulse detonation engine involves the cyclical loading, detonating, and purging of a combustor. Figure 2-4 is a representation of a typical detonation process within a closed head-end combustion tube.

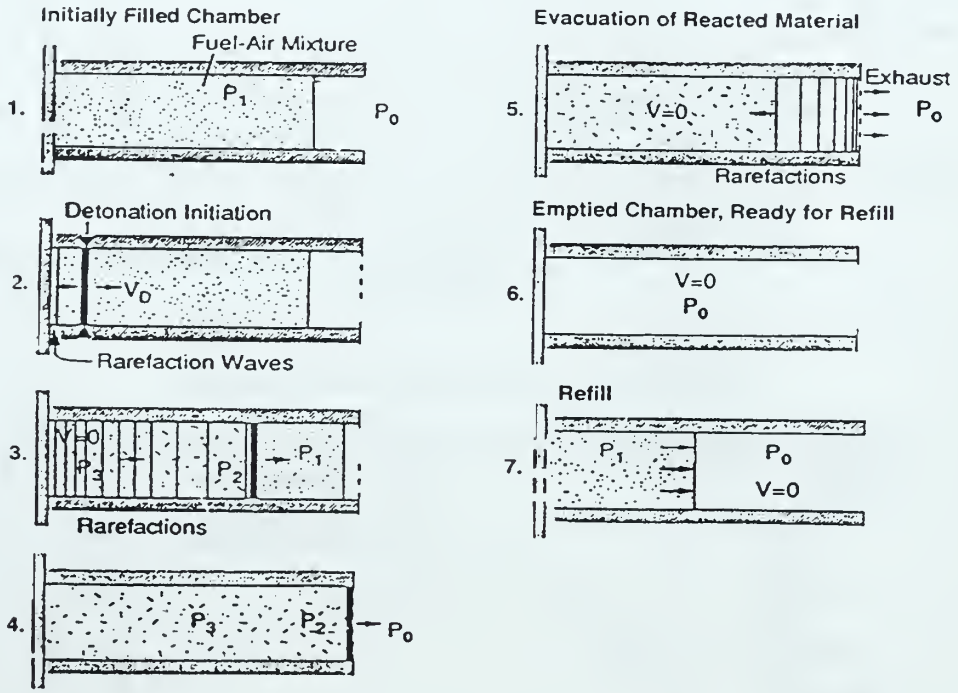


Figure 2-4. Detonation Process. From Ref. [2]

In frame 1, fuel and oxidizer are loaded into the tube and allowed to mix. In frame 2, the mixture is ignited near the closed end of the tube, creating acoustic disturbances that travel in both directions from the combustion zone. The disturbances that travel away from the closed end of the tube pre-compress the unburned reactants and accelerate the combustion process. Assuming that the mixture obeys the Perfect Gas Law, temperature will rise with the increasing pressure and the reactants burn faster, generating additional disturbances. The pressure disturbances that traveled toward the

closed end of the tube reflect off of the closed end and traverse back toward the combustion wave at a faster rate due to the higher sound velocity, resulting from heat addition, and eventually catch up to the initial waves. This phenomenon increases the compression ahead of the combustion wave. This further generates waves, which eventually coalesce and form a shock wave that is strong enough to directly ignite the reactants. The reaction zone behind the shock continuously feeds the compression wave with energy that keeps the shock front from decaying. This sustained chain of events generates a shock wave coupled to the deflagrating reaction zone shown in frame 3 and is a diabatic process known as a detonation. Frame 4 depicts the detonation wave reaching the end of the tube, leaving only the burned reactants behind it. Once the shock wave leaves the tube (frame 5), the pressure differential causes rarefaction waves to propagate into the tube towards the closed end. The remaining products are expelled through this self-aspirating process. The entire process can be repeated once the tube is empty (frames 6&7).

### 2. Detonation Ignition

There are two primary ways to initiate a detonation wave: direct ignition and a deflagration-to-detonation transition (DDT) process. In the latter case, an igniter is used to establish a deflagration process that eventually develops into a detonation wave through the process described in section II-C-1. This method, also known as thermal ignition, is heavily dependent on tube length and geometry, ignition source, and combustion reaction rates. The length of the deflagration-to-detonation transition is affected by the combustible mixture used, internal dimensions and geometry of the combustor, possible heat addition, and the equivalence ratio used [Ref. 7]. Ideally, the

DDT length should be as short as possible so that realistic propulsion system designs can be created. In reality, a tradeoff must be made between achieving the shortest possible DDT length and using fuel/oxidizer mixtures that are relatively benign for safety reasons. Prior work done at the Rocket Propulsion and Combustion Laboratory at the United States Naval Postgraduate School in Monterey, California has validated this method using liquid JP-10 and oxygen. [Ref. 7]

Direct ignition, a faster means to initiate detonation, can be done using an extremely high-energy spark or plasma delivered in a short period of time, although this only works for a few fuel and oxidizer mixtures. Another method is to propagate an ignition blast wave or strong shock wave into unburned reactants. In this thesis a thermal ignition shock wave generated by a liquid JP-10 and oxygen mixture from a "pre-detonation tube" was employed. The "pre-detonation tube" needed to be sufficiently longer than the deflagration to detonation transition length for a JP-10/oxygen mixture in order to directly initiate a detonation in a mix of JP-10 and air in the main combustion tube. According to established criteria the detonation will only successfully propagate from the "pre-detonation tube" into a larger tube or area if the diameter of the "pre-detonation tube" is greater than or equal to 13 times $\lambda$ (the cell size, which is a function of the fuel used). [Ref. 8 & 9] For example, the cell size for a JP-10/$O_2$ mixture is estimated to be 2 mm. Therefore, as long as the "pre-detonation tube" diameter is greater than or equal to 26 mm ($\approx$ 1 Inch), a detonation should have no problems propagating into, but not necessarily sustaining, the main combustion tube as long as a JP-10/$O_2$ composition exists at the interface plane.

## D. THERMODYNAMICS OF DETONATIONS

To understand what occurs during the detonation process, one needs to revisit some basic chemistry for equilibrium combustion and to find the heat released as a result. An "ideal" or complete combustion process between a fuel and oxidizer at a stoichiometric mixture ratio results in products consisting of only water and carbon dioxide. The complete combustion of ethylene and oxygen can be represented by:

$$C_2H_4 + 3O_2 \Leftrightarrow 2H_2O + 2CO_2$$

In the real world, nature will take the reaction all the way to an equilibrium combustion condition, in which combustion radicals and combustion intermediates will be present (such as OH, NO, CO, $NO_2$, etc.) on the right hand side of the above expression. A combustion program, such as the Thermodynamic Equilibrium Program (TEP), can be used to determine the product conditions after the detonation wave has passed. To determine the heat released during the combustion event, the enthalpies of formation and of change, available in pre-published tables using the temperature $T_2$ of the products found in the TEP solution, need to be considered. In the above complete combustion example, the heat released (q) would be:

$$1mol(12.54\frac{kcal}{mol}) + 3mol(0\frac{kcal}{mol}) \Leftrightarrow 2mol(-57.798\frac{kcal}{mol}) + 2mol(-94.054\frac{kcal}{mol}) + q \Rightarrow q = 316.24\frac{kcal}{mol}$$

The heat released from an equilibrium combustion will be significantly less than a complete combustion because a portion of the heat will go into the formation of radicals and the absorption of heat by the formed water molecules to create water vapor. Section II-E contains theoretical cycle analyses of a constant pressure and a C-J detonation equilibrium combustion process that includes the effect of radicals on the heat generated.

There are five primary equations, one being the Perfect Gas Law, used to determine the post-combustion state thermodynamic properties [Ref. 5]:

Continuity
$$\dot{m} = \rho_1 u_1 = \rho_2 u_2 \tag{1}$$

Momentum
$$P_1 + \rho_1 u_1^2 = P_2 + \rho_2 u_2^2 \tag{2}$$

Energy
$$C_P T_1 + \frac{1}{2}u_1^2 + q = C_P T_2 + \frac{1}{2}u_2^2 \tag{3}$$

$$C_P = \left(\frac{\gamma}{\gamma - 1}\right) R \tag{4}$$

By manipulating equation (3) through the use of equation (4), and combining the new equation with equation (1) and (2), the Rankine-Hugoniot relation is generated:

$$\left(\frac{\gamma}{\gamma - 1}\right)\left(\frac{P_2}{\rho_2} - \frac{P_1}{\rho_1}\right) - \frac{1}{2}(P_2 - P_1)\left(\frac{1}{\rho_1} + \frac{1}{\rho_2}\right) = q \tag{5}$$

Figure 2-5 is a P-V diagram of the theoretical final conditions achievable in a combustion process for given initial conditions (point A) and a value of q, also known as the Hugoniot curve. Regions I through V are regions of possible mathematical solutions. In reality, not all of the regions are physically realizable. For example, region V implies that the initial internal energy is imaginary. Careful analysis of the Hugoniot curve shows that there are two possible combustion processes: those in which pressure and density increase (detonations) and those in which pressure and density decrease (deflagrations). For the points at which the Hugoniot curve and the Rayleigh line are tangent, known as the upper (U) and lower (L) Chapman-Jouget points, the post combustion gas velocity is sonic, as dictated by heat addition in a constant area tube.

Table 2-2 depicts the type of combustion process and Mach numbers of the reactants and products for each region in Figure 2-5.

Figure 2-6 depicts possible real paths that can be taken to reach the upper C-J point. Path (a) requires the chemical equation reaction to occur everywhere along the path, but since there is no significant compression early in the path there will not be a sufficient temperature to initiate a reaction or enough energy to sustain the wave. Path (d) would occur when a rapid compression coincided with a slow chemical reaction, which is not very likely either. The most likely paths (path b or c in Figure 2-6), for conventional chemical kinetic rates, occur because of the fast shocking of the combustion gases, leading to the Von Neumann pressure spike seen in Figure 2-6. This pressure spike is created by the fact that the shocking occurs faster than the gases can achieve an energy equilibrium in the vibrational state.

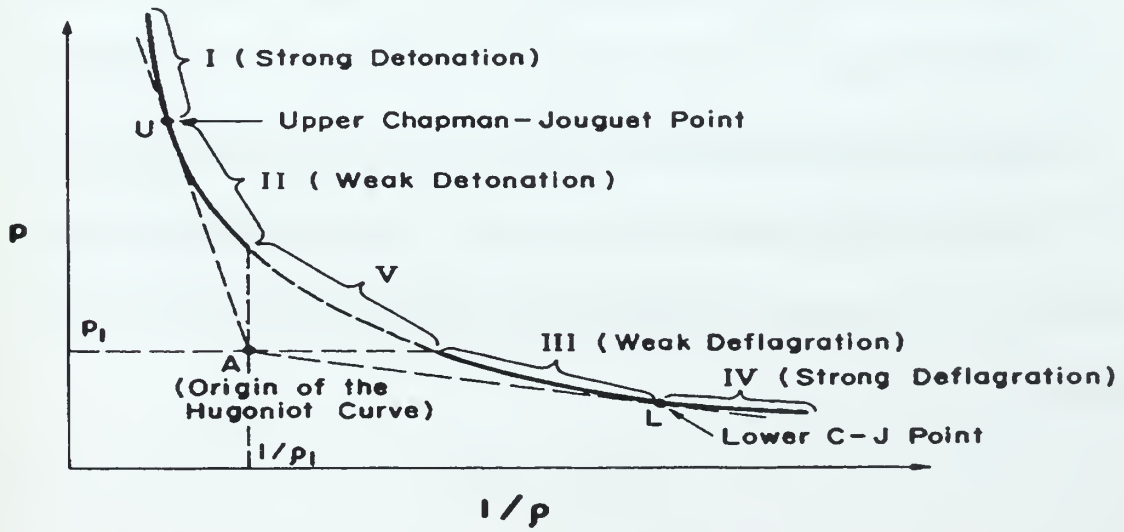


Figure 2-5. Physical Breakdown of Hugoniot Curve. From Ref. [5]

| Region | Combustion Wave | $M_1$ | $M_2$ |
|---|---|---|---|
| I | Strong Detonation | >1 | <1 |
| II | Weak Detonation | >1 | >1 |
| IV | Weak Deflagration | <1 | <1 |
| V | Strong Deflagration | <1 | >1 |

Table 2-2. Hugoniot Curve Regional Properties.

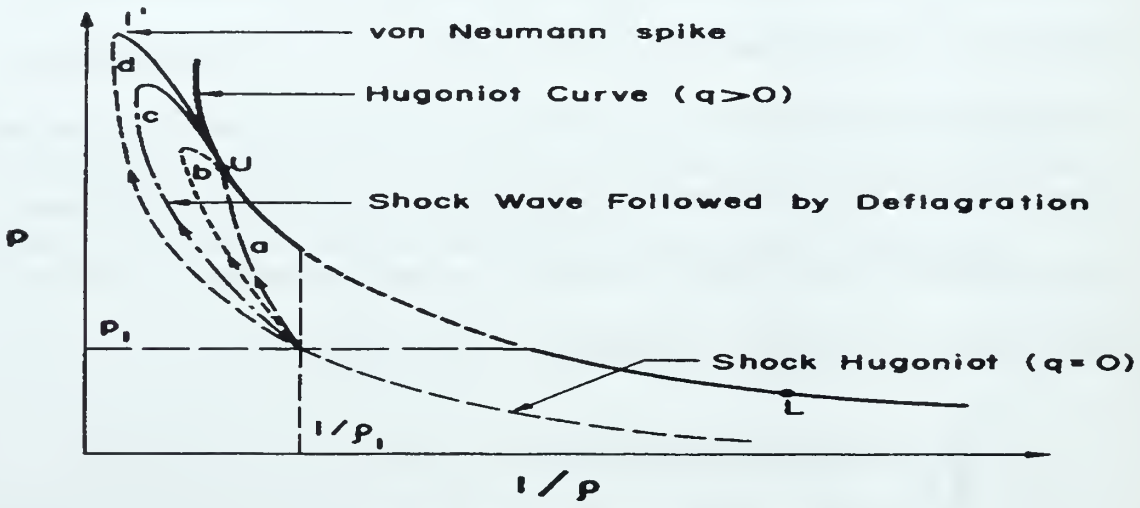


Figure 2-6. Hugoniot Curves for a Given Value of q and q=0. From Ref. [5]

By differentiating equation (5) with respect to $\rho_2$, and noting that the Rayleigh and Hugoniot curves intersect at the upper and lower points, the following equation is generated:

$$\frac{P_2 - P_1}{\left(\frac{1}{\rho_2} - \frac{1}{\rho_1}\right)} = -\gamma P_2 \rho_2 \tag{6}$$

By combining equations (1) and (2) and setting the result equal to equation (6), one finds:

$$u_2^2 = \frac{\gamma P_2}{\rho_2} = c_2^2 \Rightarrow |u_2| = c_2 \tag{7}$$

In other words, at the upper C-J point (point U in Figure 2-5) the velocity after the wave is limited by the local speed of sound at the C-J detonation condition even though the detonation wave is moving supersonically into the unburned mixture.

## E. THEORETICAL WAVE MECHANICS

A theory for a simplified detonation wave structure, independently arrived at by Zeldovich, von Neumann, and Doring (ZND), assumed that a steady, one dimensional flow existed relative to the detonation front and that very limited reactions and heat release occurred in the shock wave itself due to its thickness relative to the mean free molecular path. They theorized that the detonation wave consists of a planar shock moving at the detonation velocity with chemical reactions occurring behind the shock over a region thicker than the shock wave, and that the shock wave initially heats the reactants to a temperature that can result in a sufficiently fast reaction rate to generate the required energy to support the preceding shock wave.

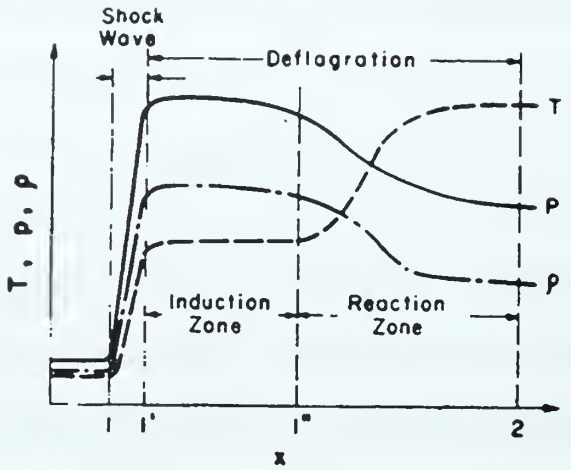

Figure 2-7. ZND Wave Structure. From Ref. [5]

Figure 2-7 depicts the variation in properties through a one dimensional ZND detonation wave, with the property magnitudes dependent upon the fraction of gaseous mixture reacted. The induction zone immediately behind the shock, where the temperature is not very high, demonstrates a slow increase in reaction rate and relatively flat pressure, temperature, and density profiles. After the induction period the properties change rapidly as the reaction rate increases drastically. The reaction is completed within a distance on the order of 1 centimeter and the properties reach their equilibrium values. [Ref. 5]

## F. THEORETICAL CYCLE ANALYSIS

One of the primary benefits of a pulse detonation cycle is reported to be its higher thermodynamic efficiency and lower entropy rise relative to other combustion processes. To determine the potential performance gain, a theoretical cycle analysis was performed for a constant pressure and a C-J detonation process using JP-10 fuel and air as the reactants.

Determination of the resulting heat addition for both cases was done using the post-combustion product conditions generated by the Thermodynamic Equilibrium

Program (TEP) for the same given set of initial conditions (P = 1 atmosphere, T = 300 degrees Kelvin, equivalence ratio of one) for each case and pre-published tables containing the enthalpies of formation and change for the reactants and products. The synthesis of this work was used in equation (8) to find the heat added, where $u_2$ is the detonation velocity and $c_2$ is the sonic velocity behind the wave.

$$\frac{1}{2}(u_2 - c_2)^2 + C_{P_2} T_2 - C_{P_1} T_1 - \frac{1}{2} u_2^2 = q_{add} \tag{8}$$

To determine the net work and the thermal efficiency for each case, several assumptions had to be made:

- The working fluid is both a thermally and calorically perfect gas during isentropic compression and expansion.
- The working fluid has constant but different specific heats prior to and after the combustion.
- The energy of combustion is determined using thermodynamic considerations contained in TEP.

Equations (1) through (4) and the Perfect Gas Law were all used in this analysis. The entropy relationship across the wave was determined using the following relationship:

Entropy $$s = C_p \ln\left(\frac{T}{T_{REF}}\right) - R \ln\left(\frac{P}{P_{REF}}\right) \tag{9}$$

The net work for each case was determined by integrating the area under the curve in their respective P-v diagrams. The Brayton (constant pressure) and Detonation cycles, using data from Tables 2-3 and 2-4, are included as Figures 2-8 and 2-9.

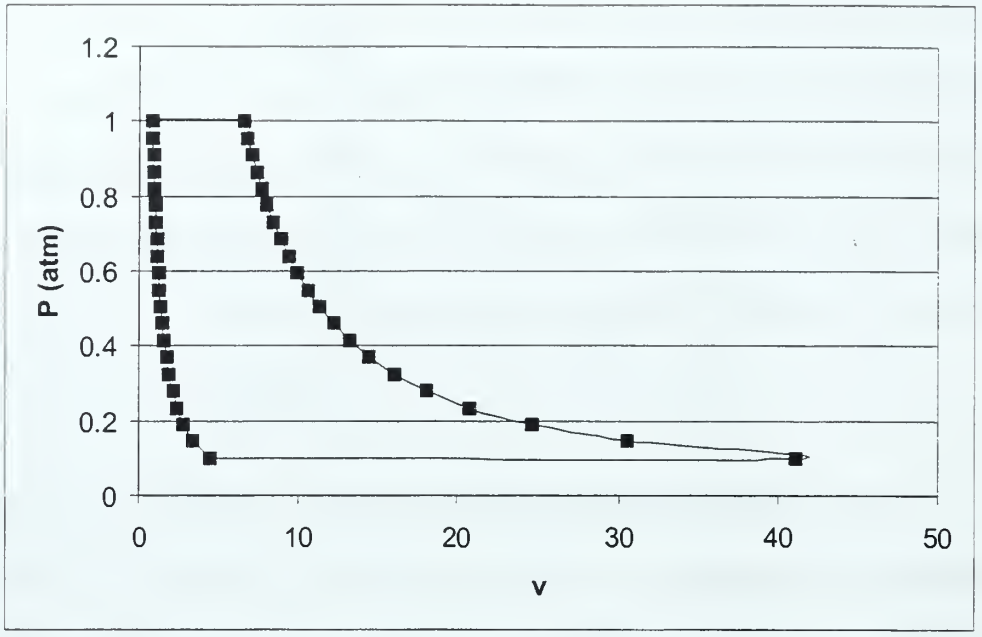


Figure 2-8. Brayton Cycle.

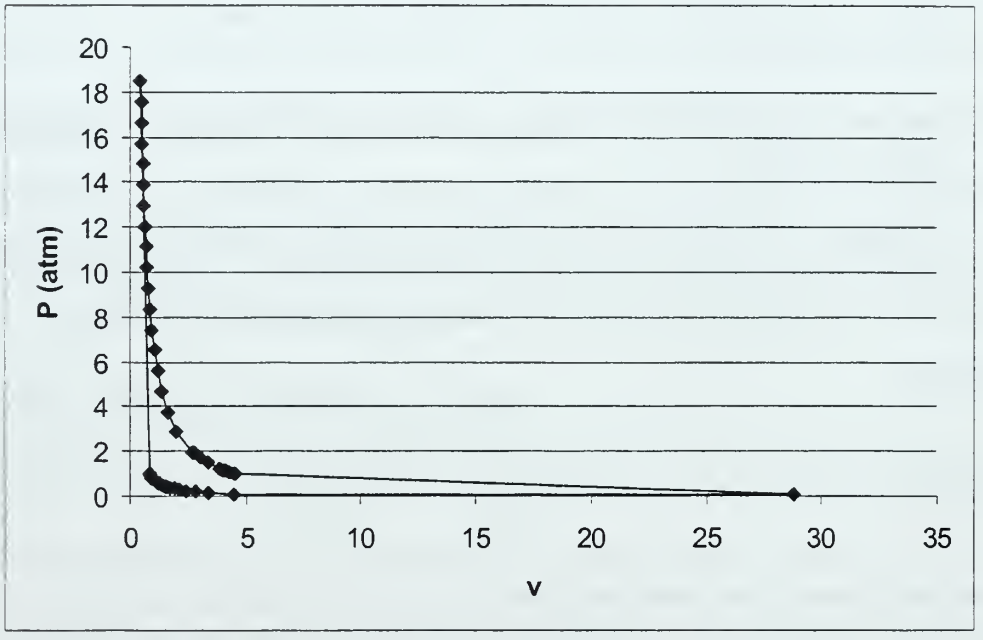


Figure 2-9. Detonation Cycle.

For both combustion processes, the temperature and pressure at State 0 was determined by first selecting initial conditions ($P_{REF}$ = 0.1 atmosphere, $T_{REF}$ = 164.873 degrees Kelvin) and applying these to representative pressure and temperature values that

would be expected to be encountered by the reactants in a supersonic missile traveling at high altitude. Specific volume and entropy at State 0 were then determined using equations (8) and (12) and the Perfect Gas Law with a pre-burned gas ratio of specific heats and specific heat at constant pressure. The process from State 0 to 1 assumes an isentropic 10:1 compression in the missile inlet to a final static pressure of 1 atmosphere.

The conditions at state 2 for both processes were taken from the TEP analysis and were used in the final calculation of the net work for each cycle. The process from State 2 to 4 for both processes assumed an isentropic expansion back to the pressure at State 0. The results of this analysis can be seen in Tables 2-3 and 2-4.

| State | Pressure (atm) | Temp. (K) | Spec. Vol. ($m^3$/kg) | Entropy (J/kgK) |
|---|---|---|---|---|
| 0 | 0.1 | 164.9 | 4.445 | 0 |
| 1 | 1 | 300 | 0.809 | 0 |
| 2 | 18.464 | 2851 | 0.446 | 2614.4 |
| 4 | 0.1 | 996.33 | 28.791 | 2614.4 |

Table 2-3. Thermodynamic States of Working Fluid for a Detonation Process.

| State | Pressure (atm) | Temp. (K) | Spec. Vol. ($m^3$/kg) | Entropy (J/kgK) |
|---|---|---|---|---|
| 0 | 0.1 | 164.87 | 4.445 | 0 |
| 1 | 1 | 300 | 0.8088 | 0 |
| 2 | 1 | 2293 | 6.536 | 3104.3 |
| 4 | 0.1 | 1444 | 41.10 | 3104.3 |

Table 2-4. Thermodynamic States of Working Fluid for a Constant Pressure Process.

The net work for the detonation and constant pressure combustion cycles was calculated using the following equations:

$$w_{C-J} = \left(\frac{Pv_1 - P_0v_0}{1-\gamma}\right) + \frac{1}{2}\left(\frac{P_2 - P_1}{v_2 - v_1}\right)\left(v_2^2 - v_1^2\right) + \left(P_2 - \left(\frac{P_2 - P_1}{v_2 - v_1}\right)v_2\right)\left(v_2 - v_1\right) + \left(\frac{P_4v_4 - P_2v_2}{1-\gamma}\right) + P_4\left(v_0 - v_4\right)$$

$$w_{C_P} = \left(\frac{P_1v_1 - P_0v_0}{1-\gamma}\right) + P_2\left(v - v_1\right) + \left(\frac{P_4v_4 - P_2v_2}{1-\gamma}\right) + P_4\left(v_0 - v_4\right)$$

Finally, thermal efficiency was found by dividing the net work by the heat added for each process. The calculated heat addition, net work, and thermal efficiency can be seen in Table 2-5.

| Process | Heat addition | Net Work | $\eta_{th}$ (%) |
|---|---|---|---|
| Constant Pressure | 2970.5 KJ/kg | 1078.1 KJ/kg | 36.3 |
| Detonation | 2555.4 KJ/kg | 1401.9 KJ/kg | 54.9 |

Table 2-5. Thermal Efficiencies.

The calculated values demonstrate that the thermal efficiencies are higher and the entropy rise lower for a given detonation process relative to a constant pressure process.

## G. MULTI-CYCLE EFFECTS

As discussed in section II-C-1, a typical single detonation cycle consists of loading a fuel/oxidizer mixture, ignition, propagation of a detonation wave down the tube, and the products being expelled from the tube by rarefaction waves created by the sudden expansion to atmospheric pressure within the tube after the detonation wave exits. Ideally, this cycle could be repeated indefinitely at a very fast cycle frequency without having to account for each cycle's effect on the next and without affecting the

performance of the engine. In reality, there are several key issues, delineated below, that need to be accounted for in order to maximize engine performance.

First, the thrust developed by the engine can be determined by either the momentum flux out of the engine or by integrating the head-end pressure over time. The average thrust can actually decline due to the expansion below atmospheric pressure after the detonation wave exits the combustion tube. Coupling of the next cycle's fuel/oxidizer loading time to the previous cycle's detonation wave leaving the tube can be used to eliminate this effect by preventing the pressure within the tube from dropping below the local atmospheric value. Also, a valveless detonation engine in which a continuous mass flow rate of air is allowed, as in a jet engine, could help mitigate a reduction in average thrust.

Second, the cycle repetition rate, or frequency, is limited by the physical size of the detonation tube, the finite times required for loading the reactants, frequency capability of the ignition system, and purging the products, e. g. the air mass flow rate which is a function of flight conditions. A valveless engine design would shorten the product purge time, thereby theoretically increasing the potential cycle frequency.

Third, the importance of matching the fuel/oxidizer load time of the next cycle to the detonation wave exit of the previous cycle must be balanced against the potential of this new mixture to be prematurely combusted due to remaining products of the previous combustion event still present in the tube. This possibility will again limit the cycle frequency and could affect the maximum average thrust produced by the engine.

THIS PAGE INTENTIONALLY LEFT BLANK

# III. EXPERIMENTAL APPARATUS AND SETUP

Three experimental setups were used in this study: an atomization characterization setup, a vitiated air heater, and the pulse detonation engine setup. All three will be described, including the apparatus used for atomizer and vitiator characterization.

## A. PHASE DOPPLER PARTICLE ANALYZER

The atomizer characterization was done using an Aerometrics Phase Doppler Particle Analyzer (PDPA) system capable of measuring particle sizes from 0.50 to 155 microns and injection velocities from 5 to 300 meters per second. Sauter Mean Diameters ($D_{32}$), volumetric mean diameters, and other spatial statistics were obtained for the atomization system used. The tip of the atomizer was placed seven centimeters (2.76 inches) upstream from the sample volume to obtain an appropriate sample with an allowable obscuration. Figure 3-1 is a picture of the PDPA apparatus layout, showing the Argon-Ion laser, the optical section, and the computer setup to record the data.

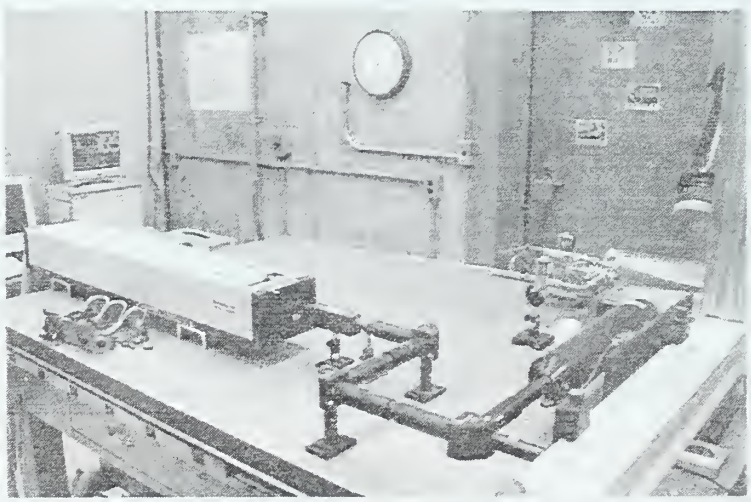

Figure 3-1. Phase Doppler Particle Analyzer System Layout.

## B. MALVERN MASTERSIZER

A determination of particle size distribution entering the main combustion tube was done using a Malvern Mastersizer system placed near the exit of the four main air arms.

The Malvern Mastersizer measurement system was fitted with a 100-millimeter focal length lens, which allowed particle diameter measurements from 0.5 to 148 microns. The end of the manifold flange (item a in Figure 3-2) was placed approximately 5.08 cm (2 inches) from the sampling volume to obtain an appropriate sample with an allowable obscuration. Item d in Figure 3-2 is the interface flange between the fuel injection manifold and the main air arms. Item c is the pre-detonation tube used to directly initiate a detonation in the main combustion tube. The experimental setup can be seen in Figure 3-3.

Once the "inlet air" was heated, it was diverted into the "inlet" of the pulse detonation engine, where it was mixed in a fuel injection manifold (item e in Figure 3-2) with discrete amounts of JP-10 injected using the BETE XA-F-PR200 injector. The mixing of heated "inlet air" and fuel aerosol led to additional vaporization of the already small fuel droplets, giving a more homogeneous mix of fuel and air vapor prior to arrival in the main combustion tube, particularly since the mixture travels through a tube with an L/D greater than ten (item b in Figure 3-2). For clarity, an exploded diagram of the engine, with the main combustion tube removed, is included as Figure 3-2.

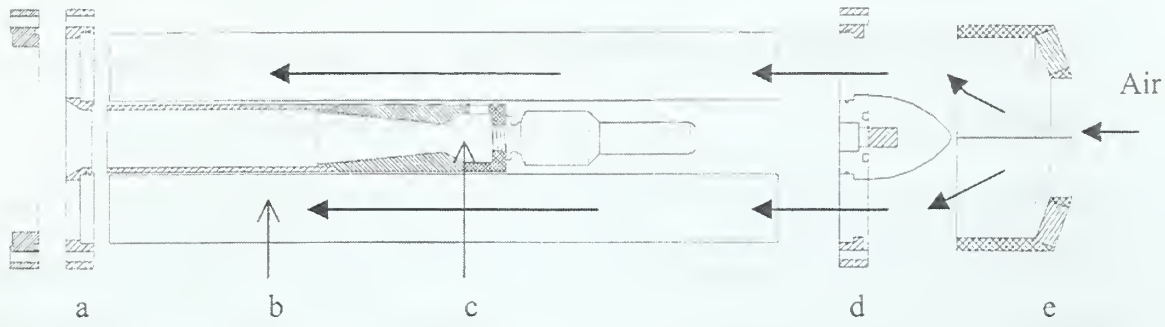


Figure 3-2. Pulse Detonation Engine Segment.

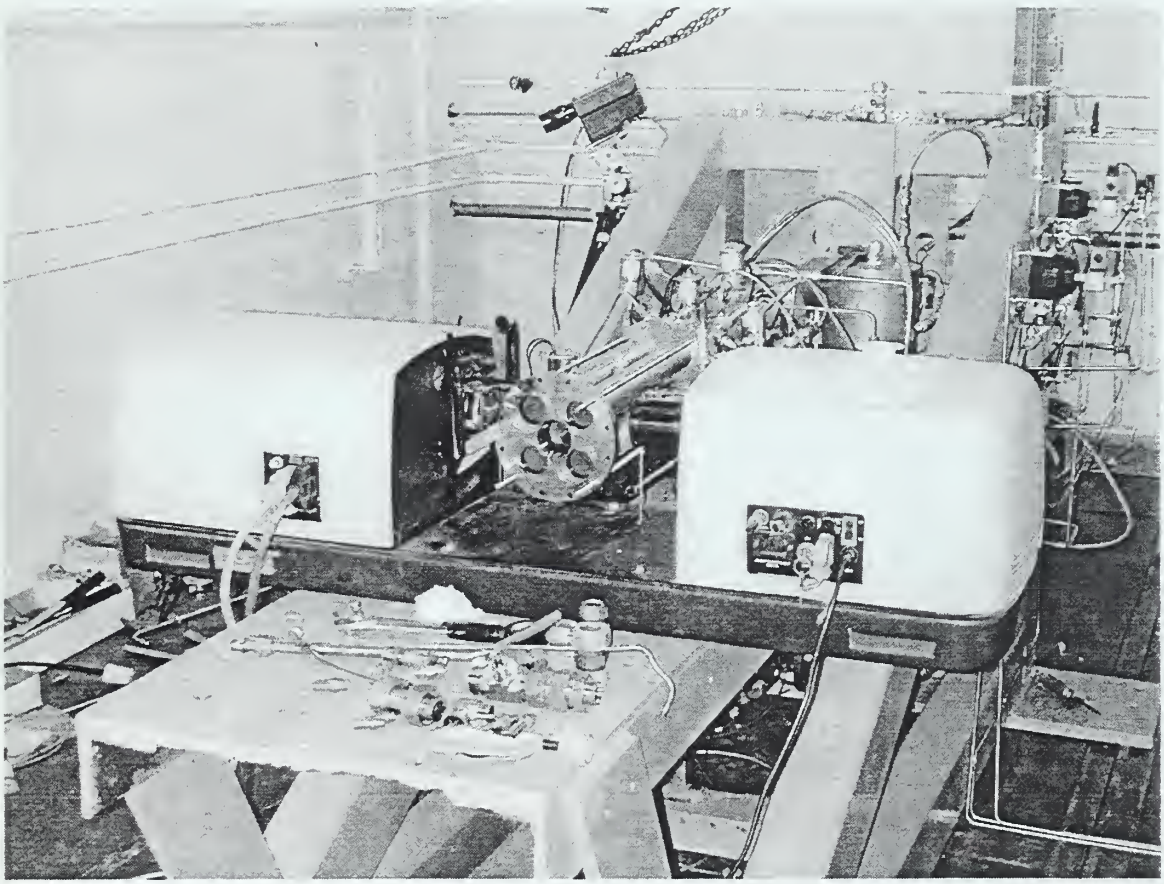

Figure 3-3. Malvern Mastersizer Measurement System.

## C. VITIATOR

A hydrogen/oxygen vitiator was used to raise the temperature of the "inlet air" of the engine to temperatures approaching 533 Kelvin (500 °F). This was done to simulate typical inlet conditions that a pulse detonation engine would experience in-flight at

supersonic speeds. Compressed air was routed into the vitiator, where an $H_2/O_2$ igniter was initially used to light a self-sustaining hydrogen/air combustor that raises the temperature of the "inlet air". Because the vitiator combusts externally provided hydrogen and oxygen in the air, "make-up" oxygen is added downstream of the vitiator to bring the "inlet air" back to the proper oxygen molar concentration in air. A picture of the vitiator is provided in Figure 3-4.

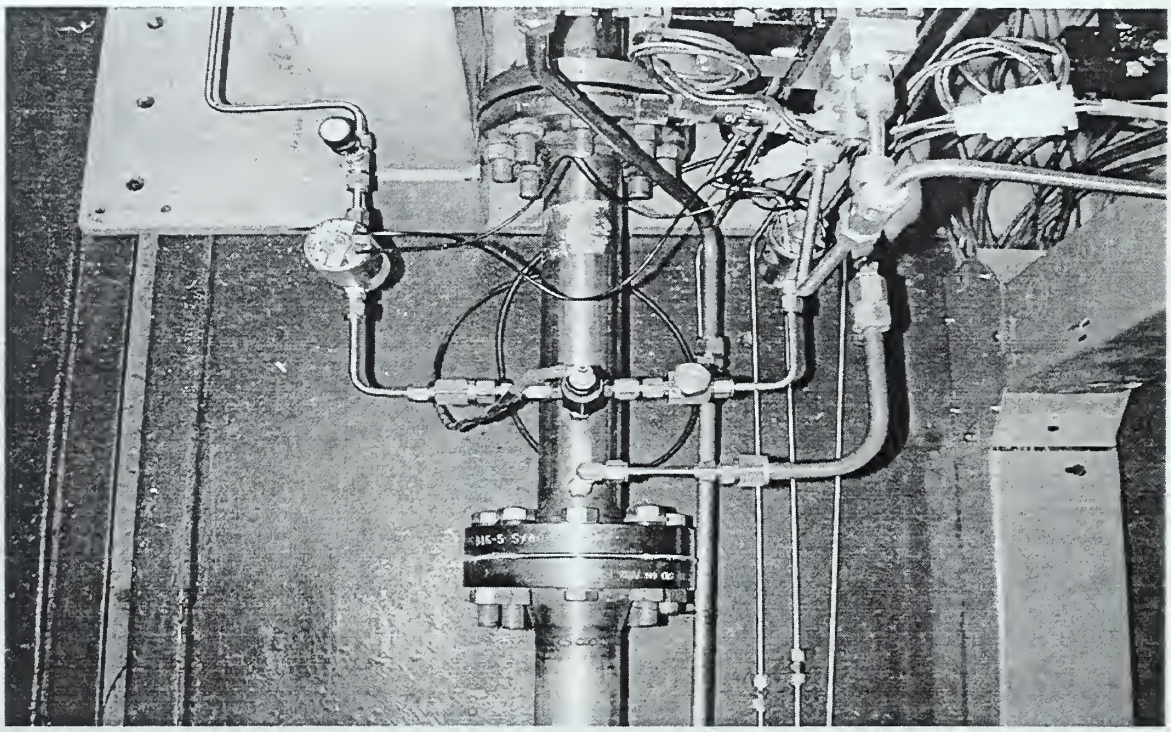

Figure 3-4. Vitiator.

## D. PULSE DETONATION ENGINE

The author designed and built a valveless pulse detonation engine based on previous work done at the Rocket Propulsion and Combustion Laboratory located at the United States Naval Postgraduate School in Monterey, California. A schematic of the engine is provided as Figure 3-5.

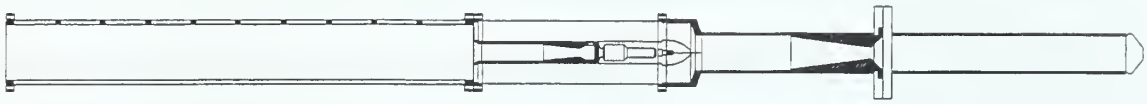

Figure 3-5. Pulse Detonation Engine Schematic.

The Pulse Detonation Engine components were designed using a computer aided design program and were machined from stainless steel. The drawings are included as Appendix A. Additional work was required for the pulse detonation engine experiment to operate (such as injector and vitiator plumbing, test cell electrical development, and transducer calibrations) but was omitted from this paper for brevity. The code developed for engine operation is included as Appendix B.

Vitiated air flows through the inlet nozzle, placed upstream of the engine in order to isolate upstream pressure fluctuations and set inlet conditions prior to the engine, and into a fuel injection manifold (item e in Figure 3-2). The fuel and air mixture created in the manifold continues from the manifold through the fuel/air mixing arms (homogeneity is assumed at the end of the arms) and into the 12.7 cm (5 in.) diameter main combustion tube, where a detonation wave propagating from a 4 cm (1.5625 in.) pre-detonation tube (item c in Figure 3-2) combusts the unburned reactants. [Ref. 7] Four Kistler 603B1 transducers and 5010B dual mode amplifiers with 540 kHz notch filters were used in varying locations along the pre-detonation tube and the main combustion tube to monitor the pressure time traces through the engine. The signals from the amplifiers were sampled by a National Instruments High Speed Data Acquisition board using a sample rate of 500,000 samples per second for 600,000 samples on all four amplifiers simultaneously in order to calculate the detonation wave speed. A 1.4-Joule Unison Industries ignition system was used as the ignition source for the combustor and was

capable of cycle frequencies up to 10 Hz. The ignition system had an estimated delivery efficiency of 35% and was able to deliver the spark in 30-100 microseconds resulting in power levels of approximately 4.90 kW to 16.2 kW. A Visual Basic 5.0 GUI was written to control all facility valves and ignition. Switching of all valving and ignition TTL signals was handled by a Keithley PIO24 board connected to a bank of Crydom 6321 solid-state relays. The actual engine can be seen in Figure 3-6.

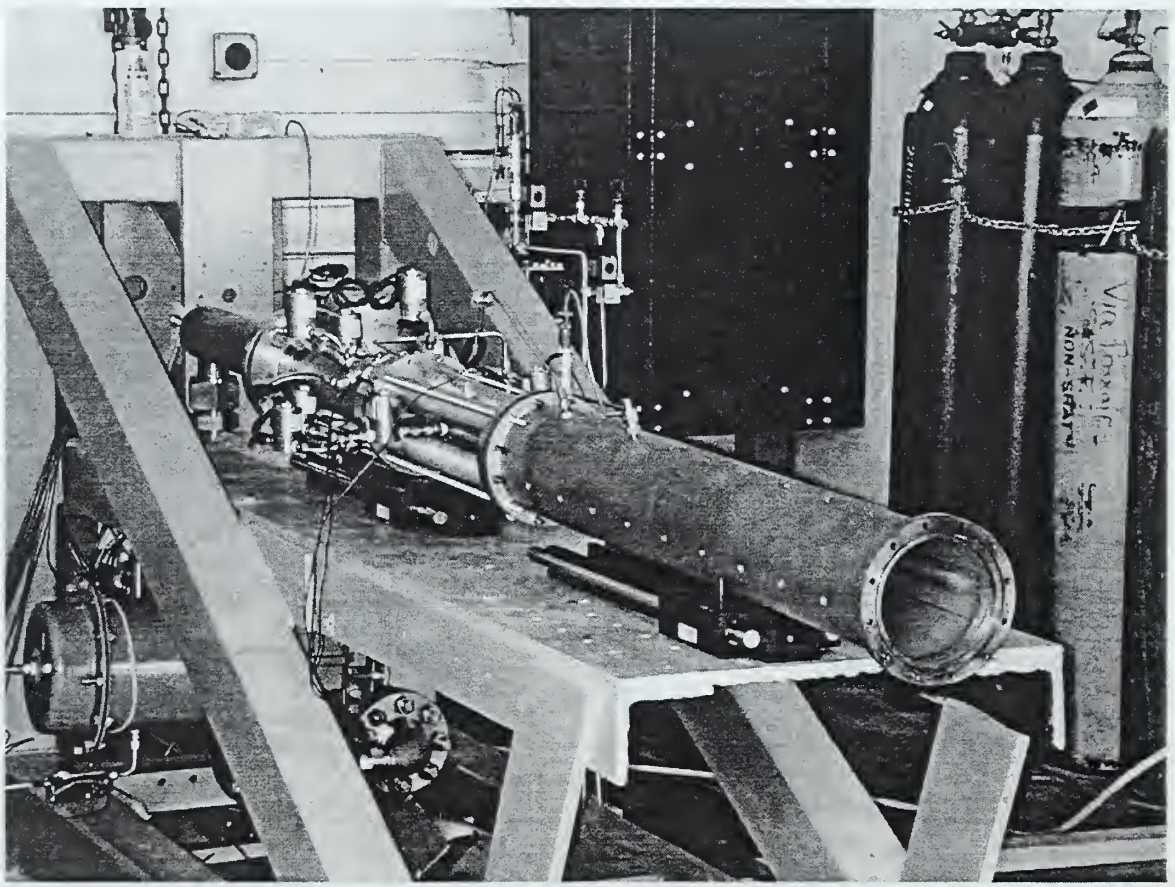

Figure 3-6. Pulse Detonation Engine.

# IV. RESULTS

## A. ATOMIZER CHARACTERIZATION

### 1. Particle Distribution

The BETE XA-F-PR200 system was chosen to be the atomizer for the pulse detonation engine in this thesis due to its clean discrete operation at transients and it's wide range of fuel delivery rates while maintaining low SMD values. The BETE system is advertised to be capable of flowing between 0.7 and 10.7 gallons per hour depending on the pressurization values. This resulted in a possible JP10 ($\rho_{JP10}$=0.940 gm/cc) mass flow rate range of 0.0415 kg/min to 0.6346 kg/min, respectively. The atomizer is an internal air blast design and is depicted in Figure 4-1.

Figure 4-1. Fuel Injection Element. From Ref. [10]

The atomizer mixes and ejects the fuel and oxidizer when a fuel shut off cylinder is pressurized using compressed air. A Peter Paul 9.5 Watt 24 VDC coil solenoid three-way valve provided and vented compressed air to the fuel shut off cylinder. Oxygen and air to the BETE atomizers were each provided by individual Peter Paul 9.5 Watt 24 VDC coil two-way solenoid valves. The solenoids were controlled by Crydom 6321 optically isolated relays with 100 microsecond response times.

The observed droplet distributions from the PR-200 atomizer as a function of fuel and atomization pressure is shown in Figure 4-2. Small droplet diameters are critical for the successful detonation of JP10 in a gaseous oxidizer environment. An approach similar to one by Tulis [Ref. 11] was taken to model droplet heating, evaporation, and

oxidation. It was concluded from that analysis that fuel droplets in a JP-10/O2 aerosol of approximately 10 microns in diameter and smaller, and fuel droplets in a JP-10/Air aerosol of approximately 5 microns in diameter and smaller, could be heated and vaporized in the necessary time scales required for detonation to occur. Figure 4-2 indicates production of Sauter Mean Diameters below 10 microns for fuel pressures less than 0.2965 MPa (43 psi) and air pressures ranging from 0.5516 to 0.6205 MPa (80 to 90 psi) at room conditions ((P = 1 atmosphere, T = 291.5 degrees Kelvin).

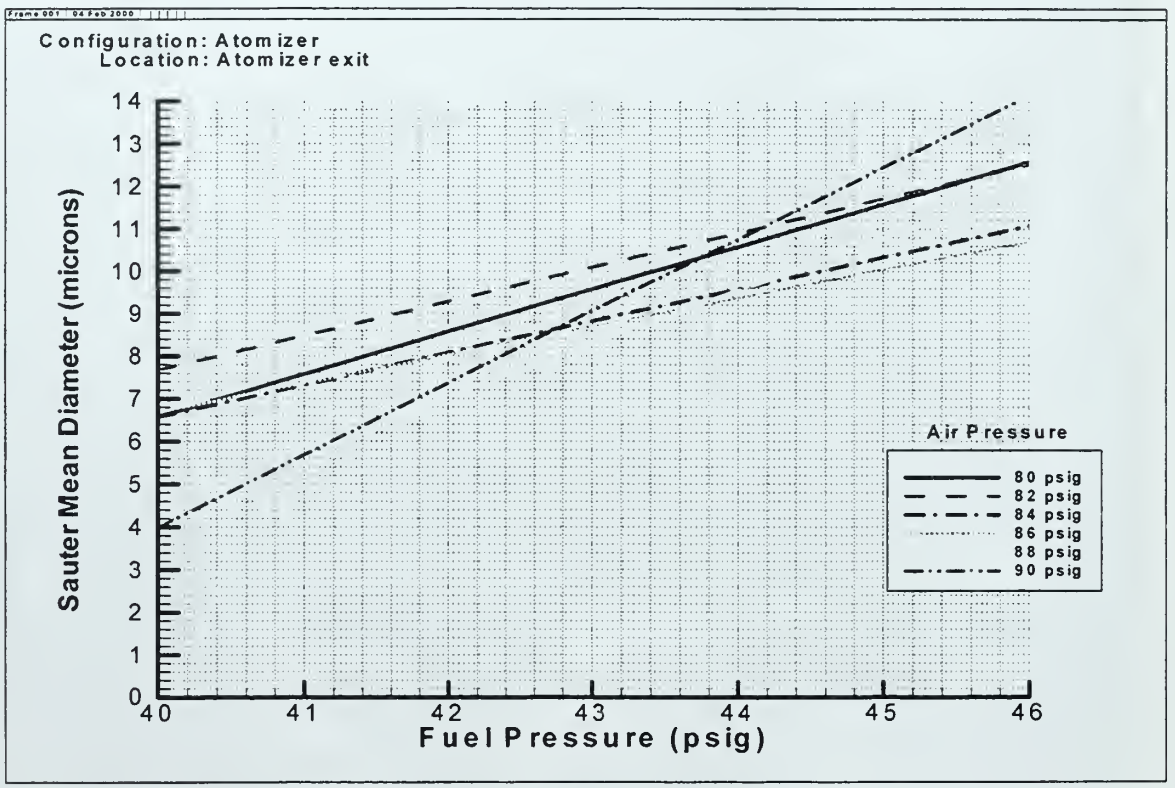


Figure 4-2. Droplet Sauter Mean Diameter as a Function of Pressure.

Since the BETE atomizers were placed at the end of a tube and forced to inject the aerosol through five to ten tube diameters (items b and c in Figure 3-2) into the main combustion tube, further flow characterization was done using 12.7-cm and 25.4-cm acrylic extensions attached to the end of the atomizer, as depicted in Figure 4-3. This simulated the effect of ducting the aerosol to the main combustion tube.

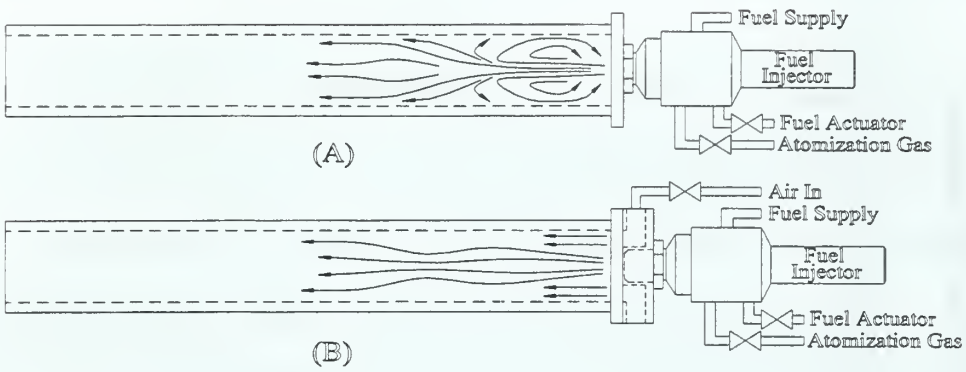


Figure 4-3. Atomizer with Acrylic Extension. From Ref. [4]

Figure 4-3 gives an indication of the flowfield that takes place once the injector is placed inside the pre-detonation tube or fuel/air mixing arms, both with and without bypass air. The simplest condition was the injection of a JP10/air aerosol mixture into a tube from the head end. The recirculation patterns resulted in fuel rich conditions at the head end that promoted rapid fuel agglomeration. The flow field observed for this setup is depicted in Figure 4-3 (A). The flowfield observed for the bypass air configuration, depicted in Figure 4-3 (B), enabled a specified fuel and oxidizer ratio to be loaded and minimized wall agglomeration. The bypass configuration also allowed for a wider range of equivalence ratios to be analyzed. Figures 4-4 and 4-5 depict the SMD's attained using the 12.7 and 25.4-centimeter acrylic extensions, respectively. In both configurations the minimum SMD attained was near 10 microns for a fuel pressure of 0.2758 MPa (40 psi) and an air pressure of 0.6067 MPa (88 psi), and the range of SMD values varied from 10-15 microns for all fuel/air pressure ratios.

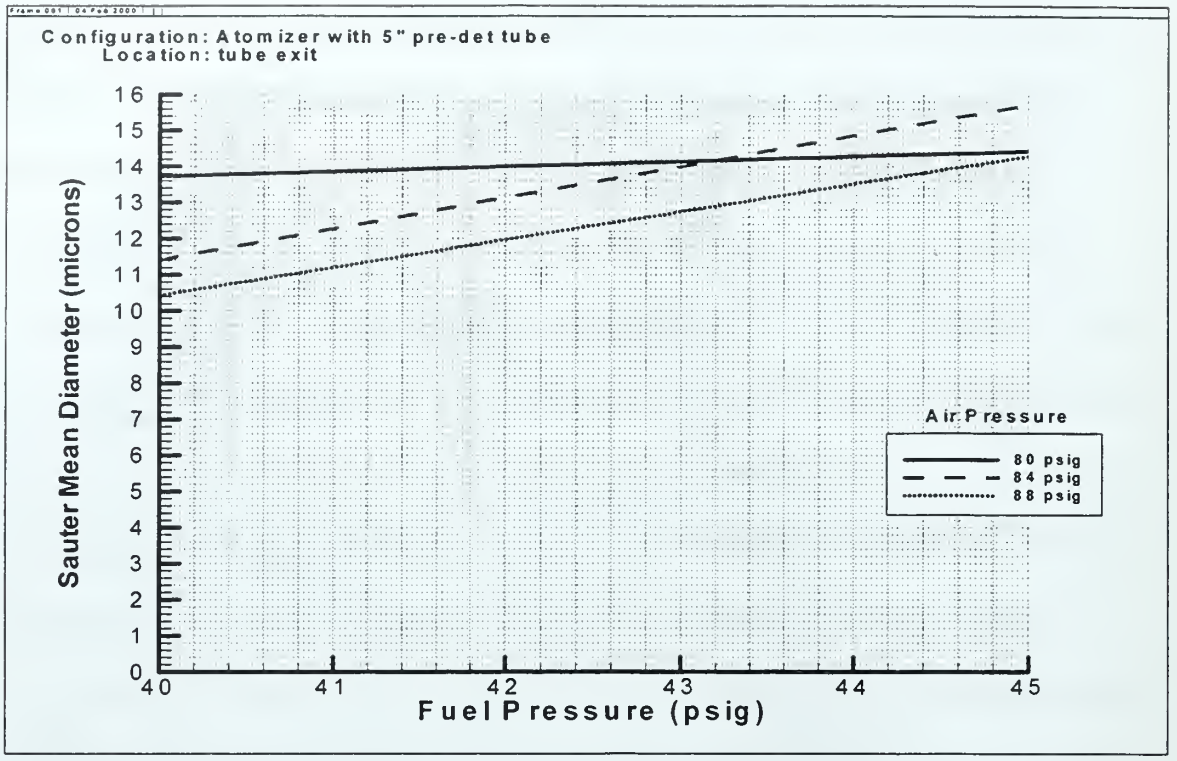


Figure 4-4. Aerosol SMD with 12.7-cm. pre-detonation tube as a function of pressure.

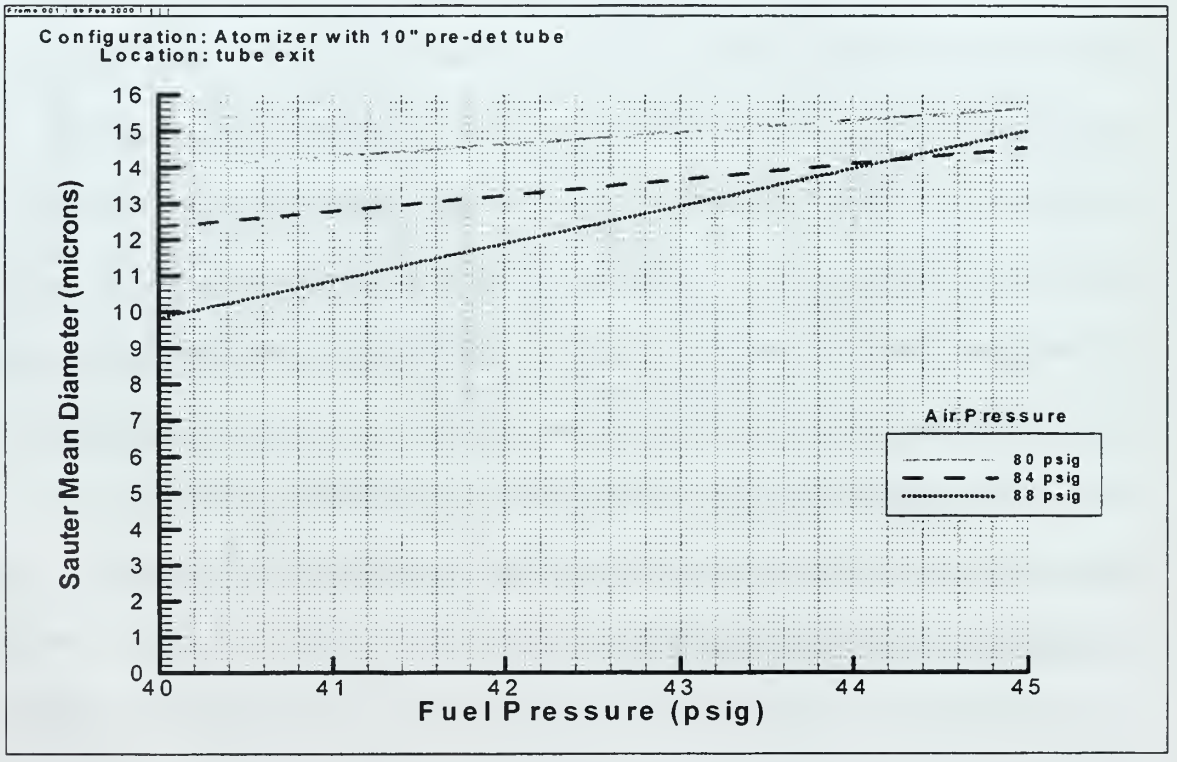


Figure 4-5. Aerosol SMD with 25.4-cm. pre-detonation tube as a function of pressure.

### 2. Flow Rates

#### *a. Fuel Mass Flow Rate*

Mass flow rate of liquid through the atomizer was determined using a nitrogen pressurized column of water. Previous calibrations of the BETE atomizers has shown that overall water flow rates are very close to those found for JP-10 with this system. [Ref. 7] Nitrogen pressure was varied from 39 psig to 45 psig in 2-psi increments. Atomization oxygen pressure was varied from approximately 80 to 90 psig for each nitrogen pressure increment. All hardware was the same as those used on the pre-detonation tube.

For steady-state flow, the atomizer flow was recorded on video, with the spray duration taken from the time annotation at the commencement and cessation of the flow. Spray duration was typically maintained for a duration of 25 seconds. After cessation, the change in water column volume was measured using a graduated cylinder. The change in volume divided by the duration of the spray was the volumetric flow rate of the liquid. Multiplying by the density yielded the mass flow rate. The fuel mass flow rate, for each oxygen pressure at each fuel pressure, was plotted versus oxygen pressure using a linear curve fit, and is included as Figure 4-6.

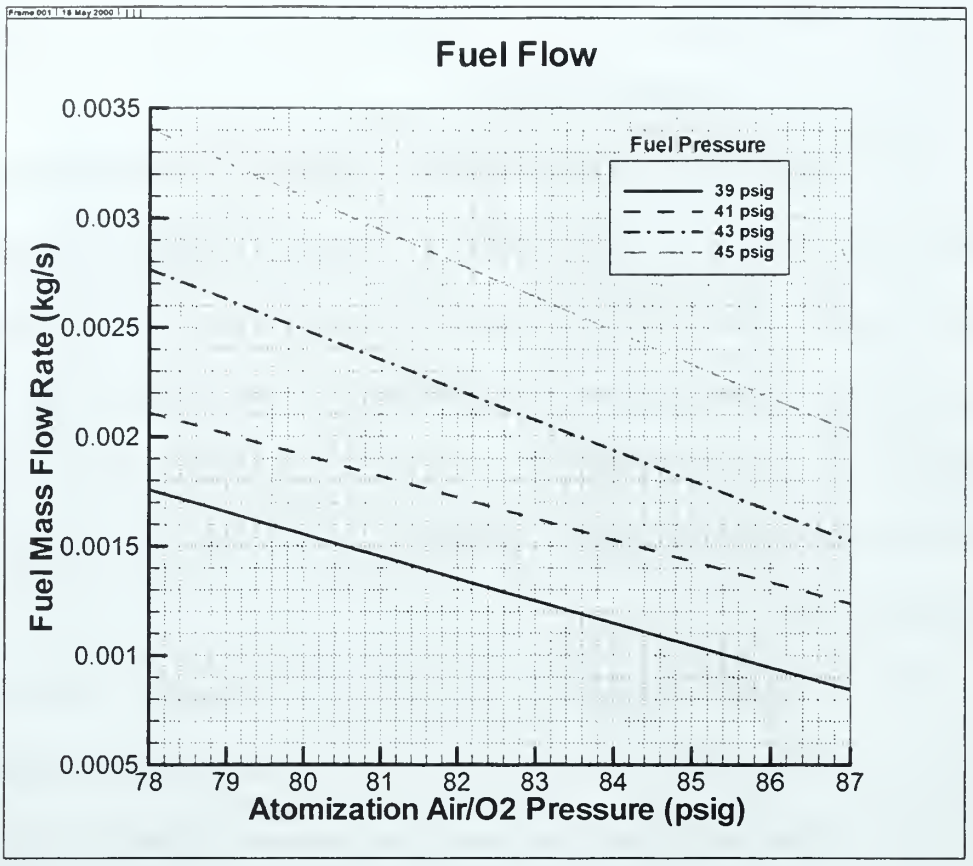


Figure 4-6. Fuel Mass Flow Rate vs. Air/$O_2$ pressure.

A similar method was used to measure the mass flow rate at different duty cycles. Pulses of 500 ms, 250 ms, and 100 ms were examined using the timing in the pre-detonation tube control code. The atomizer was pulsed at the pressure combinations above until several seconds of total on time had been achieved. The change in water level was measured as before and the mass flow rate calculated as above. Instantaneous mass flow rates were calculated every time the atomization oxygen and fuel pressures were updated, using values interpolated from the linear curve fits of the steady-state data.

### *b. Oxygen Mass Flow Rate*

The mass flow rate of oxygen through the atomizer was calculated using an evacuated cylinder and the ideal gas law. One end of the cylinder was fastened to the

nozzle of the atomizer and the other end to a pressure transducer and vacuum pump. The volume of the cylinder and connective tubing (2648 ml) were measured using water. After the cylinder was evacuated, the vacuum pump was isolated and a steady spray was initiated until pressure in the cylinder reached 15 to 17 psia. Cylinder pressure was plotted versus time and two points were selected from the linear range of the plot. The change in volume of the water column was measured using a graduated cylinder, as above, and both the water and the oxygen were at ambient temperature (measured using a thermocouple). Then the ideal gas law was used to calculate oxygen mass flow rate:

$$\frac{p_2 - p_1}{t_2 - t_1}\left(V_{cyl+tube} - V_{water}\right) = \dot{m}_{O_2}\frac{\overline{R}}{M_{O_2}}T$$

where $\overline{R}$ is the universal gas constant (8314.3 J/kgmol-K) and $M_{O_2}$ is the molecular weight of oxygen (31.9988 kg/kgmol).

This was repeated for several oxygen and fuel pressures over the range above. The oxygen mass flow rate, for each oxygen pressure and specified fuel pressure, was plotted versus oxygen pressure and is included as Figure 4-7. Over this range, oxygen mass flow rate was found to be practically independent of fuel pressure, so a linear curve fit was applied to the data.

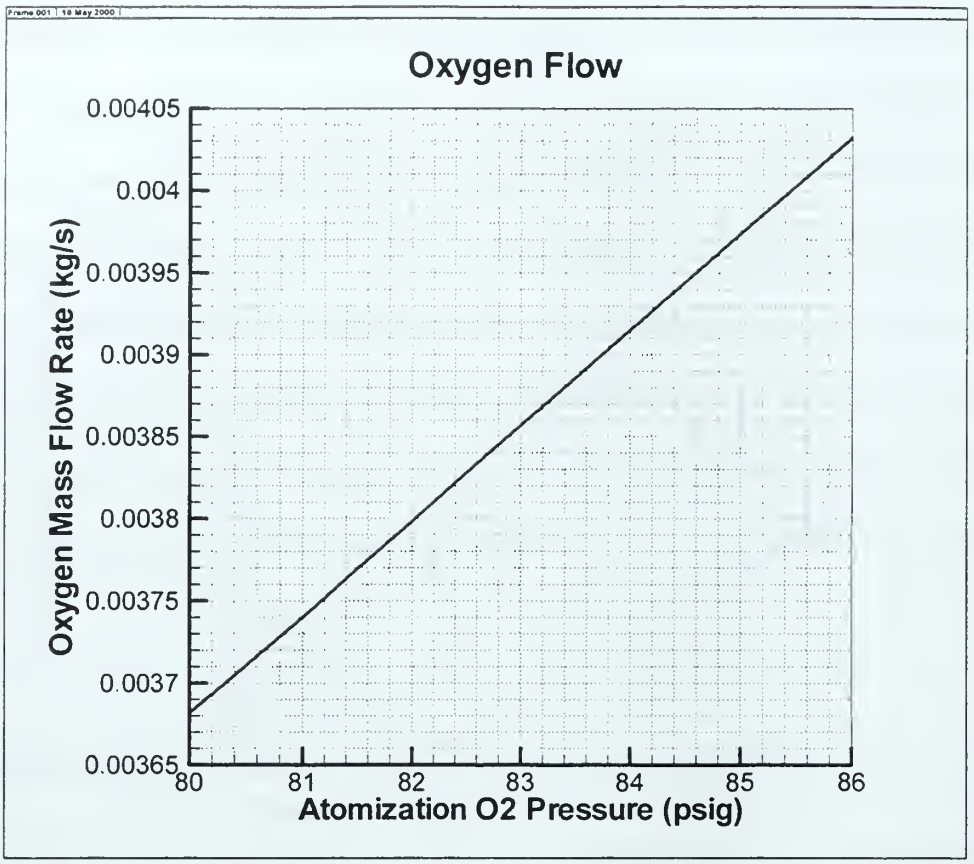


Figure 4-7. Oxygen Mass Flow Rate vs. Atomization $O_2$ pressure.

### 3. Equivalence Ratio

Equivalence ratio is defined as the ratio of the actual fuel-to-oxidizer mass flow rate ratio to the stoichiometric fuel-to-oxidizer mass flow rate ratio. The Thermodynamic Equilibrium Program (TEP) was used to find the stoichiometric fuel-to-oxidizer ratio for the combustion of both JP-10/$O_2$ and JP-10/Air independent of pressure and temperature.

#### *a. Pre-Detonation Tube*

Instantaneous equivalence ratio values of the oxygen-and-atomized-fuel mixture being injected were calculated by entering the oxygen pressure in the linear curve fits of oxygen and fuel mass flow rates, interpolating fuel mass flow for the fuel pressure, and dividing by the stoichiometric fuel-to-oxidizer ratio from TEP. Figure 4-8 depicts the equivalence ratio for varying fuel pressures versus oxygen pressure.

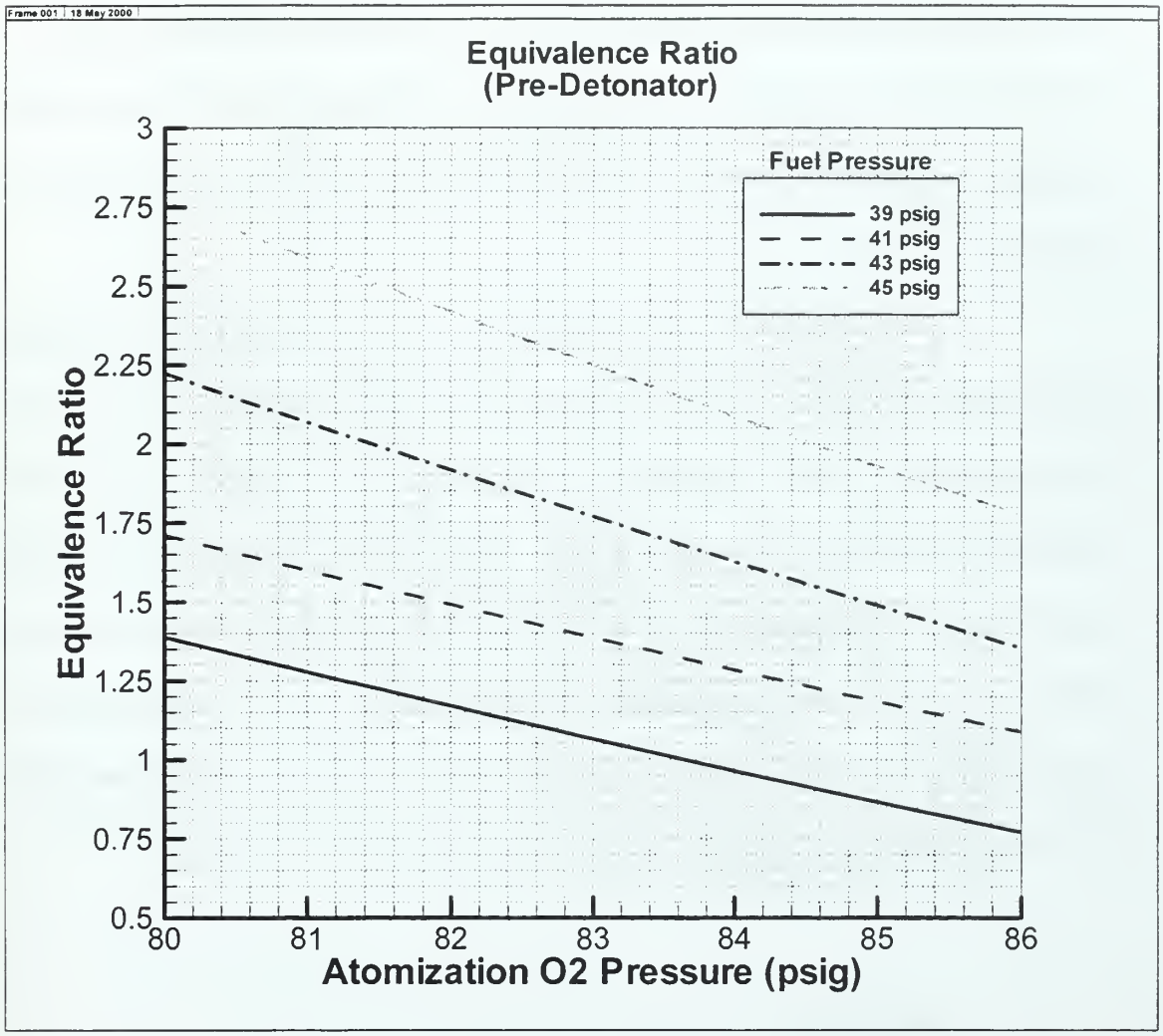


Figure 4-8. Pre-Detonation Tube Equivalence Ratio.

### *b. Main Combustion Tube*

The equivalence ratio in the main combustion tube is essentially the same as that of the air arms. Fuel mass flow rate through each atomizer is determined using the same plot as for the pre-detonation tube, except with atomization air pressure as the independent variable. However, two oxidizer flows must be considered: the air used during the atomization process and the vitiated "inlet" air.

The molar flow rate of air through the atomizer was assumed to be the same as that for oxygen. Therefore, the mass flow rate of air through the atomizer

was calculated using the same data as in section IV-2-b, with only the value of the molecular weight changed ($M_{air}$ = 28.966 kg/kgmol). The vitiated "inlet" air mass flow rate was set in the facility control code and was divided by four to give the mass flow rate in each arm.

Since the main combustion tube uses air as the oxidizer, TEP was used to find the stoichiometric fuel-to-oxidizer ratio for the combustion of JP-10 in air. Instantaneous values of the equivalence ratio of the fuel/air mixture entering the air arms were calculated by entering the atomization air pressure in the linear curve fit of the fuel mass flow rate and interpolating fuel mass flow for the fuel pressure and air mass flow for the given vitiated "inlet" air pressure. This value was divided by the stoichiometric fuel-to-air ratio from TEP. The main combustion tube instantaneous equivalence ratios for two different fuel pressures can be seen in Figures 4-9 and 4-10.

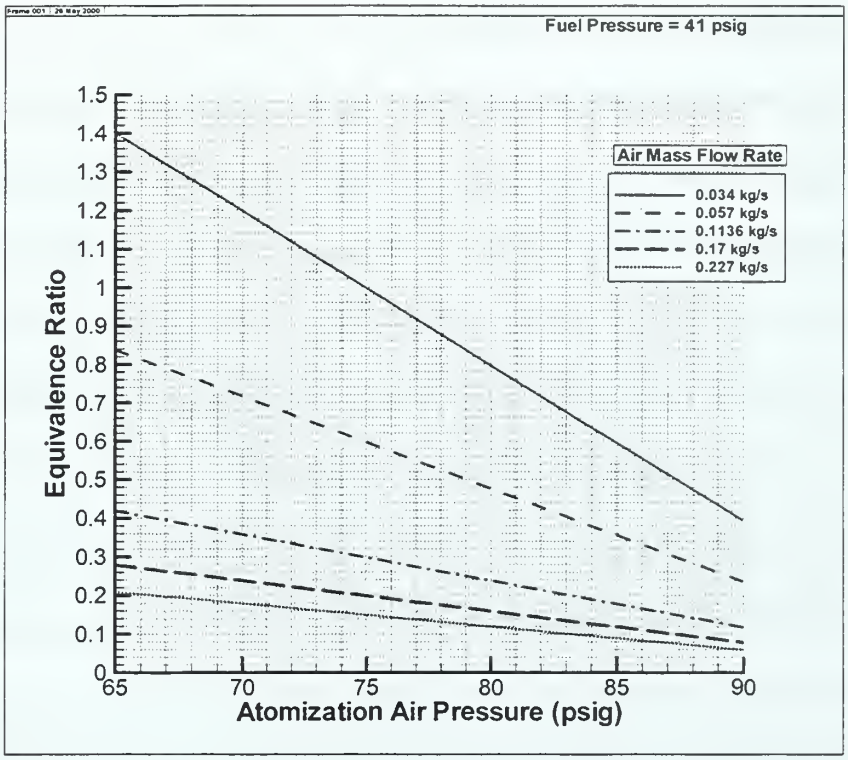


Figure 4-9. Main Combustion Tube Equivalence Ratio for a Fuel Pressure of 41 psig.

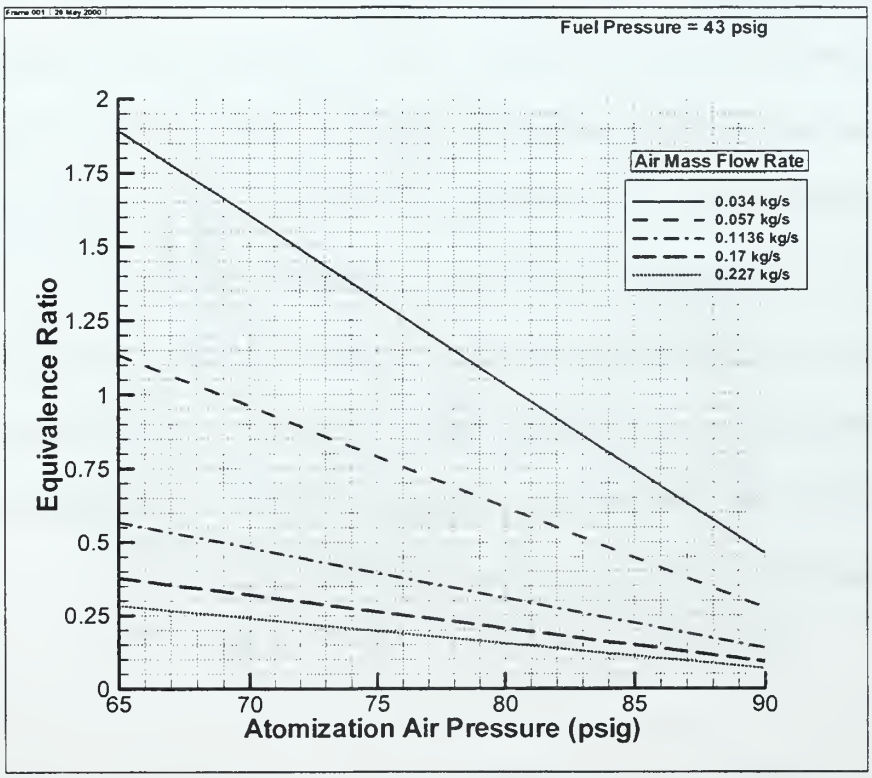


Figure 4-10. Main Combustion Tube Equivalence Ratio for a Fuel Pressure of 43 psig.

## B. VITIATOR CHARACTERISTICS

A test matrix was performed on the vitiator at various set temperatures for each of several "inlet air" mass flow rates. Representative results of the testing (actual vitiator and main combustion tube temperature) can be seen in Table 4-1. Additionally, for a mass flow rate of 0.136 kg/s and 0.226 kg/s (0.3 lbm/s and 0.5 lbm/s), the effect of heat addition on atomizer particle size and percent fuel vaporized was measured using the Malvern Mastersizer measurement system (as discussed in section III-B). The results for 0.136 kg/s are graphically depicted in Figure 4-11. As particle size decreases in Figure 4-11, the percentage of fuel vaporized increases exponentially. The heat loss between the vitiator and the main combustion tube was appreciable, and can be explained by the heating of the engine inlet ducting and lack of insulation around the engine. The highest vitiator temperature reached was approximately 521 Kelvin (478 degrees Fahrenheit), which approaches our maximum testing condition. The results of the vitiator test runs demonstrate that the vitiator can achieve temperatures within the desired range for different mass flow rates. A representative plot of run conditions obtained is included as Figure 4-12. The remainder of the plots are included as Appendix B.

Analysis of the Sauter mean diameters determined by the Malvern Mastersizer measurement system shows, for an air mass flow rate of 0.136 kg/s, the required fuel injected for the main combustion tube becomes vaporized for engine inlet temperatures greater than 339 K (150°F) for most fuel injection conditions.

| Mass Flow Rate | | Vitiator Set Temp. | | Vit. Actual Temp. | | Main Tube Temp. | |
|---|---|---|---|---|---|---|---|
| kg/s | lbm/s | K | F | K | F | K | F |
| 0.907 | 2 | 422 | 300 | 363 | 194 | 329 | 133 |
| 0.816 | 1.8 | 505 | 450 | 414 | 285 | 343 | 158 |
| 0.68 | 1.5 | 533 | 500 | 436 | 325 | 350 | 170 |
| 0.453 | 1.0 | 644 | 700 | 489 | 420 | 372 | 210 |
| 0.453 | 1.0 | 589 | 600 | 475 | 395 | 354 | 178 |
| 0.226 | 0.5 | 644 | 700 | 521 | 478 | | |
| 0.226 | 0.5 | 589 | 600 | 496 | 433 | 326 | 127 |
| 0.226 | 0.5 | 533 | 500 | 450 | 350 | 328 | 130 |

Table 4-1. Vitiator Temperature vs. Mass Flow Rate and Set Temperature.

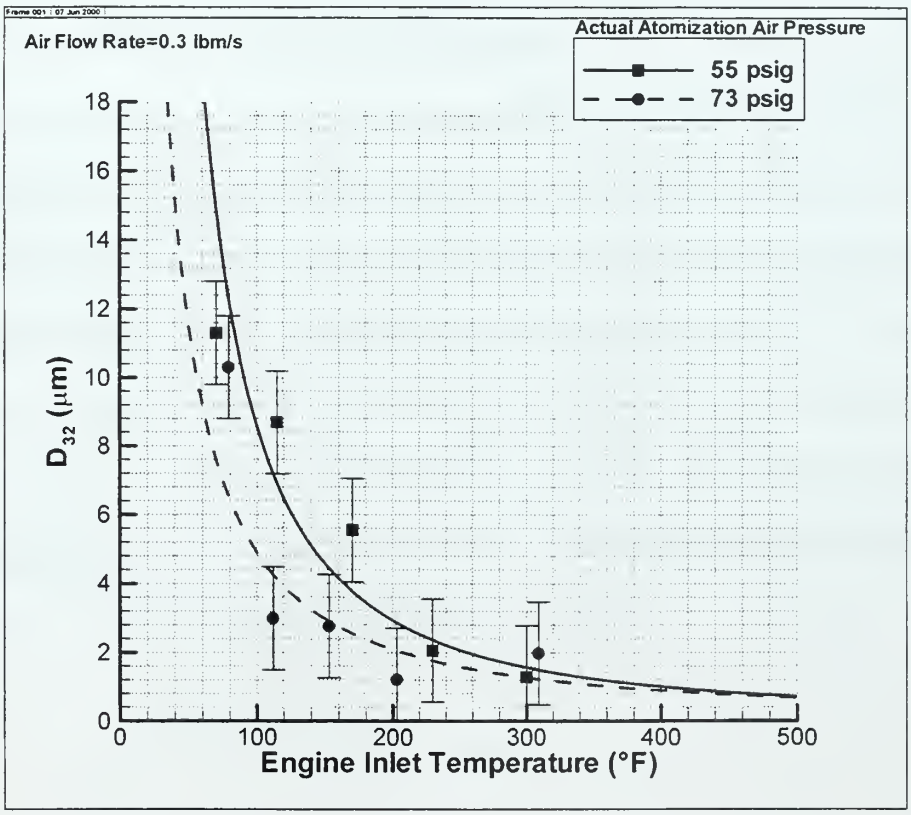


Figure 4-11. Droplet SMD as a function of Mass flow rate and Temperature.

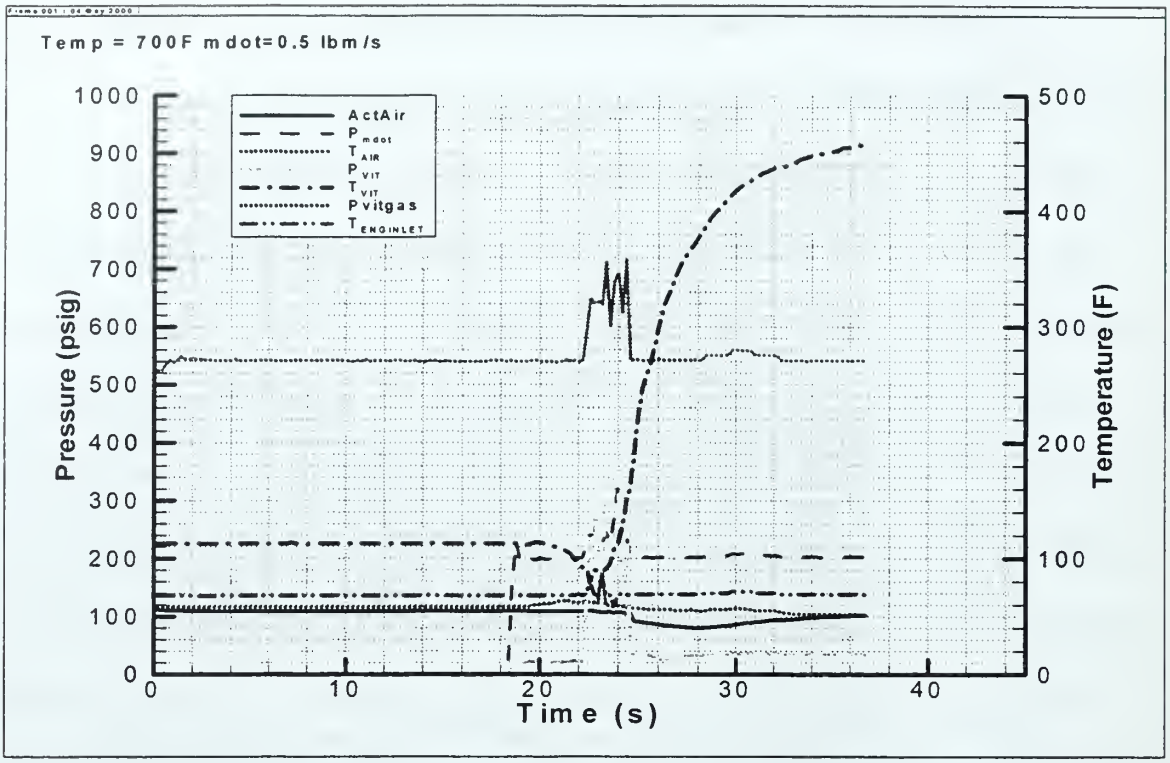


Figure 4-12. Representative Vitiator Test Run Results.

## C. BOUNDARY CONDITIONS

The pressure disturbances at the head end of the main combustion tube were able to propagate both towards the exit of the main combustion tube and up into the choked inlet section. The choked inlet was inserted upstream of the fuel injection manifold in order to isolate downstream pressure disturbances for flow rates greater than 0.454 kg/s, due to a 39.1 percent open area in the manifold flange that interfaces the four main air arms with the main combustion tube. The manifold flange can be seen in Figure 4-13.

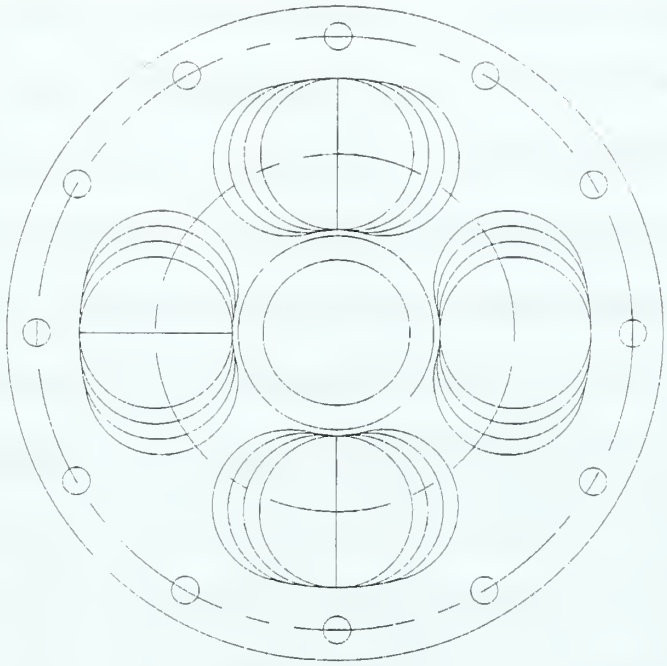

Figure 4-13. Valveless Pulse Detonation Engine Manifold Flange.

The ability of the pressure waves to propagate upstream, creating a transient increase in back pressure, could unstart the engine inlet by disgorging the normal shock through the throat of the choked inlet section. In addition, the reduction in the percent of "hard wall" reflection from the head wall could reduce the detonation strength propagating downstream. The actual nozzle can be seen in Figure 4-14.

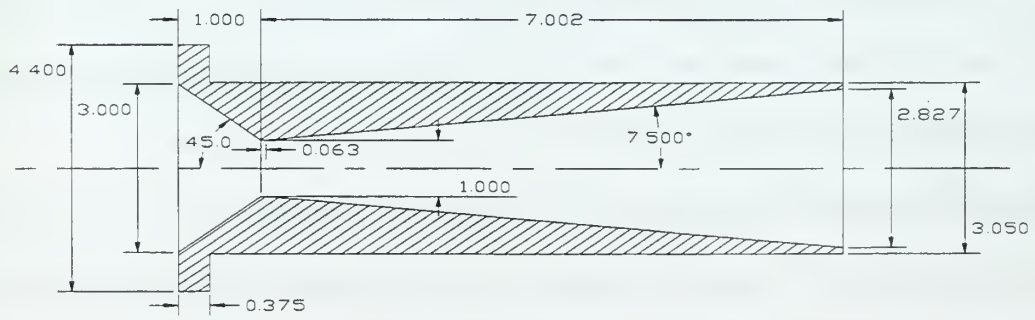


Figure 4-14. Choked Inlet.

To determine whether the inlet unchoked, the location of the normal shock within the diverging section of the choked inlet was calculated using theoretical no friction, isentropic one-dimensional thermodynamic equations for given upstream stagnation pressures. The upstream Mach number is less than or equal to 0.3, and a sudden onset sustained back pressure rise was assumed. It was found that the unstart condition would theoretically not occur for conditions expected to be seen in the engine: static back pressures of 3.40 to 5.44 atmospheres (50-80 psig) imposed on each of three stagnation pressures of 6.81, 10.21, and 13.61 atmospheres (100, 150, and 200 psig).

Next, a computational fluid dynamics analysis of the nozzle was performed to show agreement with the inviscid calculations and to determine the normal shock location with viscous effects added. A two-dimensional quarter-section of the nozzle was drawn and a grid was applied using GRIDGEN. The grid was modified to place emphasis near the entrance to the nozzle and throughout the throat area. The nozzle was then modified using GRIDED in order to provide y-axis symmetry prior to running the grid in both an inviscid and viscous OVERFLOW algorithm. The same conditions as before were imposed on the code.

In order to determine the adequacy of the initial grid, OVERFLOW was run in an inviscid condition and the Mach number prior to the shock ($M_3$), shock location relative to the throat, and Mach number at the exit plane ($M_5$) were compared with theoretical no friction, isentropic calculations. The results can be seen in Table 4-2, and the OVERFLOW product for runs two and five are included as Figures 4-15 and 4-16 in the order listed in Table 4-2. Due to an inability to precisely determine shock location and $M_5$ in the CFD plots and the failure of theoretical calculations to take into account nozzle

geometry, an "X" in Table 4-2 denotes close agreement with theory. The general trend showed that the CFD analysis closely resembled the theoretical no friction, isentropic calculations, and that the shock propagates towards, but never reaches, the throat as backpressure increases (see Table 4-2 and Figures 4-15 through 4-18). Shocks located outside of the throat (at the design condition) were not determined for either the theoretical calculations or the CFD analysis.

| RUN | $Pt_{VIT}$ | $P_3$ | $M_3$ | | Shock Location | | $M_5$ | |
|---|---|---|---|---|---|---|---|---|
| | | | Theory | CFD | Theory | CFD | Theory | CFD |
| 1 | 100 | 1 | N/A | N/A | N/A | N/A | 3.68 | 3.57 |
| 2 | | 50 | 2.48 | 2.28 | 2.31 | X | 0.15 | X |
| 3 | | 60 | 2.25 | 2.15 | 1.70 | X | 0.12 | X |
| 4 | | 70 | 2.03 | 1.98 | 1.20 | X | 0.11 | X |
| 5 | | 80 | 1.82 | 1.87 | 0.79 | X | 0.09 | X |
| 6 | 150 | 1 | N/A | N/A | N/A | N/A | 3.68 | 3.57 |
| 7 | | 50 | 2.945 | 2.58 | 3.81 | X | 0.22 | X |
| 8 | | 60 | 2.74 | 2.46 | 3.11 | X | 0.18 | X |
| 9 | | 70 | 2.56 | 2.34 | 2.55 | X | 0.16 | X |
| 10 | | 80 | 2.40 | 2.23 | 2.09 | X | 0.14 | X |
| 11 | 200 | 1 | N/A | N/A | N/A | N/A | 3.68 | 3.57 |
| 12 | | 50 | 3.25 | 3.21 | 5.01 | X | 0.29 | X |
| 13 | | 60 | 3.06 | 2.70 | 4.25 | X | 0.24 | X |
| 14 | | 70 | 2.89 | 2.57 | 3.62 | X | 0.21 | X |
| 15 | | 80 | 2.74 | 2.46 | 3.11 | X | 0.18 | X |

Table 4-2. Theoretical calculations vs. CFD analysis.

Figures 4-15 through 4-18 are plots of Mach number within the nozzle, with the shock occurring just downstream of the maximum Mach number (white area in each plot) seen in the legend included with each Figure.

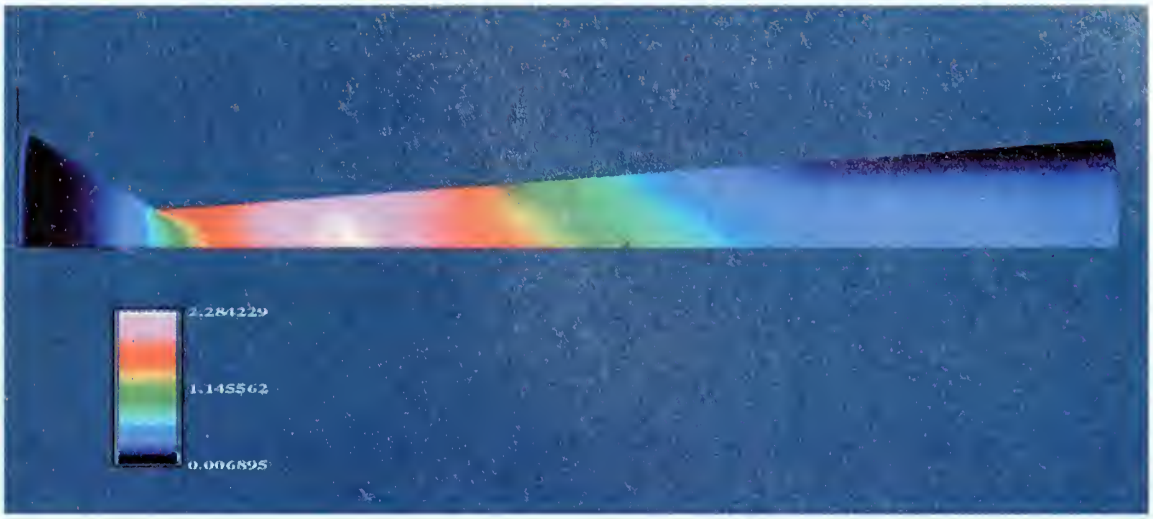


Figure 4-15. CFD Nozzle Analysis. $Pt_{VIT}$ = 100 psia. $P_3$ = 50 psia.


Figure 4-16. CFD Nozzle Analysis. $Pt_{VIT}$ = 100 psia. $P_3$ = 80 psia.

Further computational fluid dynamics analysis involved using a 2-D viscous OVERFLOW code to better simulate the actual conditions in the nozzle. This analysis produced only one run in which the normal shock just barely reached the nozzle throat, which can be seen in Figure 4-18. For this reason, emphasis was placed on obtaining solutions for runs 1 through 5 in Table 4-2 in order to image the normal shock propagating up into the throat. Runs 12 and 15 can be seen in Figures 4-17 and 4-18.

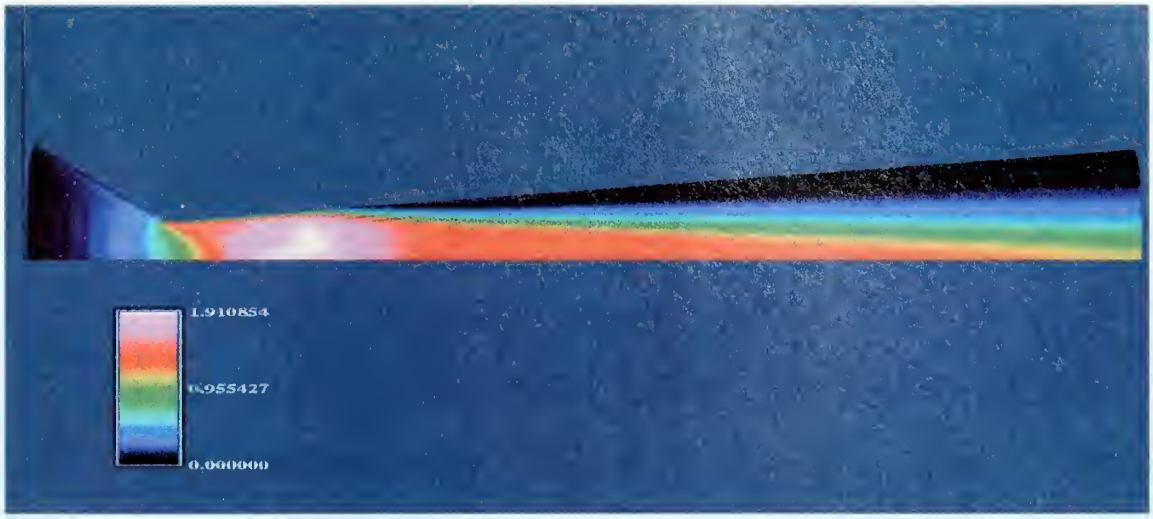


Figure 4-17. CFD Nozzle Analysis. $Pt_{VIT}$ = 100 psia. $P_3$ = 50 psia.


Figure 4-18. CFD Nozzle Analysis. $Pt_{VIT}$ = 100 psia. $P_3$ = 80 psia.

For the conditions expected to be seen in the actual nozzle, it appears computationally that the normal shock never completely reaches or disgorges from the nozzle throat, and therefore will not be able to un-start the engine inlet.

## D. PULSE DETONATION ENGINE

### 1. Pre-detonation Tube

This experiment used a pre-detonation tube sufficiently longer than the minimum required deflagration-to-detonation transition distance for a JP-10/O2 mixture as a direct ignition source to detonate a JP-10/air mixture in the main combustion tube (see section

II-C-2). The pre-detonation tube can be seen in Figure 4-19.

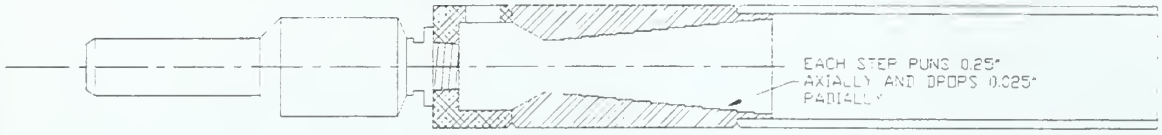


Figure 4-19. Pre-detonation Tube.

The fuel injector bolted to the head end of the pre-detonation tube provided the JP-10 and oxygen mixture, and the ignition was introduced through a hole near the head end at a location previously determined to promote good ignition of the mixture. [Ref. 7] The divergent stepped geometry immediately after the throat was designed to promote excellent mixing of the reactants prior to the introduction of the ignition and aid in shortening the deflagration-to-detonation transition process.

The initial experimentation with the pre-detonation tube was done to verify successful operation and involved setting an air mass flow rate of 0.226 kilograms per second (0.5 lbm/s) through the engine, vitiator set temperatures from 293 to 477.5 Kelvin (70-400°F), and running the pre-detonation tube at varying fuel and oxygen fill times and pressures. Table 4-3 delineates some of the conditions run in this configuration. The time of the ignition in the pre-detonation tube was set to occur 20 milliseconds after the reactant fill time was complete in order to allow the valves to close and for any transient behavior to be removed. Detonations in the pre-detonation tube were rapidly achieved because the approximate ideal conditions to achieve a detonation had been experimentally determined during previous work completed in the laboratory.

| Set Temp. (°F) | Fuel (ms) | | $O_2$ (ms) | | Ignition Time (ms) | Pressure (psig) | |
|---|---|---|---|---|---|---|---|
| | ON | OFF | ON | OFF | | Fuel | $O_2$ |
| 68 | 5 | 73 | 0 | 75 | 95 | 43 | 71 |
| 135 | 60 | 128 | 55 | 130 | 150 | 43 | 74 |
| 135 | 120 | 168 | 115 | 170 | 190 | 43 | 75 |

Table 4-3. Representative Pre-detonation Tube Run Conditions.

### 2. Initial Experimentation

Early experimentation with the main combustion tube involved running the engine at a maintained air mass flow rate of 0.226 kg/s and varying vitiator temperature, injector fuel and oxidizer fill times, equivalence ratios, and pre-detonation tube ignition times in order to achieve a successful detonation transition from the pre-detonation tube into the main combustion tube. In addition, the goal of the testing was to determine the detonable limits of the engine by controlling each of the variables discussed in the next section.

Initial testing of the entire engine produced a detonation wave in the pre-detonation tube that never successfully transitioned into the main combustion tube. The initial test conditions were all fixed except the atomization air pressure in order to vary the equivalence ratio for the main combustion tube, and can be seen in Table 4-4. Figure 4-20 is a typical plot of pressure data collected during one of these runs. The large pressure spikes seen early in each combustion process are the detonation wave exiting the pre-detonation tube, but the lack of large pressure spikes and significant wave speeds measured in the main combustion tube show that the detonation wave failed to

successfully transition into the main combustion tube. Within the pre-detonation tube, the average detonation wave speed was 1954 meters per second.

| Variable | Set Value |
|---|---|
| Inlet Air Mass Flow Rate | 0.5 lbm/s |
| Frequency | 3 Hz |
| Vitiator Set Temperature | Varied between 400 and 700 °F |
| Pre-det fuel on duration | 48 ms |
| Pre-det $O_2$ on duration | 55 ms |
| Ignition Delay | 20 ms |
| Pre-det fuel pressure | 43 psig |
| Pre-det $O_2$ pressure | Varied between 70 and 88 psig |
| Main tube fuel on duration | 175 ms |
| Main tube atomization air on duration | 200 ms |
| Main tube fuel pressure | 43 psig |
| Main tube atomization air pressure | Varied between 55 and 88 psig |

Table 4-4. Pulse Detonation Engine Variable Set Conditions.

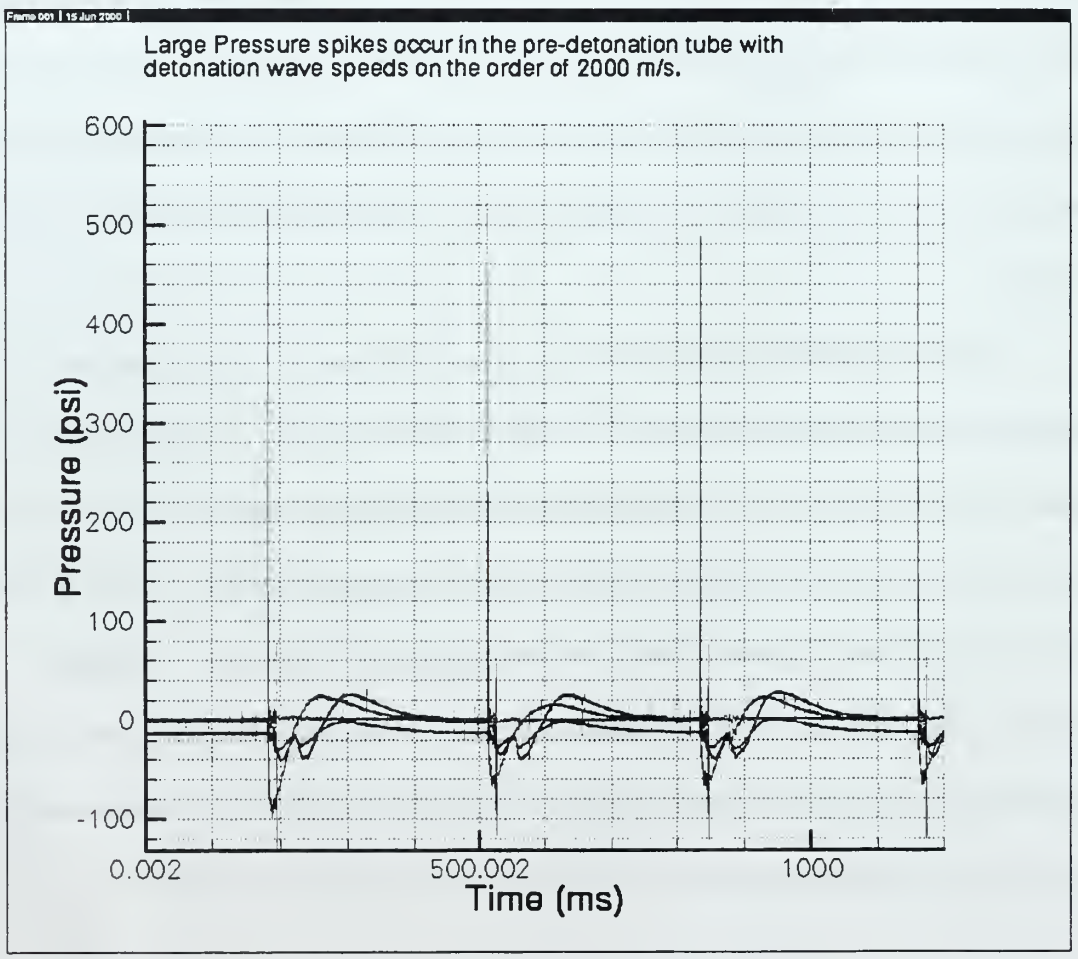


Figure 4-20. Typical Pressure Traces from Initial Engine Testing.

### 3. Troubleshooting

Modifications to the initial testing setup made to improve the diffraction condition and achieve detonation conditions in the main combustion tube also failed to produce the desired result, save for one condition.

The first set of modifications involved changing the variable set conditions seen in Table 4-4. Discussion on the set conditions led to a theory that long pre-detonation tube fill times might have caused reactant spray into the main tube, affecting the equivalence ratio and mixture of reactants that were to be detonated. Because of this, a further test matrix similar to the previous one was done with an average engine inlet temperature of 130 K (327 °F) and all fill times and ignition delays incrementally reduced by 5 milliseconds each run until a detonation was no longer achieved in the pre-detonation tube. None of these pre-detonation tube "underfills" were successful in achieving a detonation in the main combustion tube.

In order to show that a detonation could be attained in the main combustion tube, the fuel for the experiment was temporarily changed from JP-10 ($C_{10}H_{16}$) to 87-octane automotive gasoline to take advantage of gasoline's higher vapor pressure and lower combustion temperature. Further experimentation at similar conditions again failed to produce a detonation in the main combustion tube. This result indicated that the problem was most likely a mixing or diffraction issue.

One of the primary concerns generated during the experiment was whether or not the detonation wave departing the 3.81 cm (1.5 inch) diameter pre-detonation tube could successfully navigate the rapid step to a 12.7 cm (5 inch) main combustion tube. A shock focusing device, included as Figure 4-21, was inserted into the engine flush with the head

end of the main combustion tube to reflect the shock exiting the pre-detonation tube and force the fuel/air mixture emanating from the four arms into the exit plane of the pre-detonation tube in order to improve the fuel distribution on the centerline of the engine.

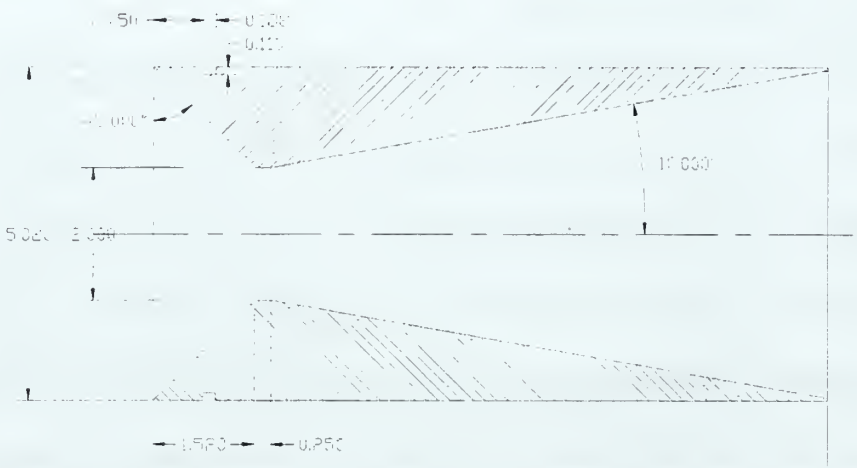

Figure 4-21. Shock Focusing Device at Head End of Main Combustion Tube.

Testing with 87-octane gasoline with the shock focusing device inserted was done using a vitiator set temperature of 300 °F and the same variable conditions as the previous test matrix. This did not produce a detonation in the main combustion tube.

Further testing entailed the addition of a short 5.08 cm (2 inch) tube to the end of the pre-detonation tube to delay the detonation wave's arrival in the main combustion tube until just prior to the throat of the shock focusing device (see Figure 4-21). It was believed that this would give the detonation wave a more gradual step into the main combustion tube as it traversed down the expanding length of the shock focusing device. Although this would improve the exiting detonation wave strength, mixing could be compromised. The pre-detonation tube fill and ignition delay times were extended by 5 milliseconds and the fuel pressure varied between 42 and 44 psig with all other variables the same as the previous test matrix. This test matrix was performed with no ignition of the vitiator, which provided oxygen enriched air to the main burner. The amount of

oxygen added was the same as required for makeup oxygen for vitiator set temperatures of 500 and 900 °F. Again, no detonation was recorded in the main combustion tube.

The final set of tests were run using JP-10 as the fuel, a vitiator set temperature of 500 °F, and the variable set conditions seen in Table 4-5. Both the shock focusing device and the pre-detonation tube extender remained in the engine.

| Variable | Set Value |
|---|---|
| Inlet Air Mass Flow Rate | 0.3 lbm/s |
| Frequency | 3 Hz |
| Vitiator Set Temperature | 500 °F |
| Pre-det fuel fill times | 200-253 ms |
| Pre-det $O_2$ fill times | 190-258 ms |
| Ignition time | 155 ms |
| Pre-det fuel pressure | 45 psig |
| Pre-det $O_2$ pressure | Varied between 85 and 95 psig |
| Main tube fuel fill times | 128-275 ms |
| Main tube atomization air fill times | 0-498 ms |
| Main tube fuel pressure | 45 psig |
| Main tube atomization air pressure | Varied between 55 and 70 psig |

Table 4-5. Pulse Detonation Engine Variable Set Conditions.

The engine was tested in this condition with only the $O_2$ and atomization air set pressures varied to test throughout the range of equivalence ratios believed to be detonable (see section IV-A-3). With no detonations forthcoming in the main combustion tube, the fill times, with the exception of the main combustion tube atomization air, were all reduced by 10 milliseconds with all other variables held constant. Extensive testing in this configuration was conducted without successful results, with the exception of one run that will be discussed in section V-B.

THIS PAGE INTENTIONALLY LEFT BLANK

# V. DISCUSSION

## A. WAVE PROPAGATION

Although the engine inlet could not be un-started for the conditions expected to be seen in the engine (see section IV-C), the pressure wave propagating upstream towards the choked inlet could have a transient effect on the performance of the engine if its effect is felt in the choked inlet prior to the completion of the pulse detonation engine cycle (see section II-C-1). In order to determine whether or not this occurred a simplified analysis was performed, using the propagation distances and speeds of propagation to solve for time.

After exiting the pre-detonation tube, the created pressure disturbance propagates both down the main combustion tube and up into the choked inlet (see Figure A-1 in Appendix A). In the latter case, the pressure disturbance propagates at 375 meters per second, the local speed of sound in the vitiated "inlet" air at 338 Kelvin (150°F), for a distance of 0.7058 meters (27.788 inches) to the exit plane of the choked inlet. However, the mass flow rate of "inlet" air offsets some of this velocity, flowing at approximately 25 meters per second for a mass flow rate of 0.136 kg/s (0.3 lbm/s). This analysis yields a total time for the pressure disturbance to reach the exit plane of the choked inlet of 2.02 milliseconds.

The pressure disturbance propagating down the main combustion tube, however, is traveling at approximately 1800 meters per second (assuming a successful detonation throughout the length of the tube) down a tube 1.018 meters (40.085 inches) in length, which takes 0.566 milliseconds to complete. However, the cycle is not complete until the rarefaction waves propagate up to, and in the case of this design, through the head wall of

the engine. The rarefaction wave will propagate at a speed approximately half of the detonation wave speed up to the head wall 1.018 meters away, which takes 1.131 milliseconds. The total time for this event up to the rarefaction wave reaching the head wall is 1.697 milliseconds, 0.32 milliseconds less than the time it takes the pressure disturbance to reach the exit plane of the choked inlet.

Beyond the head wall, the rarefaction wave will propagate at a rough speed of 450 meters per second towards the choked inlet, but will only reach a point 0.144 meters (5.67 inches) beyond the head wall at the time that the choked inlet is feeling the effect of the original pressure disturbance.

## B. EXPERIMENTAL RESULTS

As discussed in section IV-D-2, one run during the engine testing achieved a detonation wave exiting the main combustion tube, although not under ideal conditions. The variables were set in accordance with Table 5-1.

| Variable | Set Value |
|---|---|
| Inlet Air Mass Flow Rate | 0.3 lbm/s |
| Frequency | 3 Hz |
| Vitiator Set Temperature | 500 °F |
| Pre-det fuel fill times | 200-243 ms |
| Pre-det $O_2$ fill times | 190-248 ms |
| Ignition time | 145 ms |
| Pre-det fuel pressure | 45 psig |
| Pre-det $O_2$ pressure | 90 psig |
| Main tube fuel fill times | 125-265 ms |
| Main tube atomization air fill times | 0-498 ms |
| Main tube fuel pressure | 45 psig |
| Main tube atomization air pressure | 55 psig |

Table 5-1. Pulse Detonation Engine Variable Set Conditions.

Ideal conditions implies that the direct initiation of a detonation (see section II-C-2) in the JP-10/air mixture in the main combustion tube was expected through the propagation of a strong shock wave or detonation wave from the pre-detonation tube. As

can be seen in Figure 5-1, the pressure rise at the exit of the pre-detonation tube (blue and green traces) did not exhibit signs of being a strong shock wave or detonation wave, but the measured pressure wave at the exit of the main combustion tube (black and red traces) had a peak pressure exceeding 600 psig and a velocity of approximately 2000 meters per second.

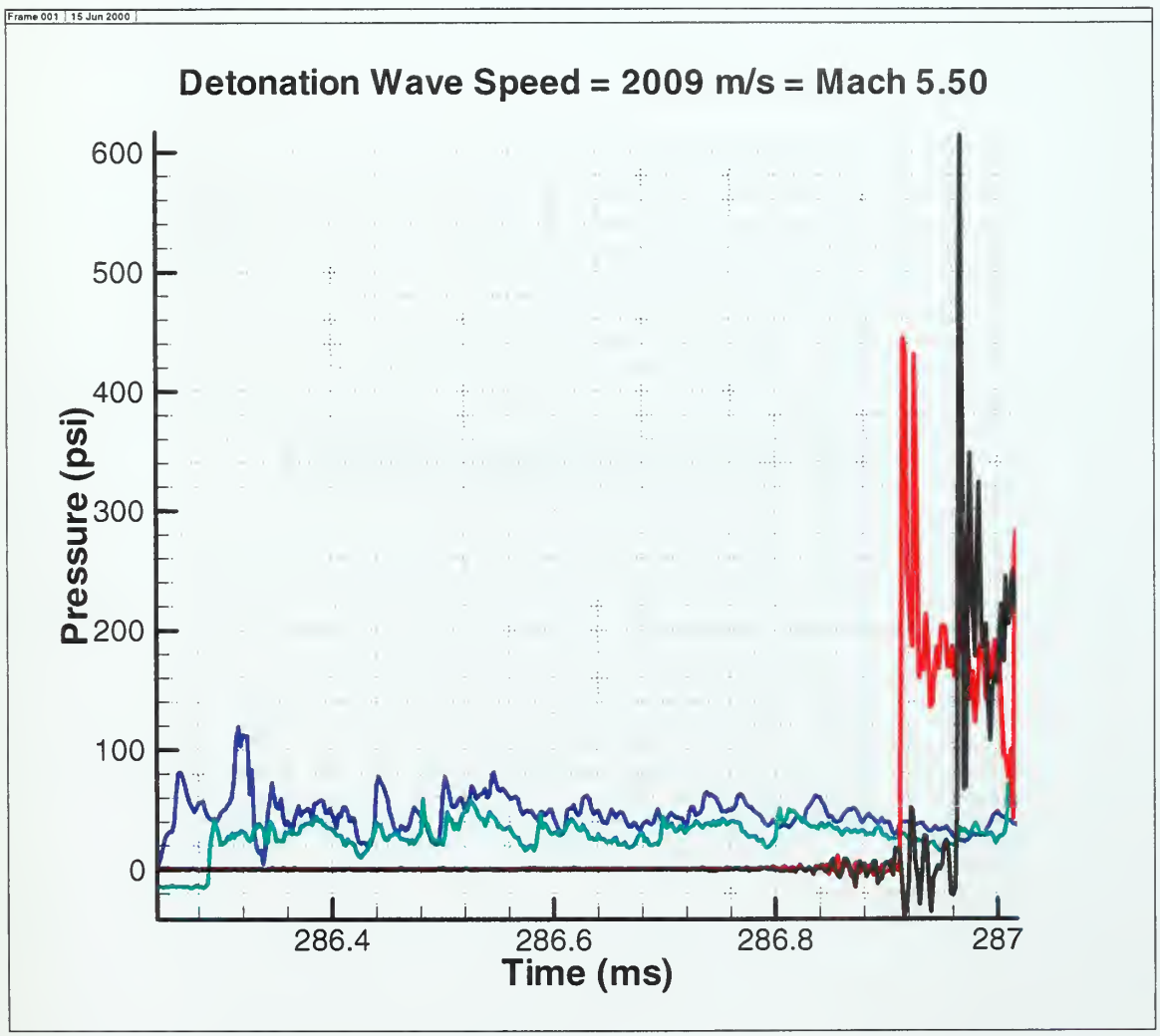


Figure 5-1. Successful Detonation in the Main Combustion Tube.

The detonable mixture in the main combustion tube was at a fuel-rich equivalence ratio of approximately 1.4. Further work will be needed to determine the detonable limits of the engine under ideal, as well as non-ideal, conditions.

THIS PAGE INTENTIONALLY LEFT BLANK

# VI. CONCLUSIONS

Work completed for this thesis showed that liquid fuel particle size, fuel and oxidizer fill times, and ignition delay time are critical parameters for the rapid development of a C-J detonation. In addition, detonation of a fuel/oxidizer aerosol becomes less difficult as the temperature of the surrounding environment and the fuel vapor content increases. Although detonations were quite easily achieved and repeatable in the JP-10/O2 mixture in the pre-detonation tube over a wide range of equivalence ratios, only one detonation was achieved in the JP-10/Air mixture in the main combustion tube. The inability to successfully propagate the detonation wave into the JP-10/Air mixture appears to be a result of the dissimilar mixtures that the detonation wave has to propagate through and the large diffraction that the wave encounters upon exiting the pre-detonation tube.

The addition of the short 5.08 cm (2 inch) tube to the end of the pre-detonation tube to delay the detonation wave's arrival in the main combustion tube until just prior to the throat of the shock focusing device (see Figure 4-21) was designed to give the detonation wave a more gradual step into the main combustion tube as it traversed down the expanding length of the shock focusing device. Although this would improve the exiting detonation wave strength, mixing could be compromised. Further work will be needed to isolate the diffraction issue, and several schemes are already being attempted. Follow on work for this engine entails achieving repeatable detonations and consistent performance in the main combustion tube and completing a test matrix to determine the range of equivalence ratios for successful detonation in the JP-10/Air mixture in the main combustion tube under ideal, as well as non-ideal, conditions.

For the conditions expected to be seen in the actual choked air inlet section, it appears computationally that the normal shock never completely reaches or disgorges from the nozzle throat, and therefore will not be able to un-start the engine inlet. Future CFD work on the choked air inlet could include the development of a three dimensional quarter section of the nozzle and the re-running of the conditions listed in Table 4-2 in both an inviscid and viscous OVERFLOW code to better simulate the actual nozzle. The transient effect that the pressure disturbance actually has on the performance of the engine remains to be determined, once regular repeatable detonations are attained in the engine.

# APPENDIX A. PULSE DETONATION ENGINE COMPONENTS

The following drawings detail the completed valveless pulse detonation engine and the individual components, with their exact dimensions in inches, that together make up the engine. These drawings were generated using AutoCad, a computer aided design software package readily available on the commercial market. Each component was machined from either 304 or 316 stainless steel stock. Purchased completed components (such as solenoids, injectors, and transducers) are omitted from this appendix. The first and second drawings included in this appendix are of the pulse detonation engine and the test cell layout, respectively. The drawings following these two are in order from the head end of the inlet section to the main combustion tube.

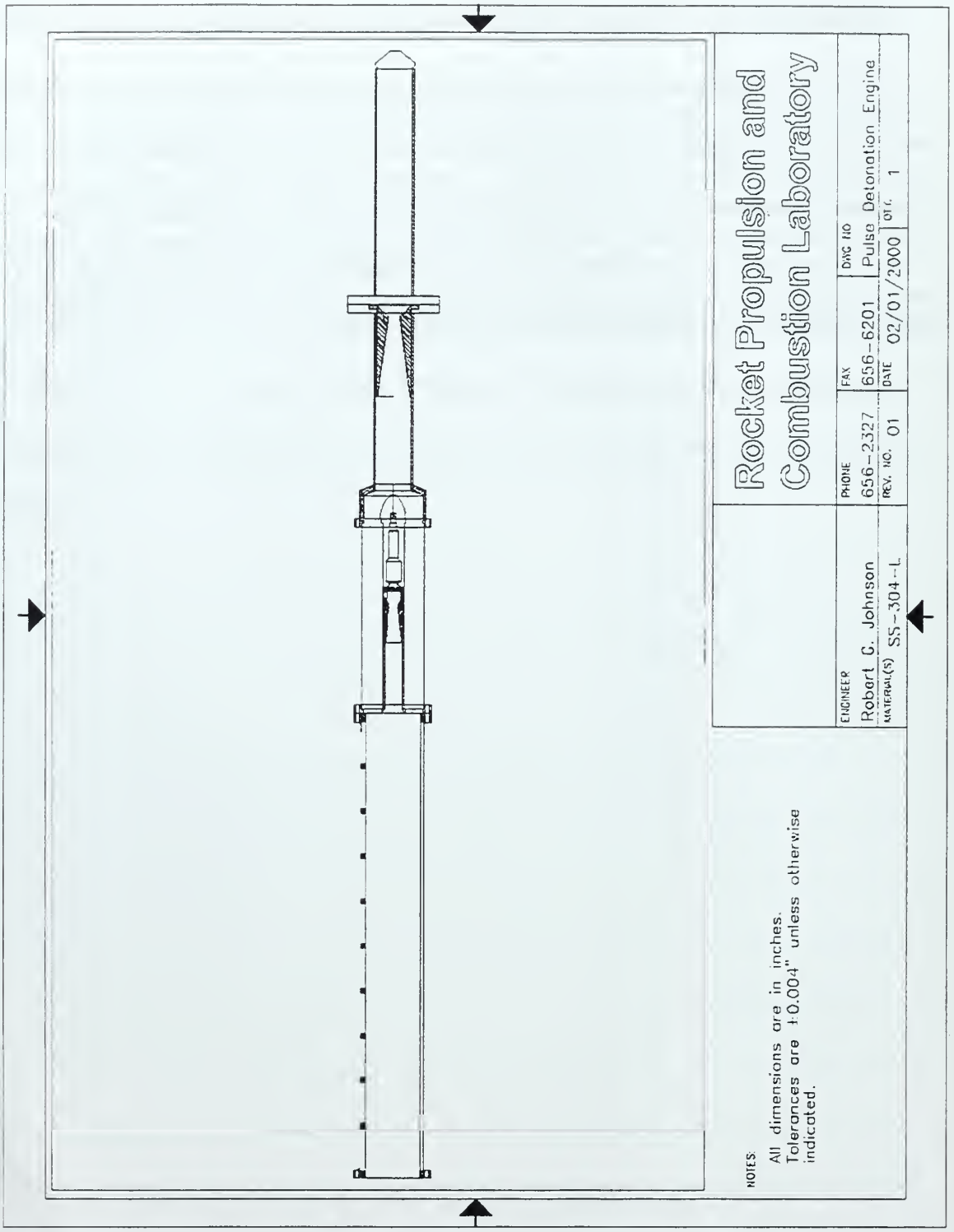


Figure A-1. This figure is a schematic of the entire Pulse Detonation Engine. A bolt was extended from the endcap and was used to measure thrust through its impingement on a piezoelectric load cell mounted to the thrust stand seen in the next figure.

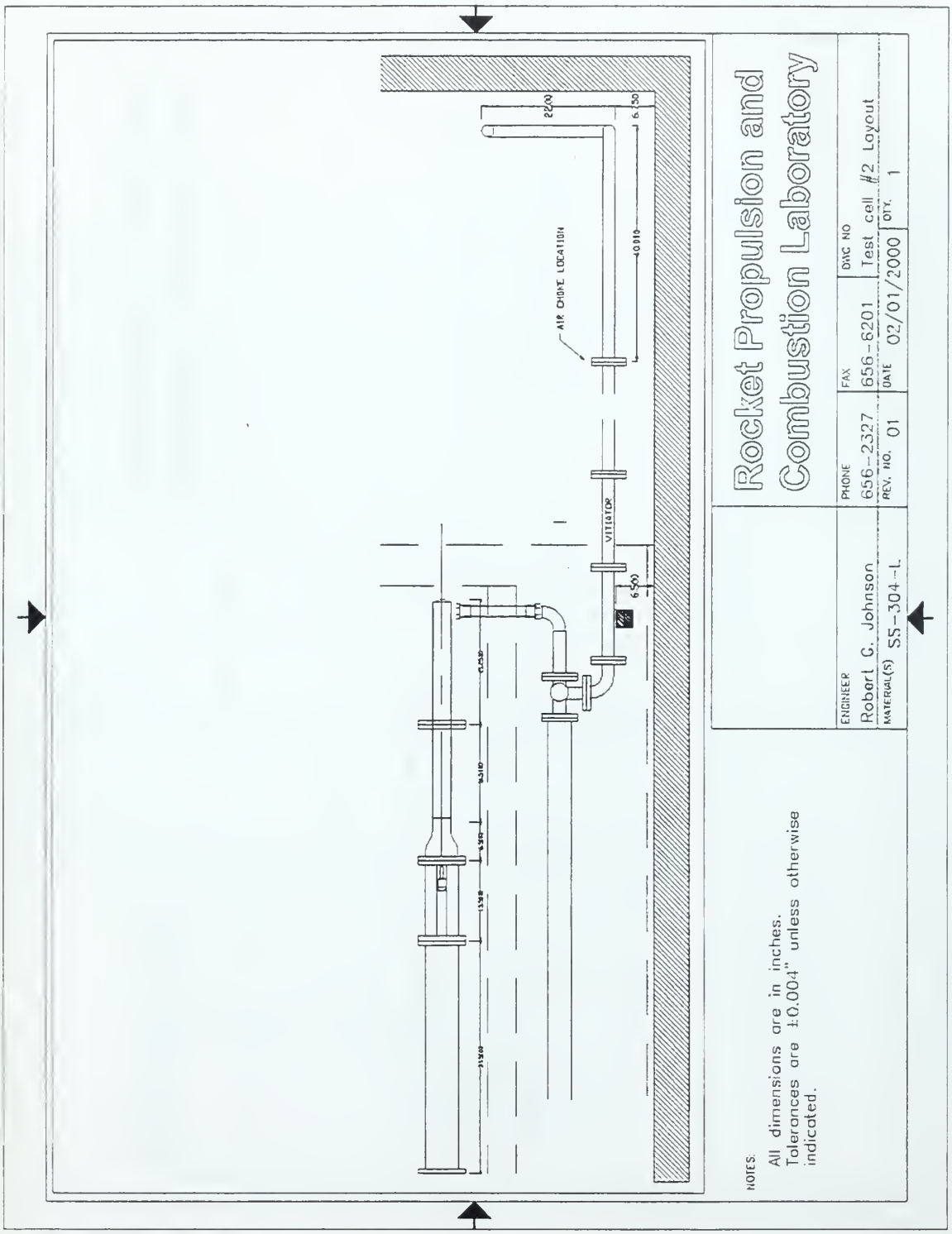


Figure A-2. This figure depicts the overall test cell layout. Pressurized air flows from the test cell wall through the vitiator to a 3-way valve. From there, the air is either dumped to the exhaust or directly into the engine for operation.

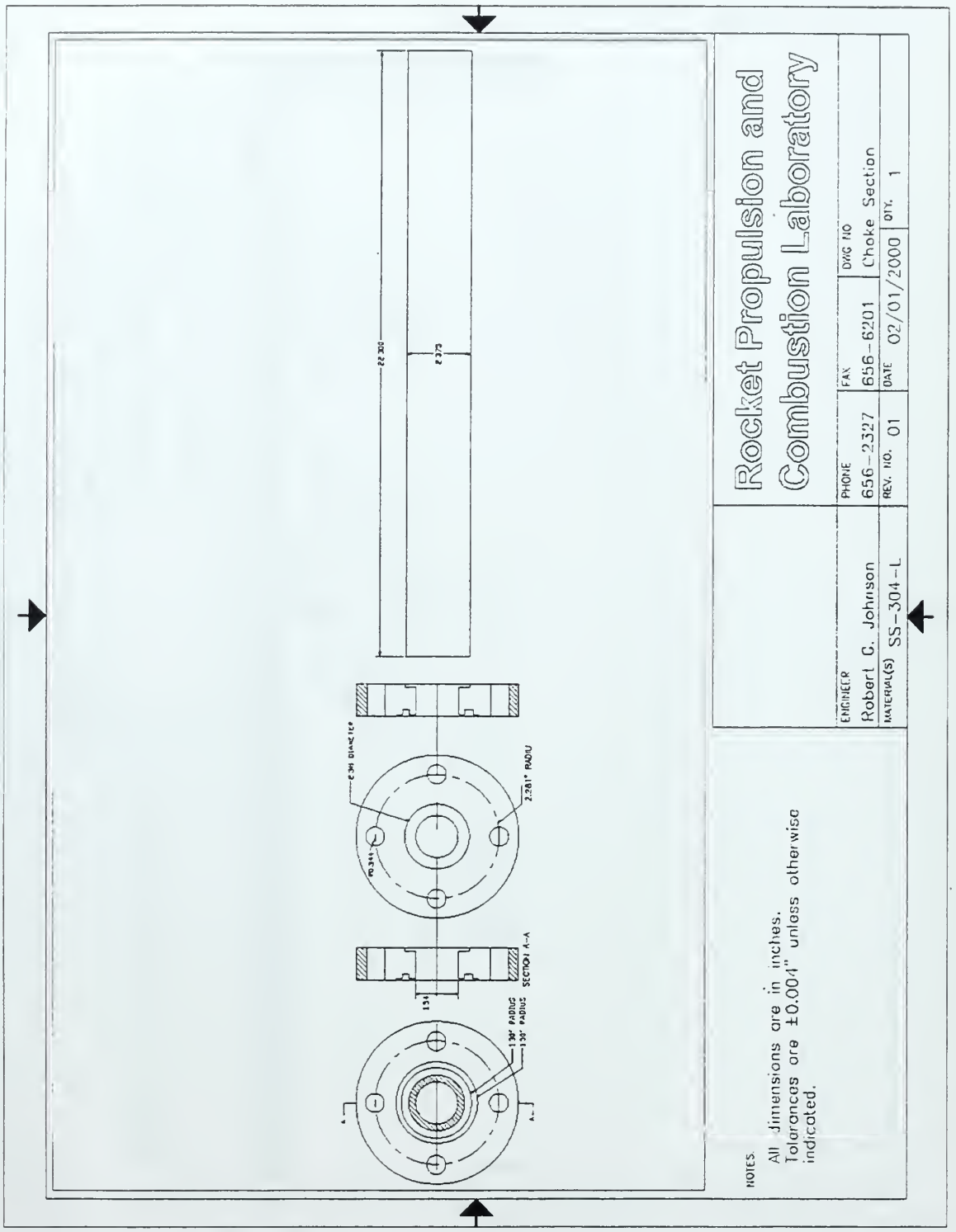


Figure A-3. These flanges, upstream of the vitiator, were used to hold a mass meter choke in place. The chokes used were 0.377", 0.5", or 0.625" in diameter and were used to determine the mass flow rate prior to heating of the air in the vitiator.

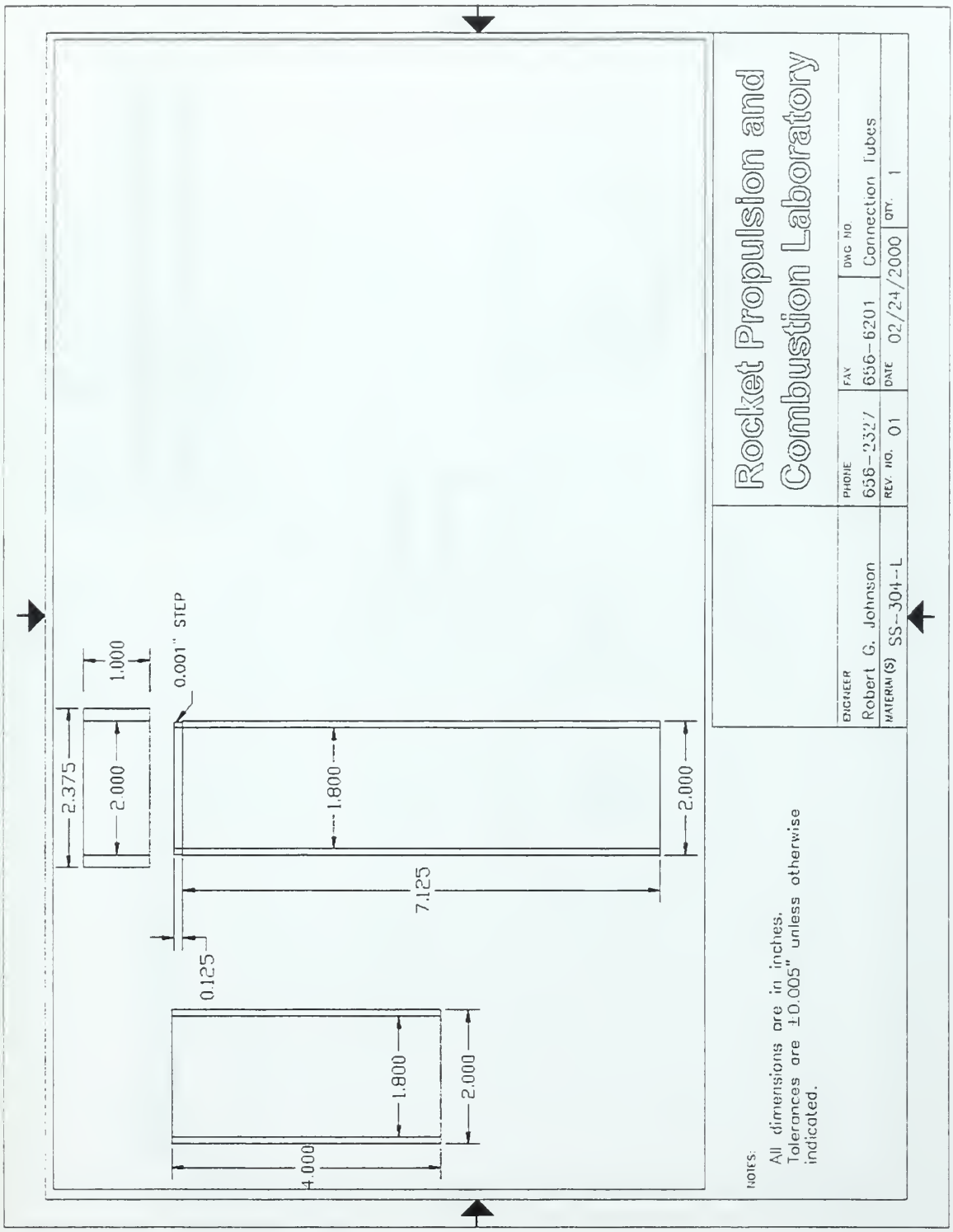


Figure A-4. These tubes were used to link a steel braided hose from the 3-way valve to the engine.

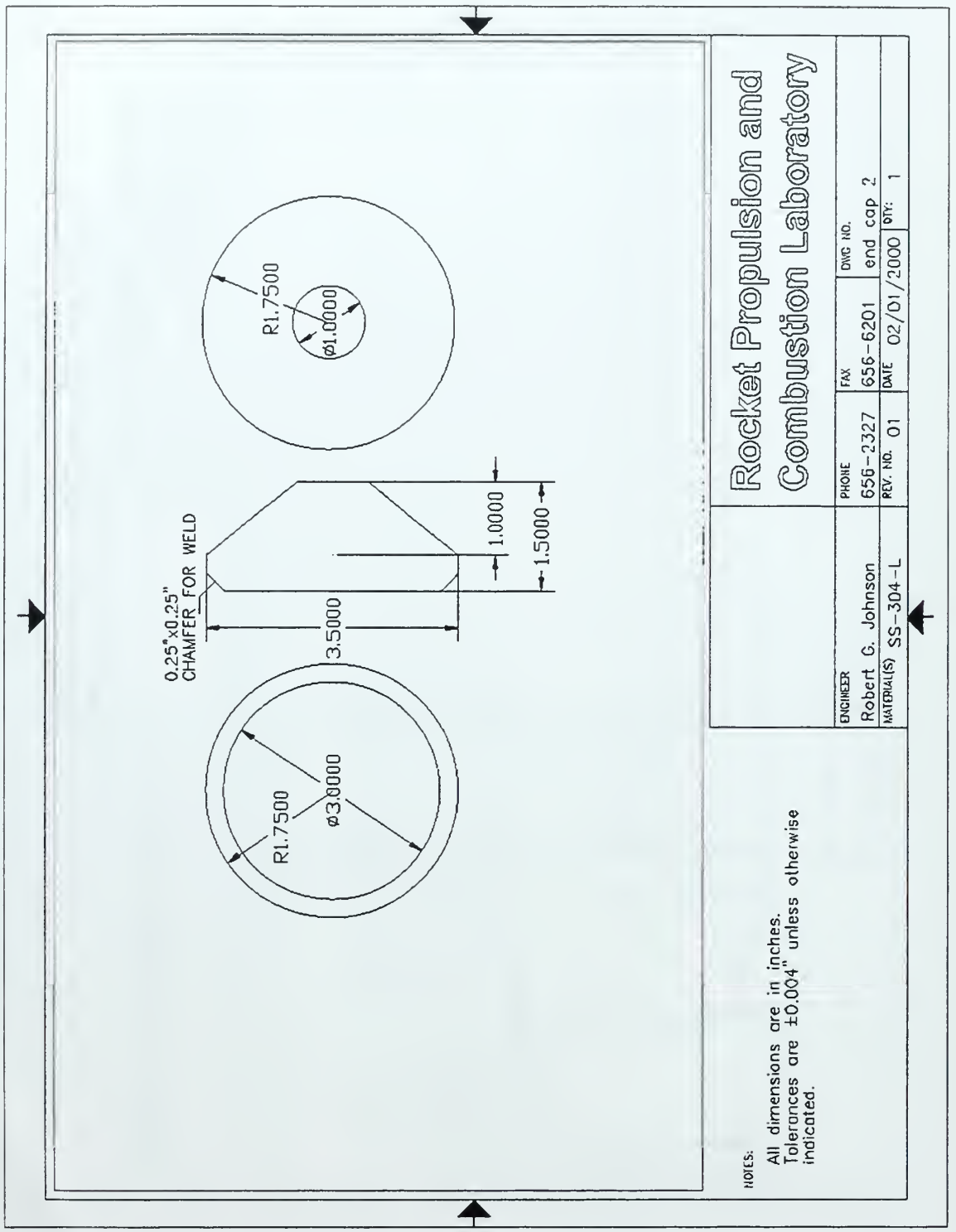


Figure A-5. This endcap was welded to the head end of the engine. The cap was used to allow flow only in one direction and to measure thrust through its impingement on a piezoelectric load cell mounted to the thrust stand.

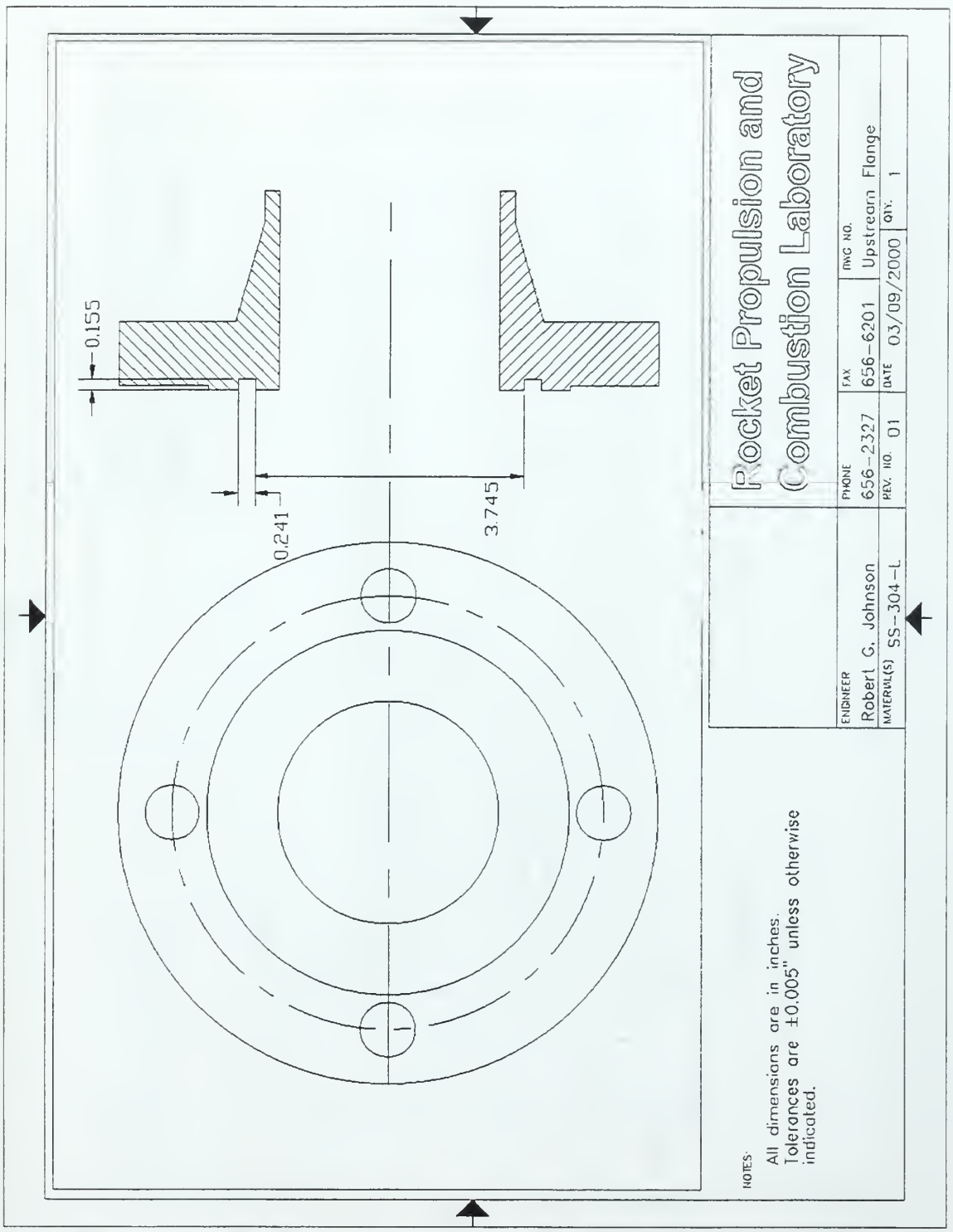


Figure A-6. This flange was the upstream mount holding the Delaval choke in place just prior to the fuel injection manifold.

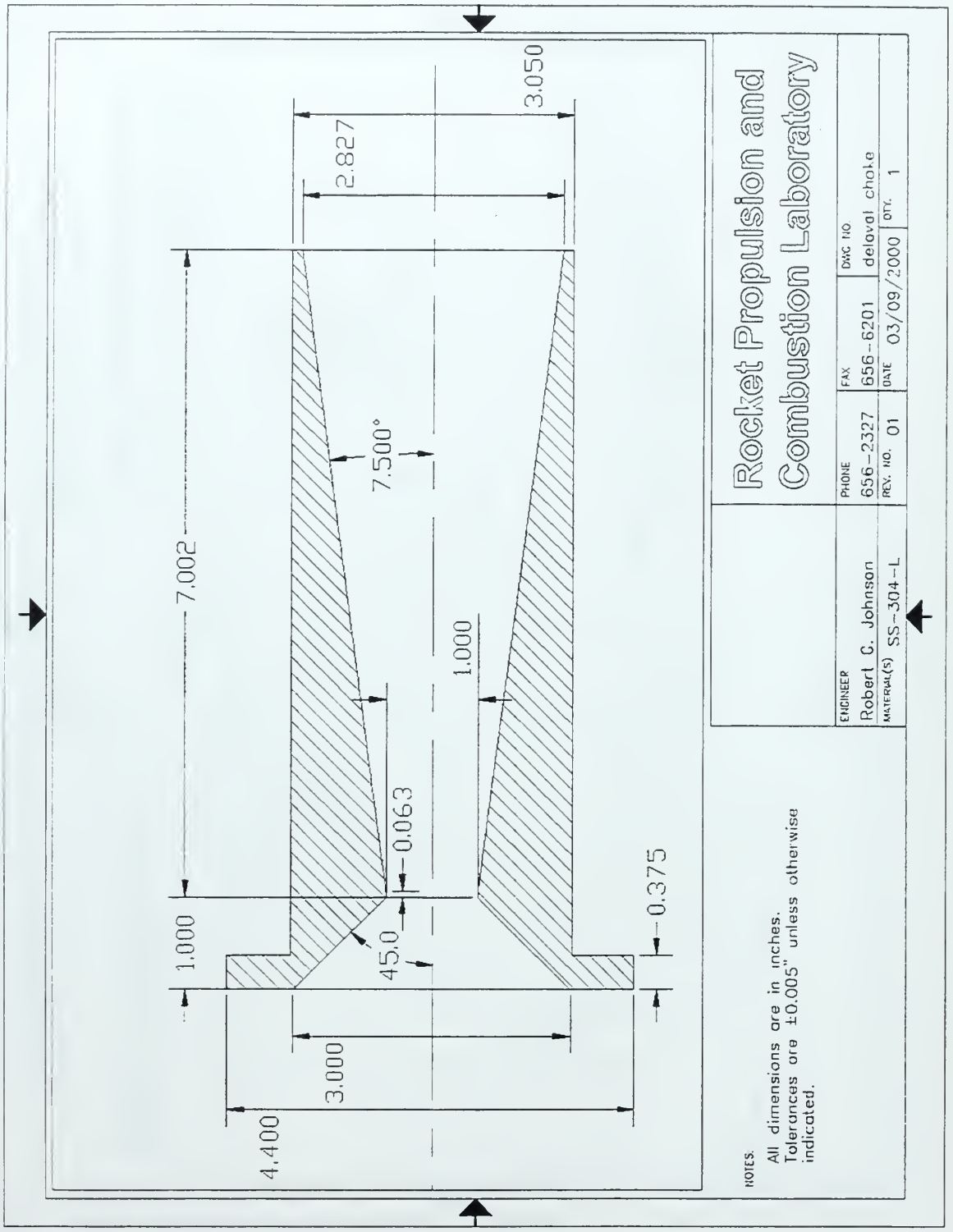


Figure A-7. This Delaval choke was placed upstream of the engine in order to isolate upstream pressure fluctuations and set inlet conditions prior to the engine.

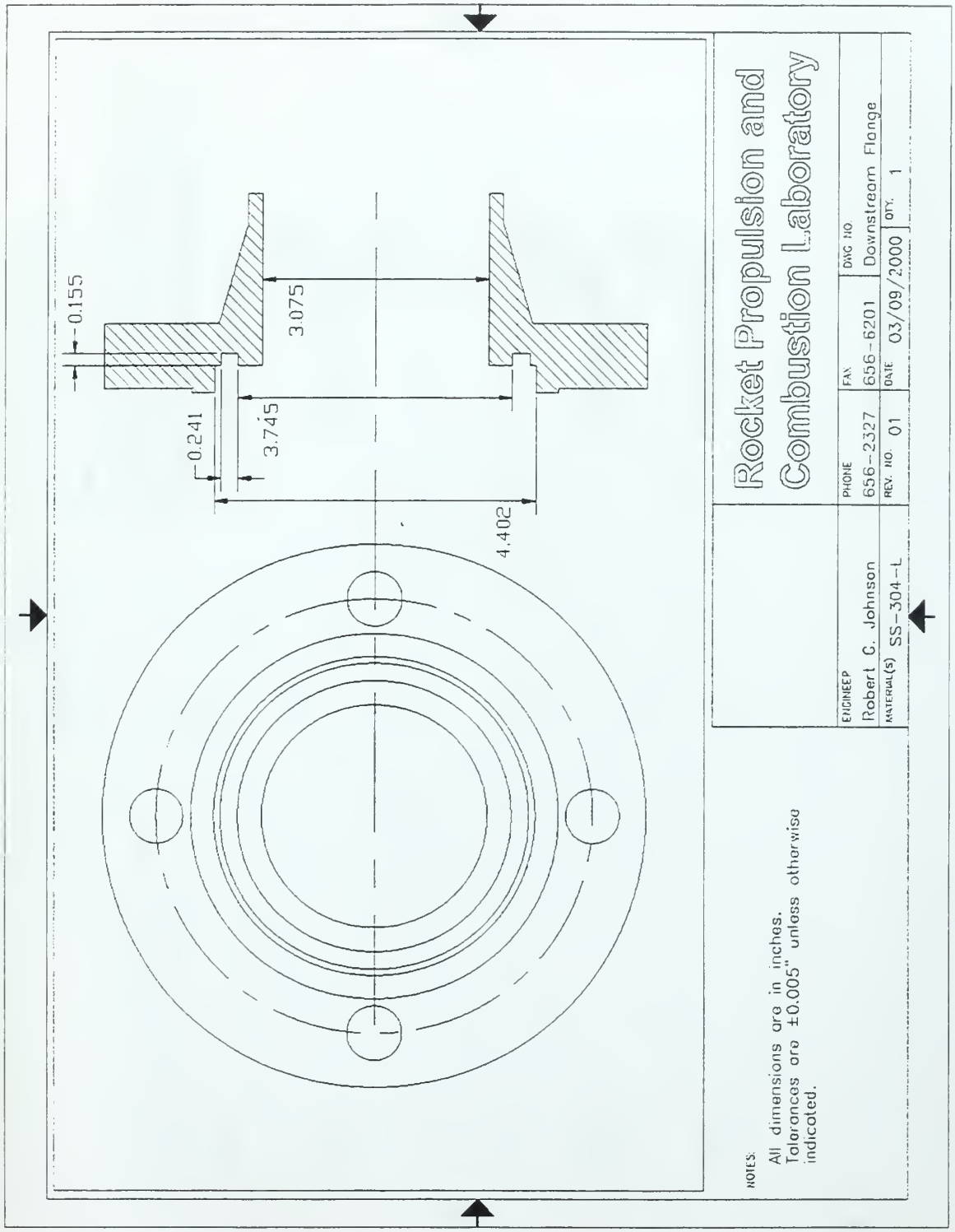


Figure A-8. This flange was the downstream mount holding the Delaval choke in place just prior to the fuel injection manifold.

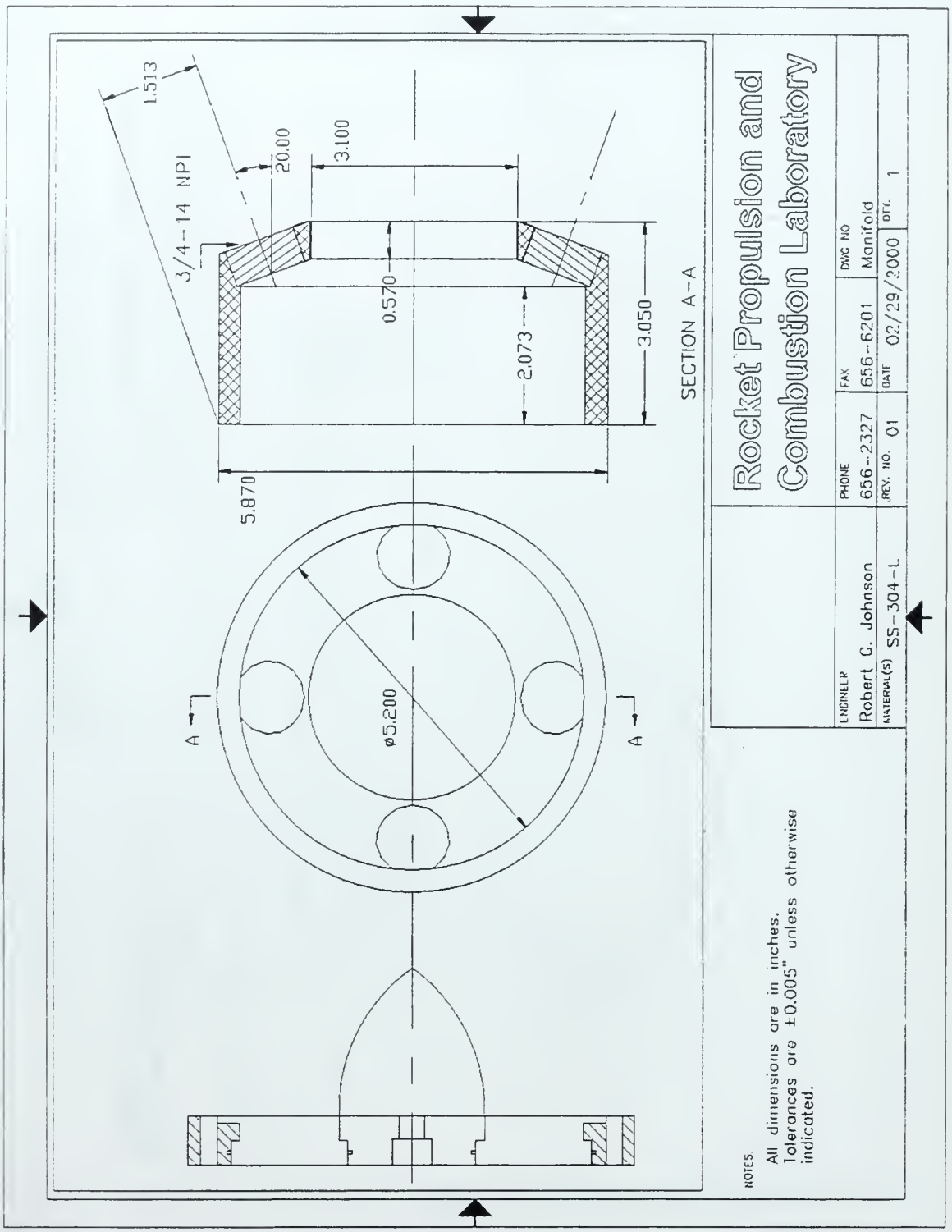


Figure A-9. This fuel injection manifold, with a 20° injection angle, was used in this thesis to inject fuel into the "inlet" air flowing at mass flow rates greater than 0.3 lbm/s.

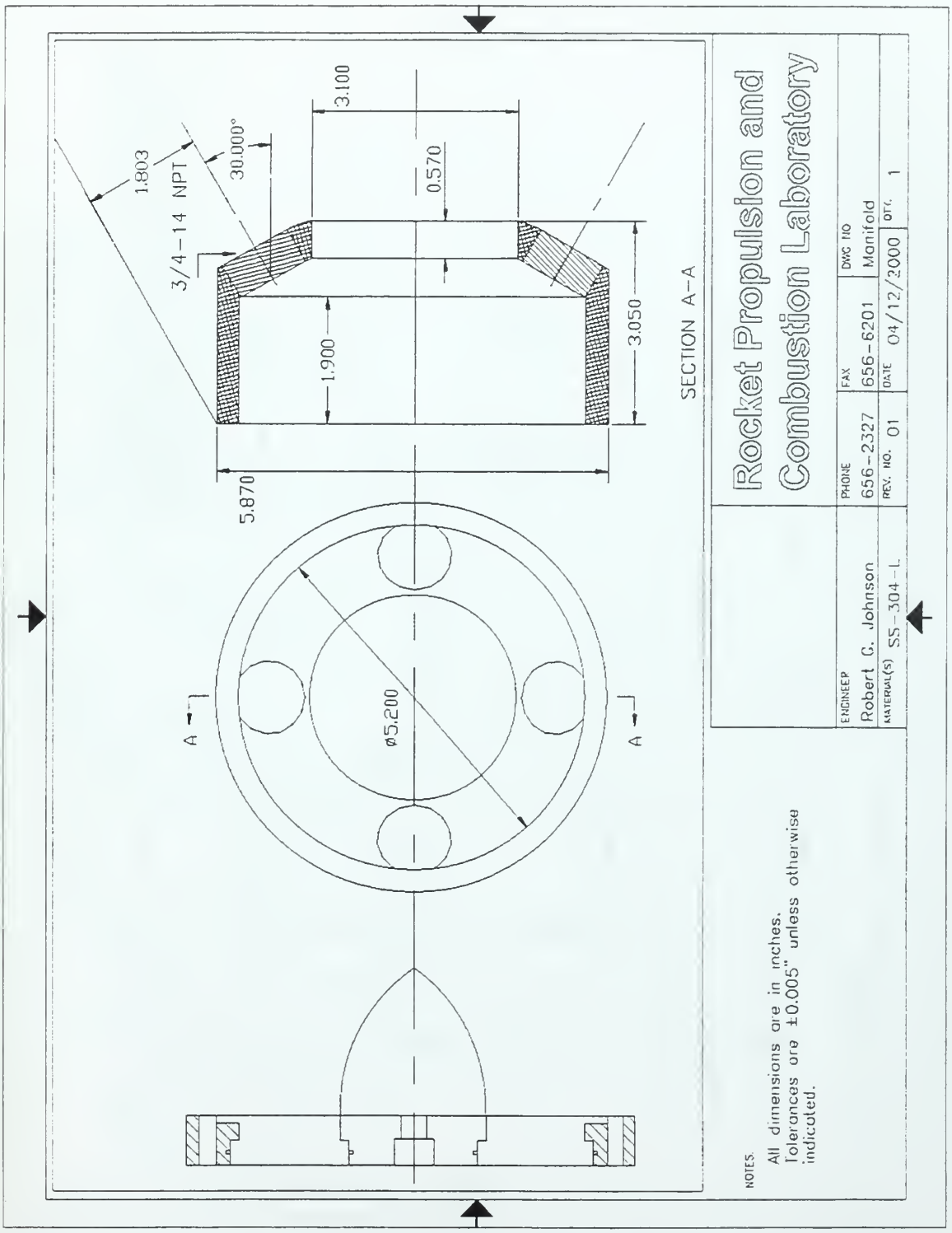


Figure A-10. This fuel injection manifold, with a 30° injection angle, was designed as an alternative to the previous fuel injector manifold to test other impingement angles to the "inlet" air flowing at mass flow rates greater than 0.3 lbm/s.

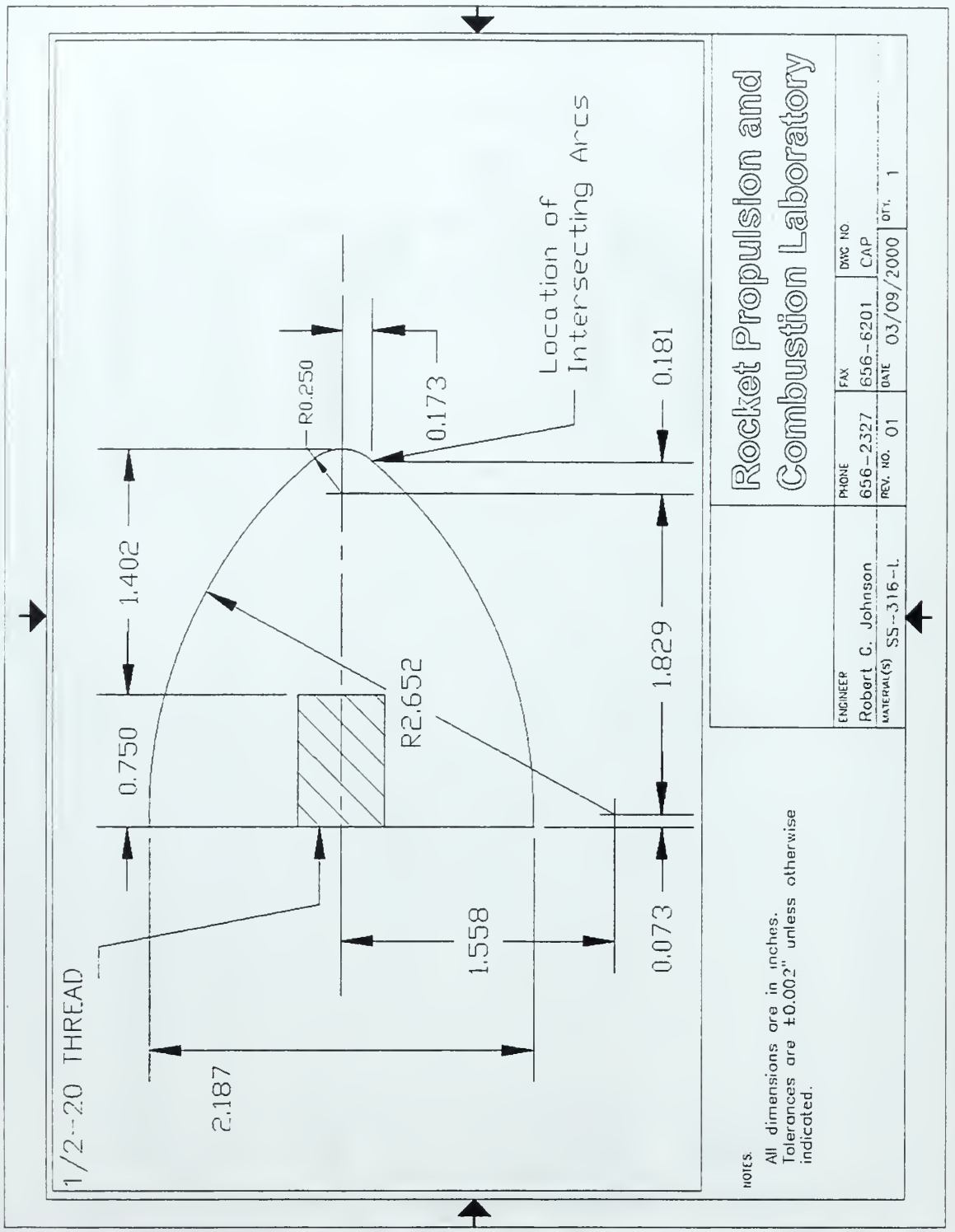


Figure A-11. This ogive was used in the fuel injection manifold to ease the "inlet" air's transition into the four main air arms.

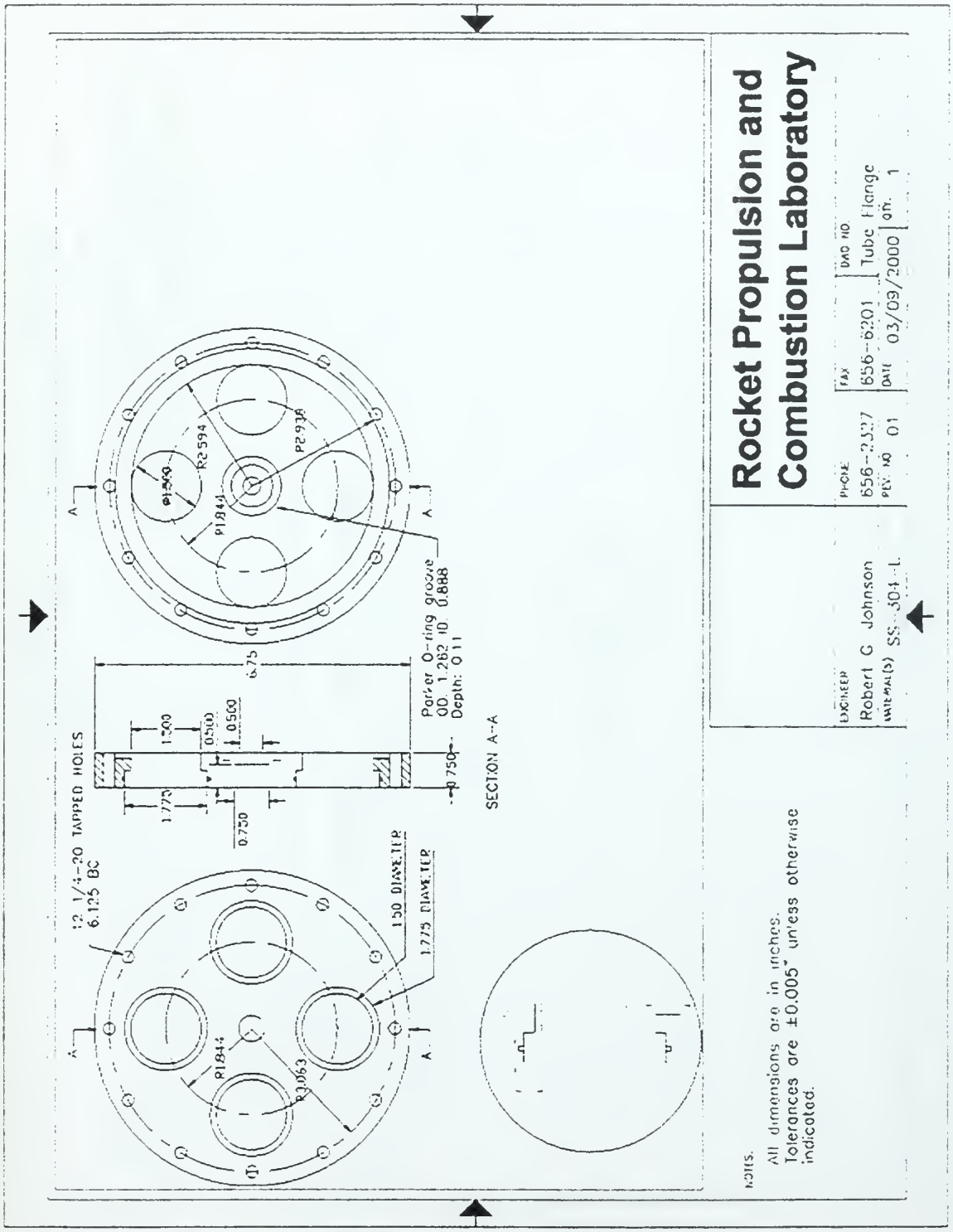


Figure A-12. The tube flange was the interface between the fuel injection manifold and the four main air arms that routes the vitiated fuel/air mixture into the main combustion tube.

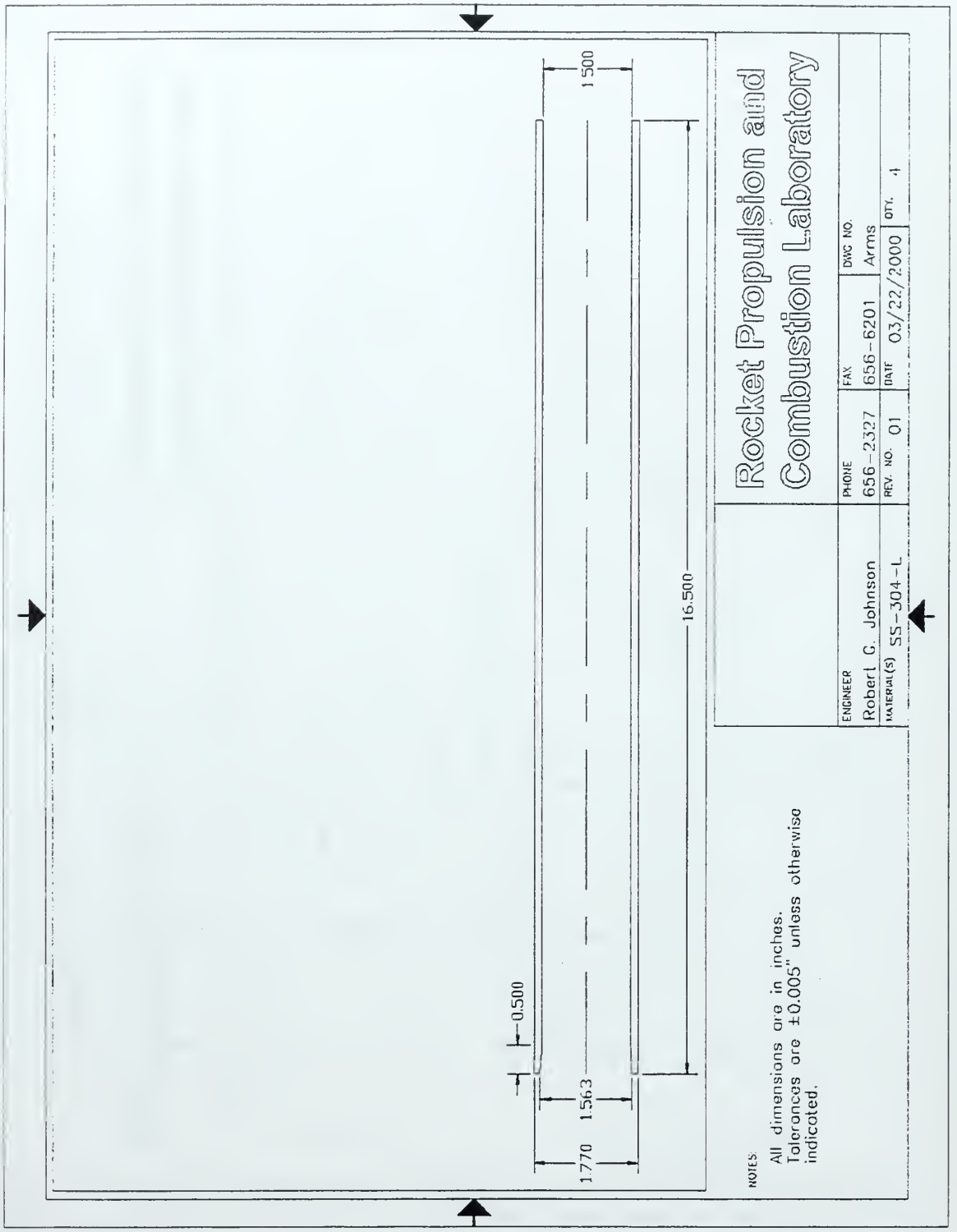


Figure A-13. This drawing is representative of the four main air arms that connect the fuel injection manifold to the main combustion tube.

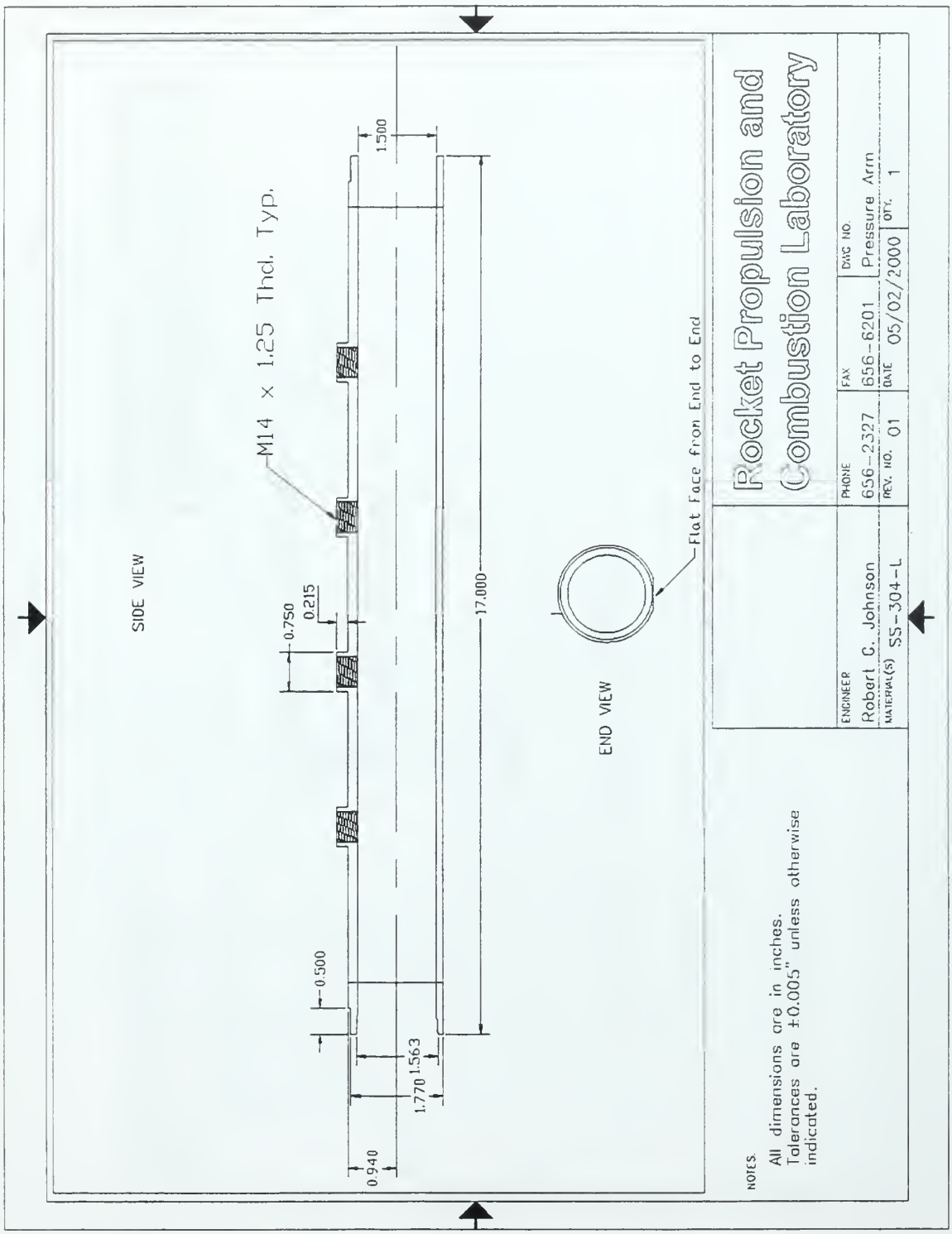


Figure A-14. This main air arm was specifically designed with welded pressure bosses to allow the operator to measure pressure waves that may be propagating backwards in the engine.

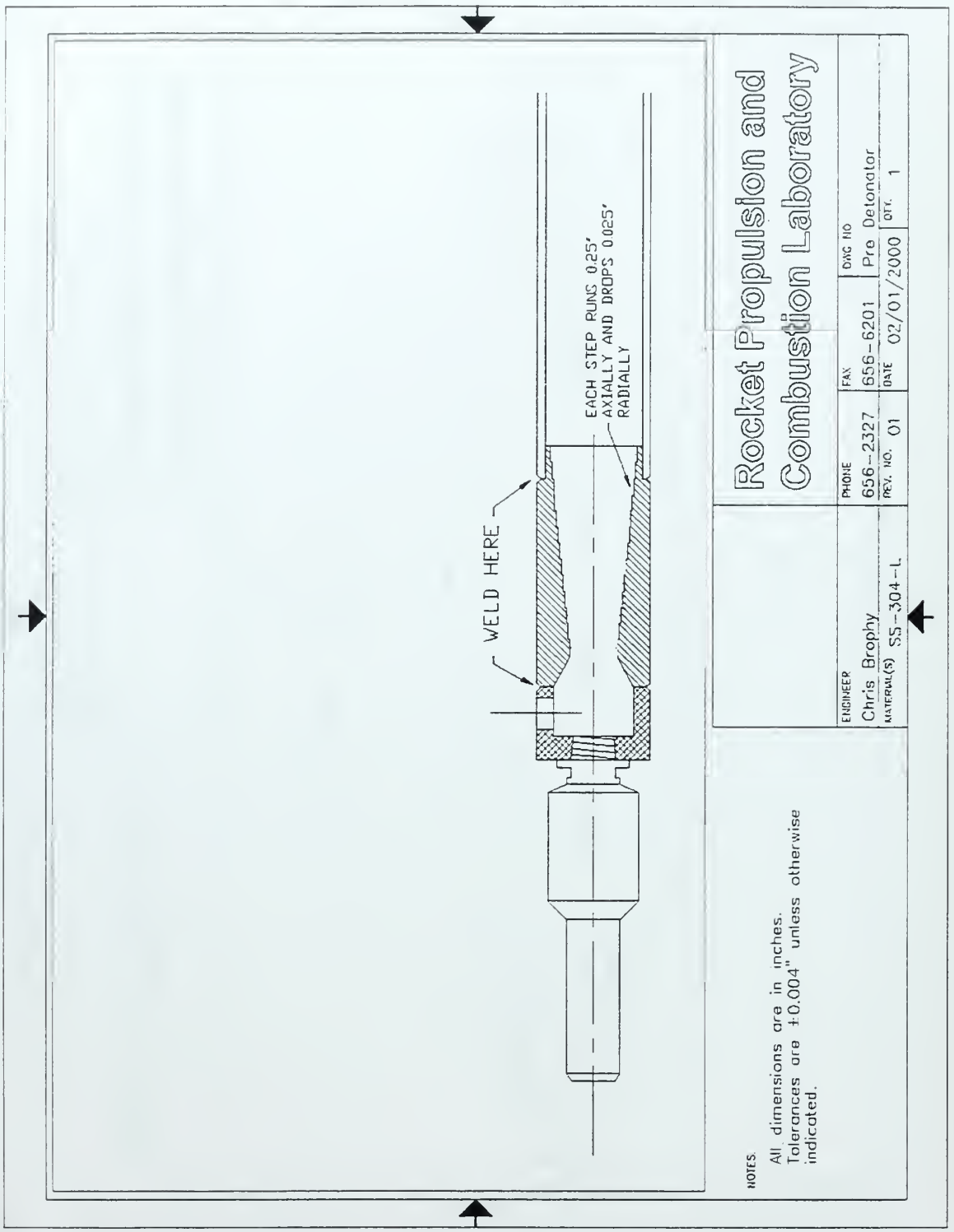


Figure A-15. This drawing depicts the pre-detonation tube that was welded to the manifold flange just prior to the main combustion tube.

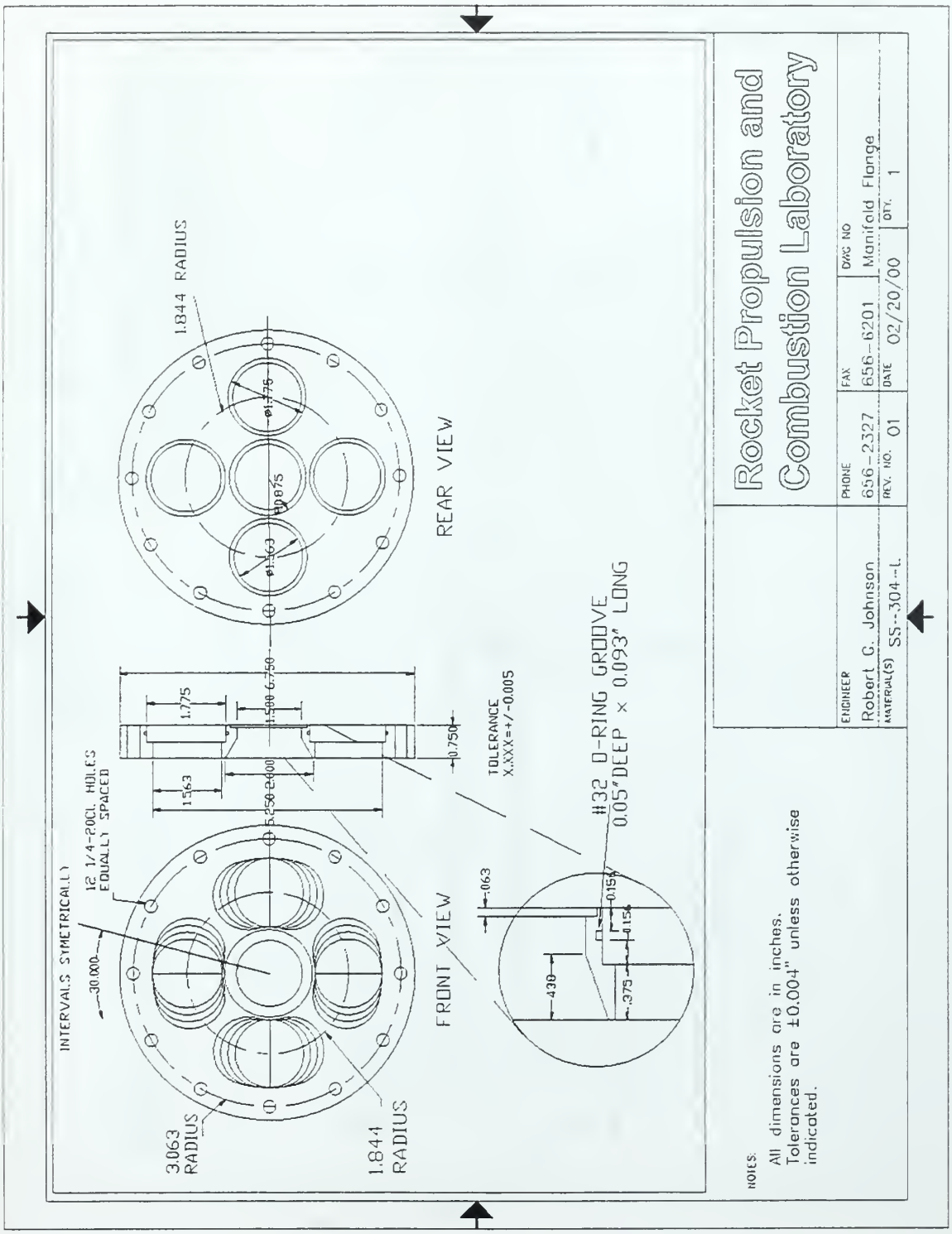


Figure A-16. The manifold flange connected the four main air arms and the pre-detonation tube to the main combustion tube flange.

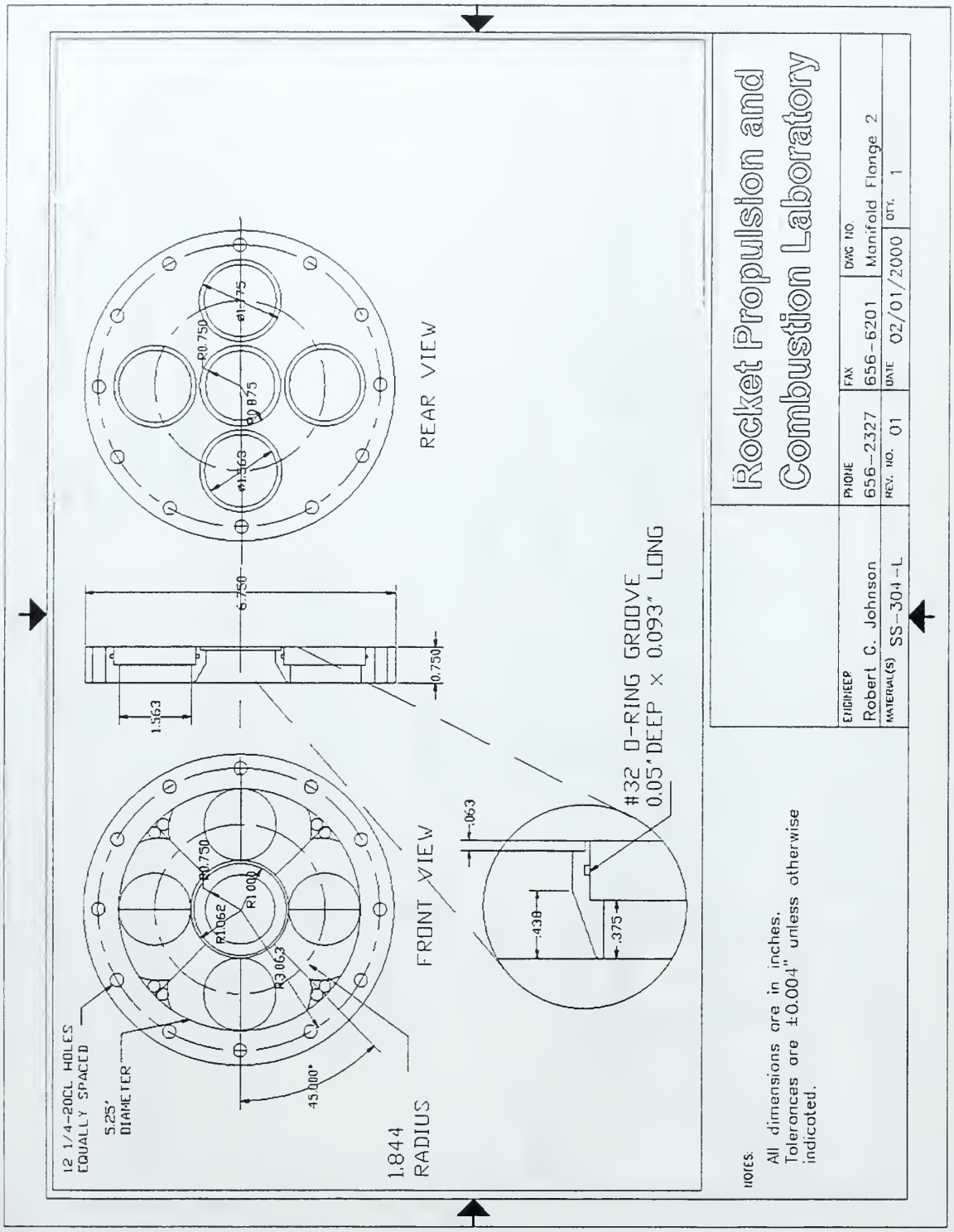


Figure A-17. This manifold flange was a modification to the previous drawing to ease the step that the detonation wave emerging from the pre-detonation tube made to the main combustion tube.

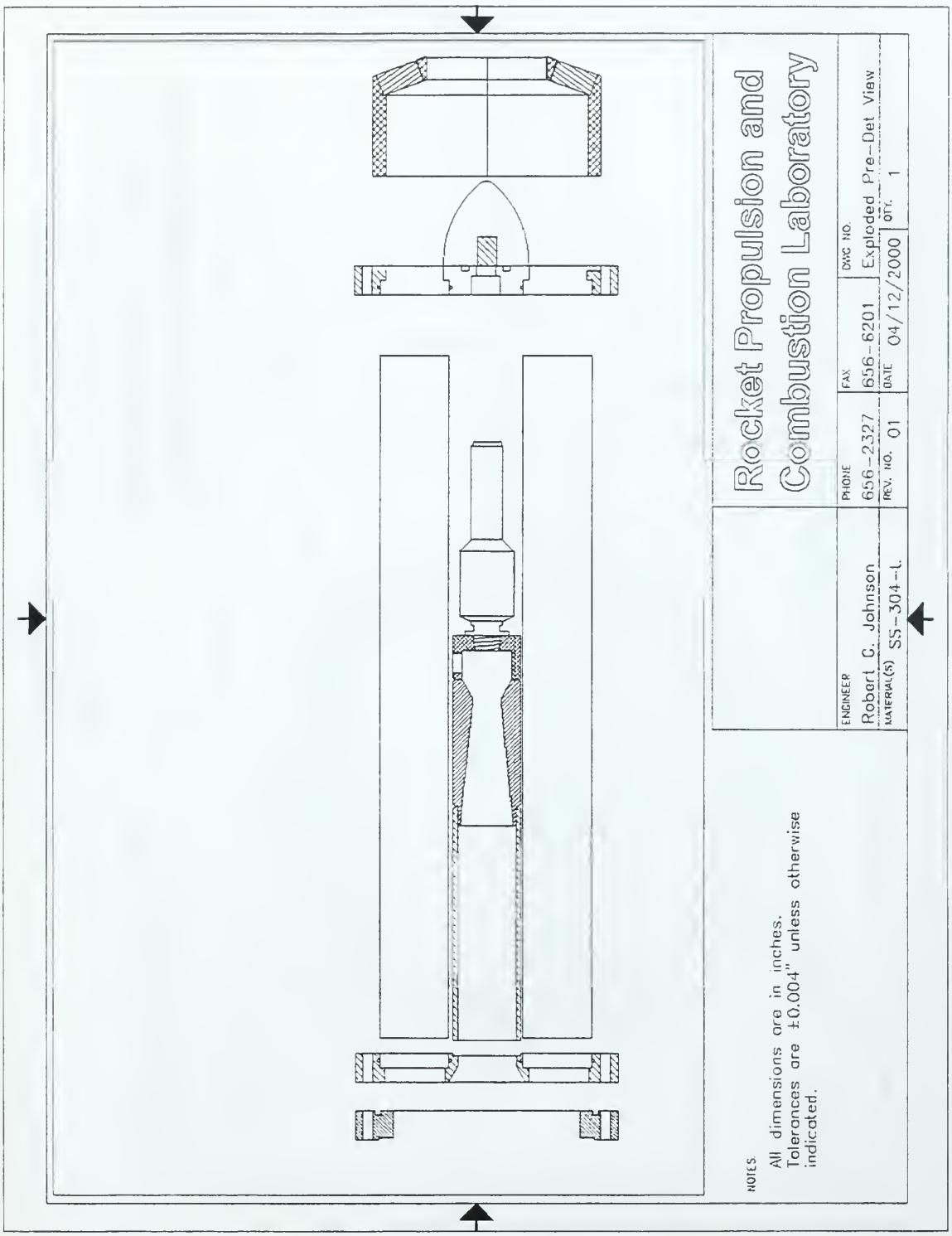


Figure A-18. This drawing depicts an exploded view of the manifold section extending from the fuel injection manifold to the main combustion tube.

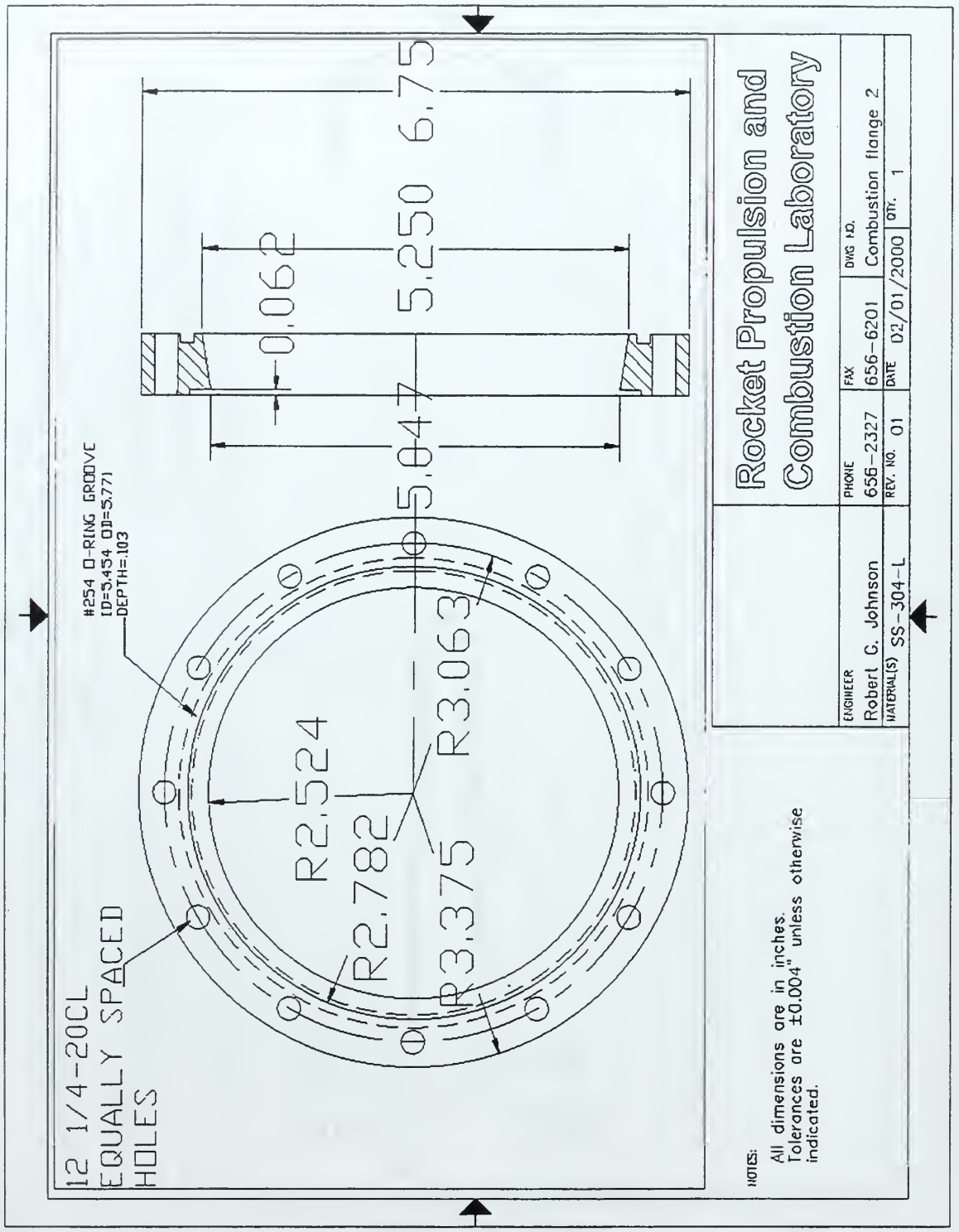


Figure A-19. This flange was welded to the inlet of the main combustion tube. The taper inside of the flange was used to match the inner diameter of the tubes through the manifold flange to the inner diameter of the main combustion tube.

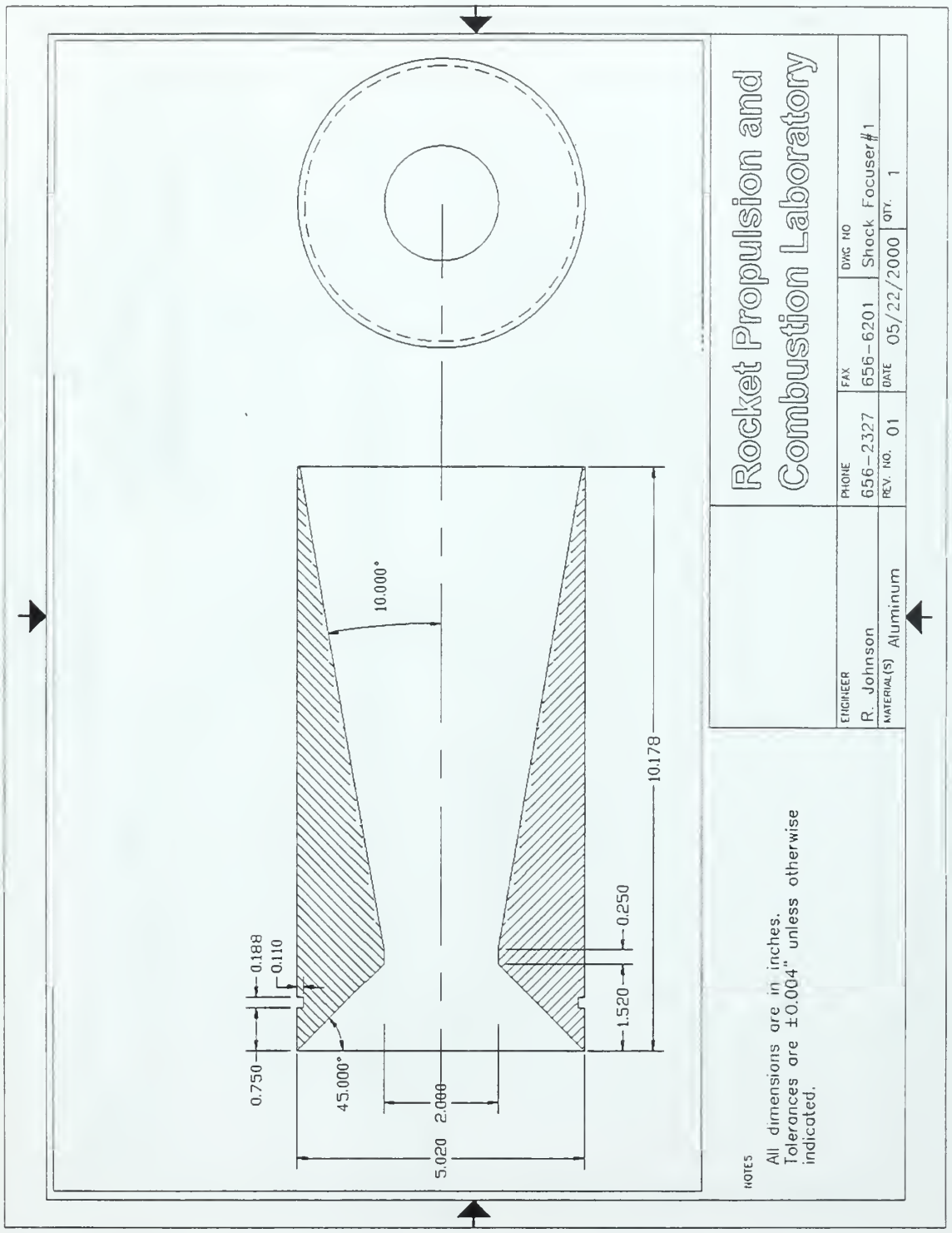


Figure A-20. This Shock Focusing Device was added after significant testing of the engine failed to produce a detonation in the main combustion tube.

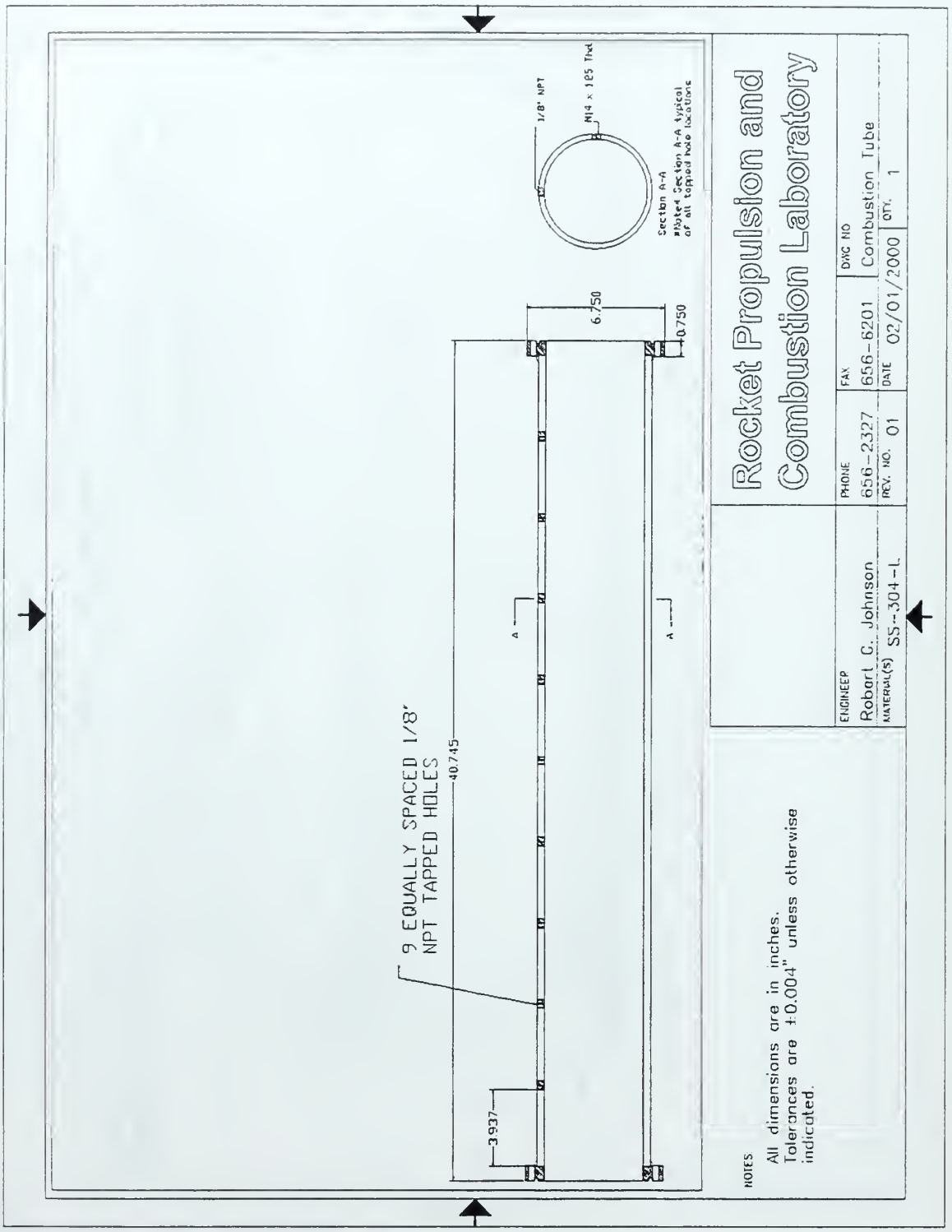


Figure A-21. A depiction of the main combustion tube with its end flanges welded in place.

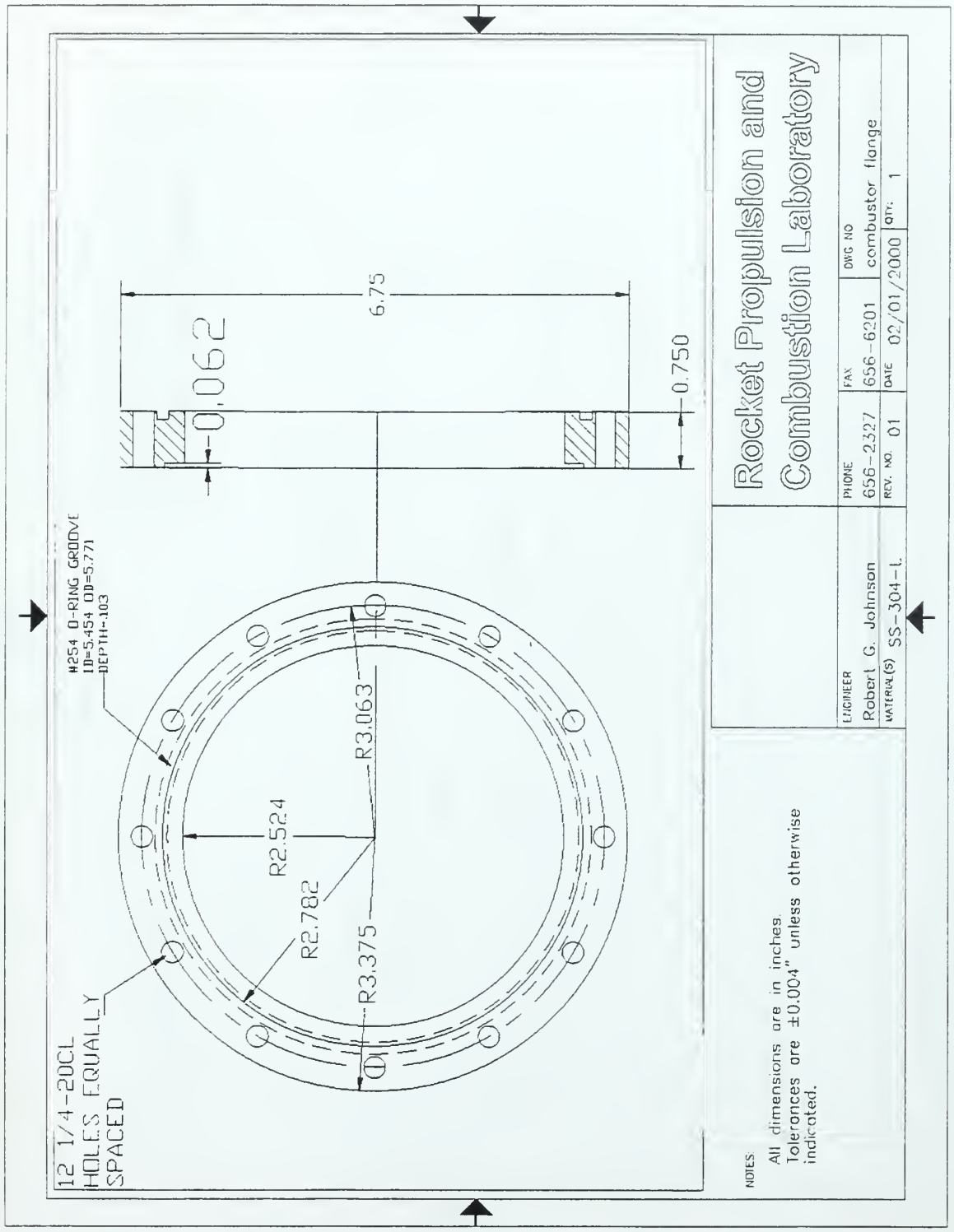


Figure A-22. This flange was welded to the exit of the main combustion tube for possible peripheral use.

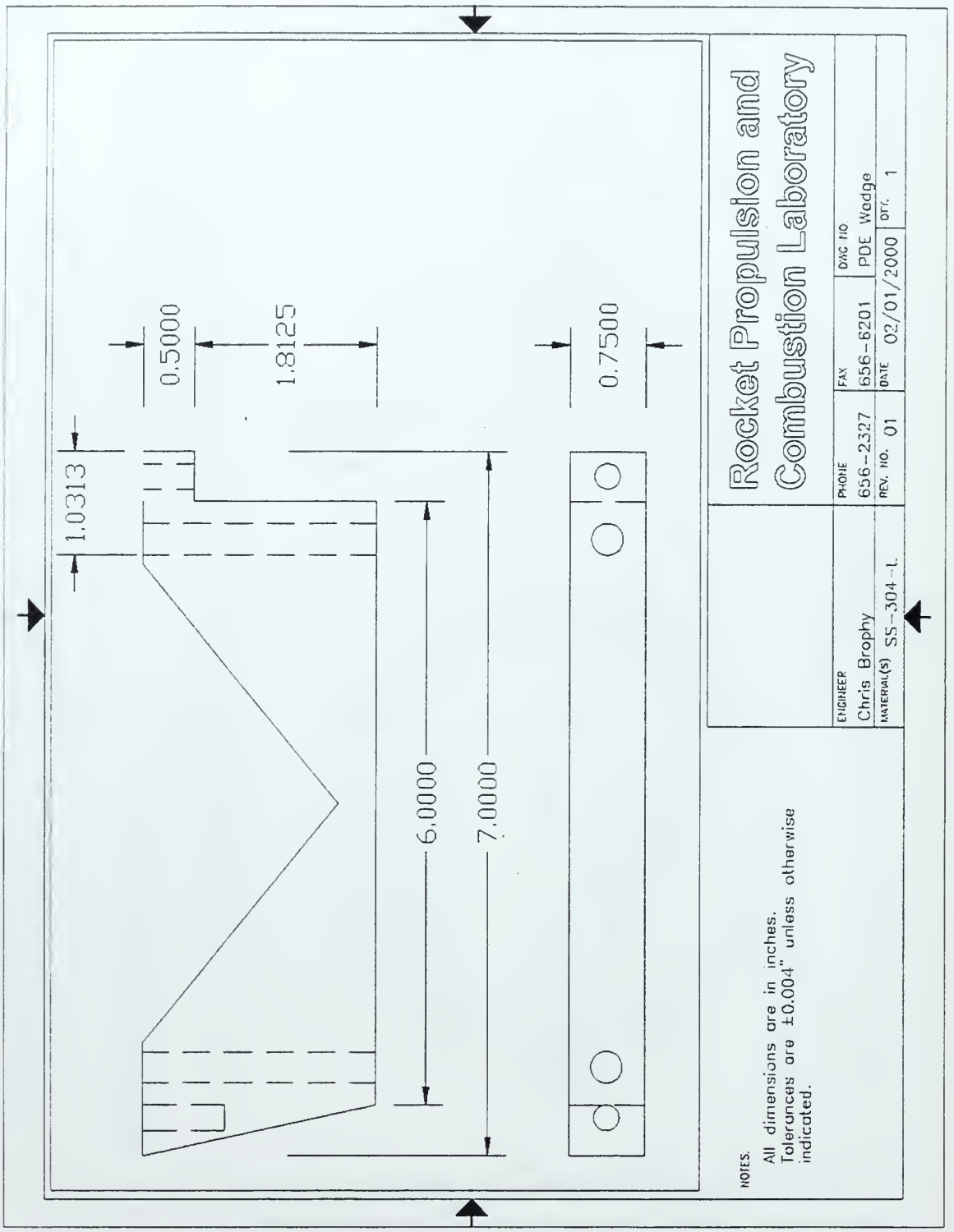


Figure A-23. This wedge was used to support the main combustion tube and fuel injection manifold on top of slide rails, allowing an accurate measurement of thrust.

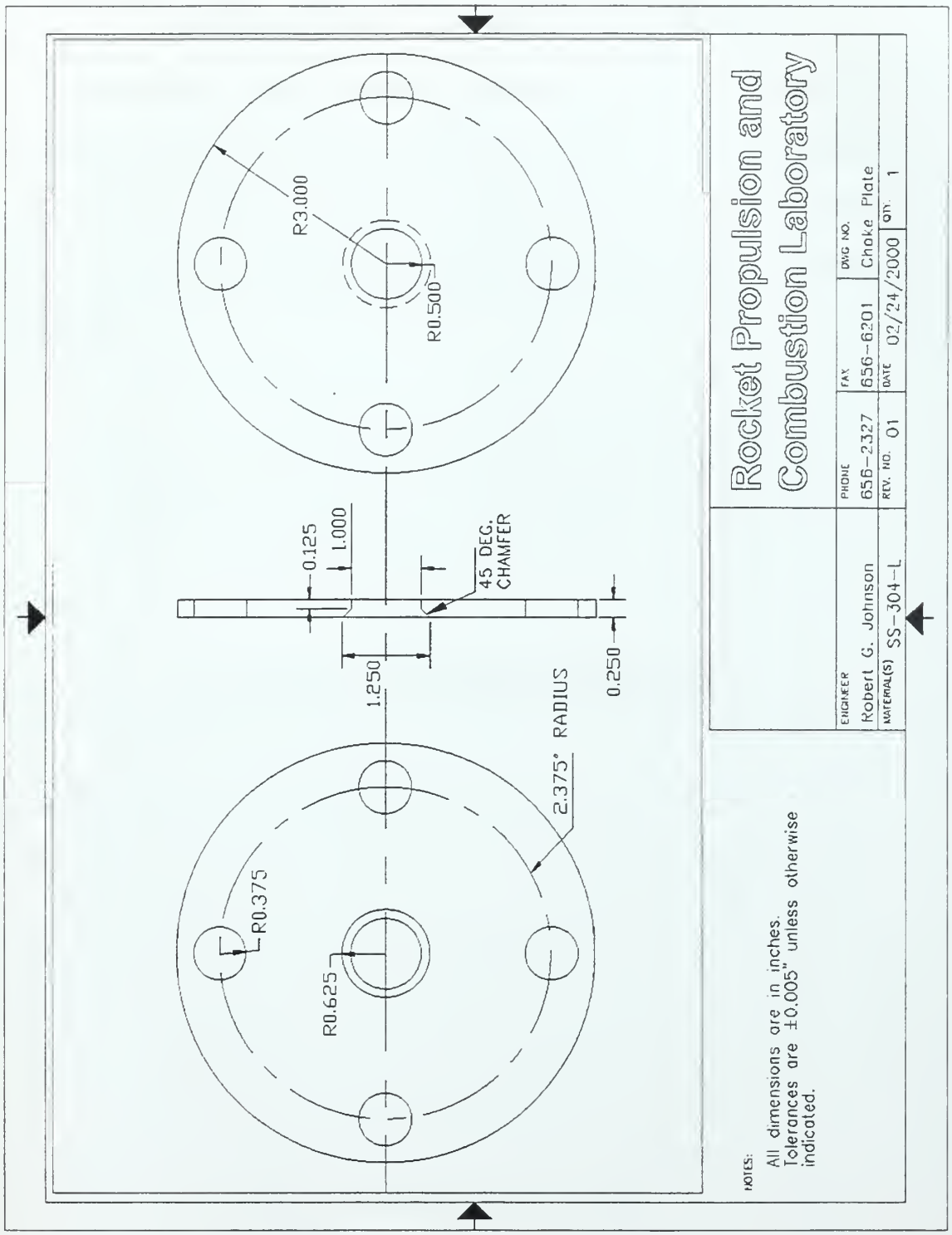


Figure A-24. This choke was placed downstream of the 3 way valve in an exhaust tube. Initially, the vitiated air was dumped overboard until a stable temperature was achieved. The 3 way valve was used to divert the vitiated air from the overboard dump to the engine. The choke was used to create sufficient back pressure on the vitiator for it to operate properly.

THIS PAGE INTENTIONALLY LEFT BLANK

# APPENDIX B. VITIATOR TEST RUNS

This appendix contains the plots of the pertinent pressures and temperatures for the vitiator and main combustion tube for all of the vitiator test runs. For the specific values attained for each run, see Table 4-1. All plots for mass flow rates of 0.5 lbm/s have incorrect data for the engine inlet temperature, and therefore that trace should be disregarded.

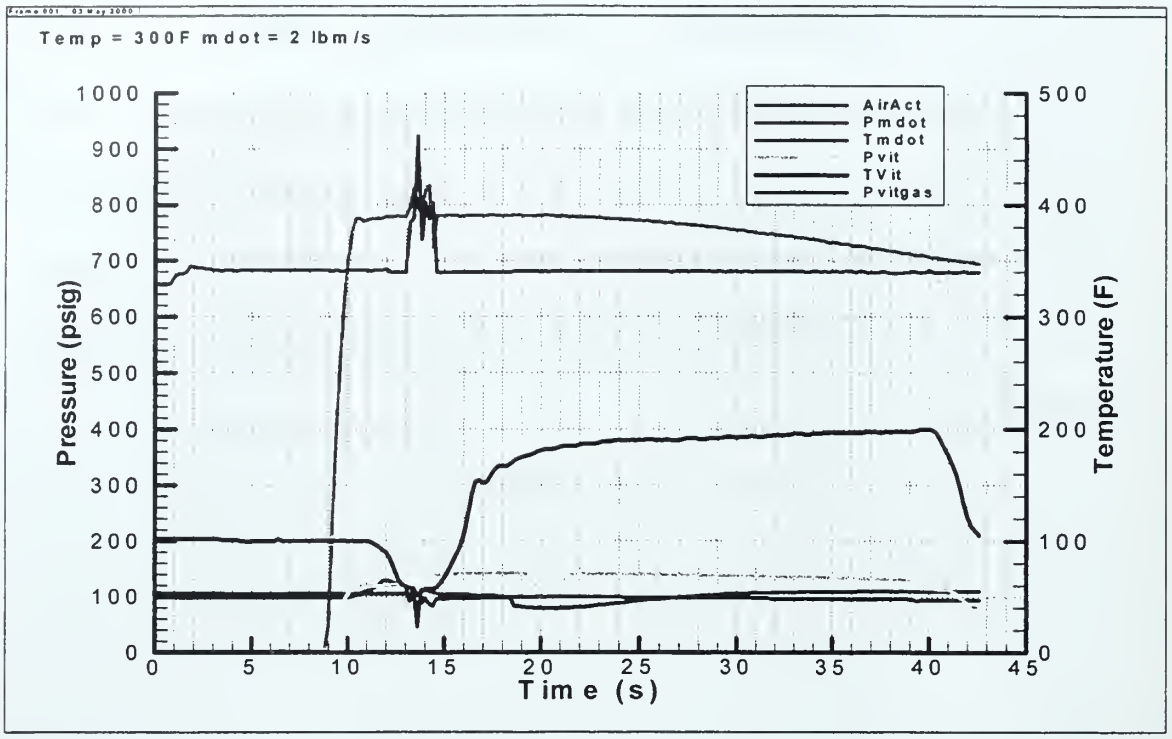


Figure B-1.

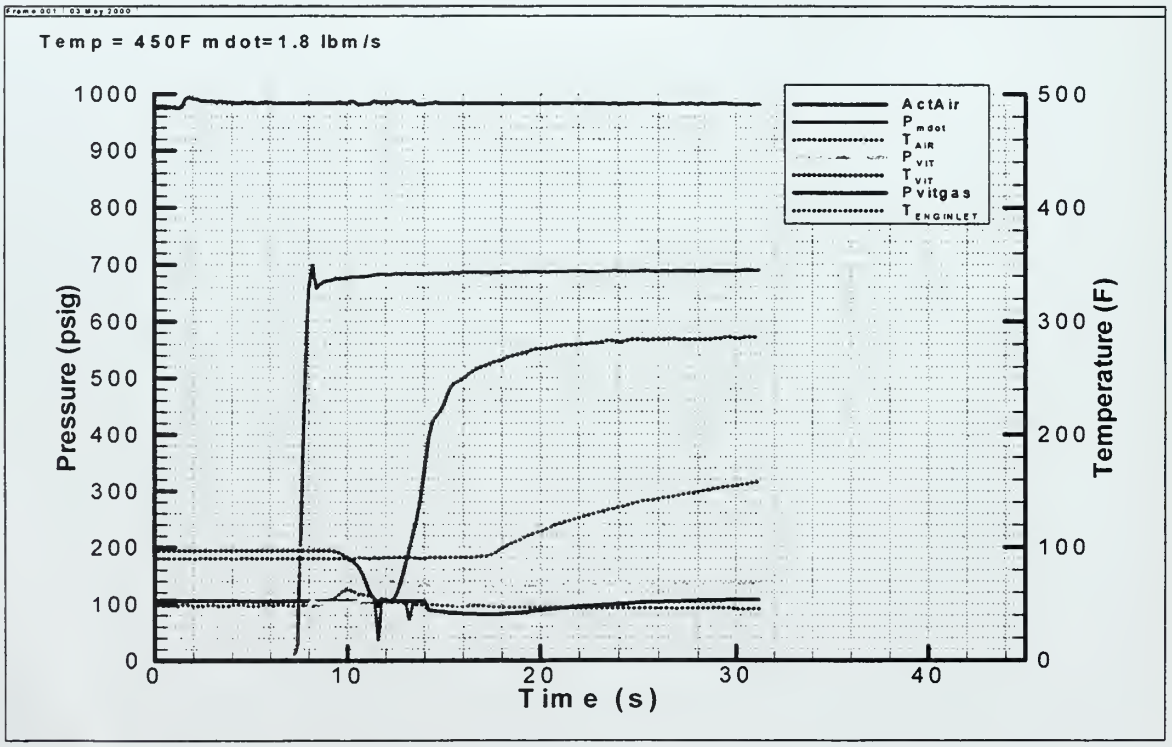


Figure B-2.

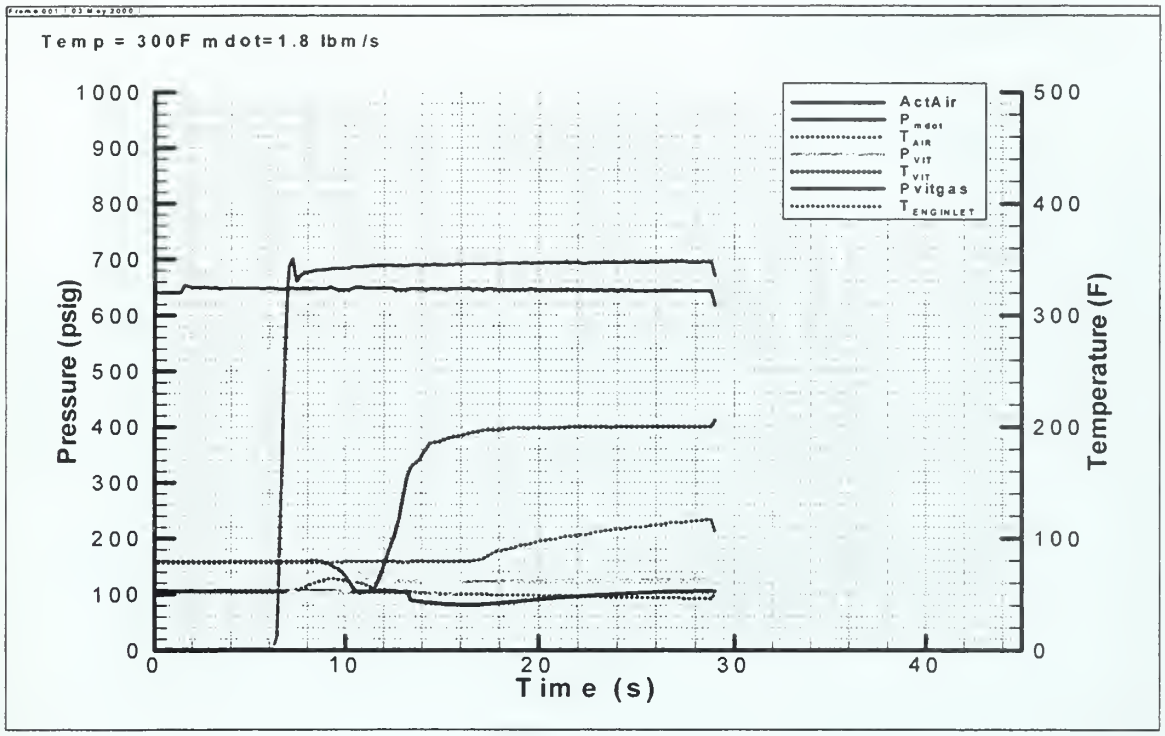


Figure B-3.

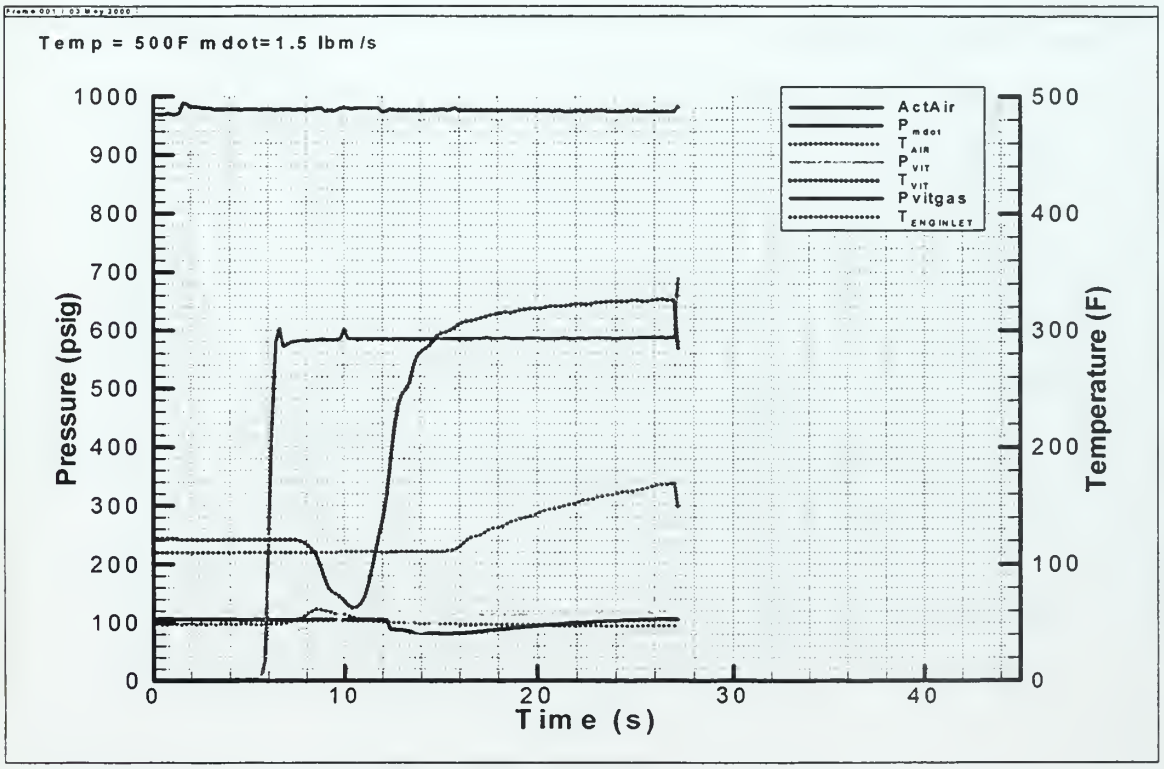


Figure B-4.

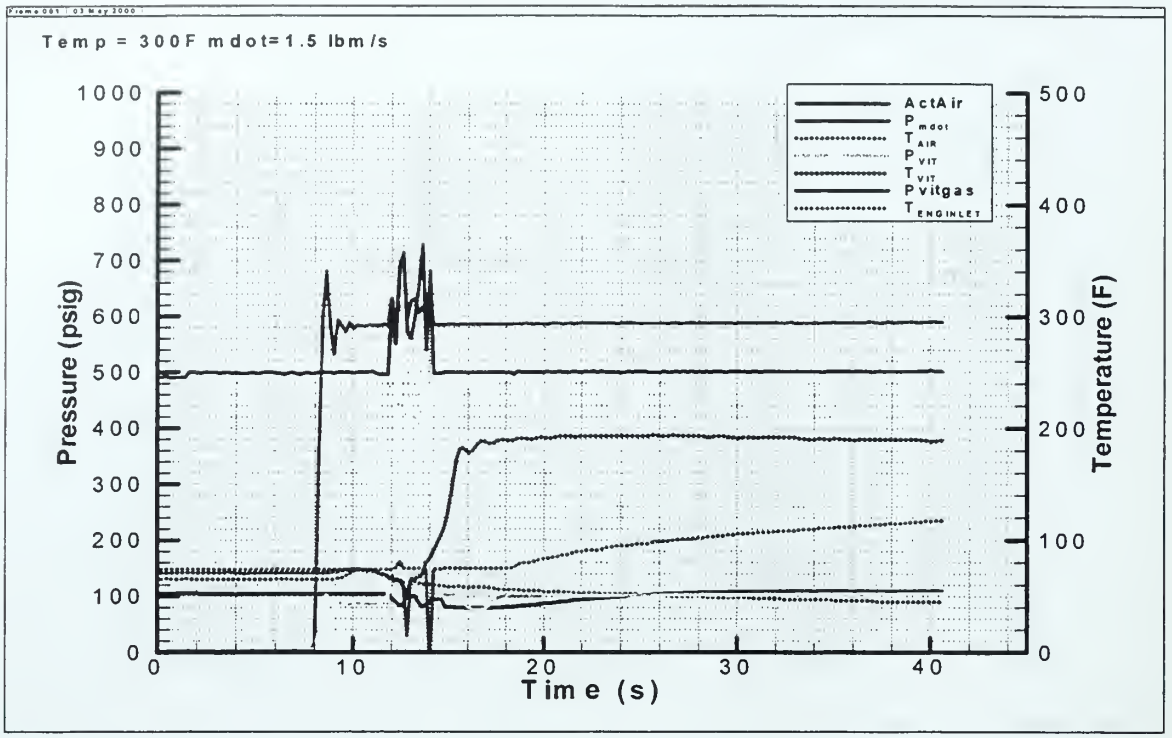


Figure B-5.

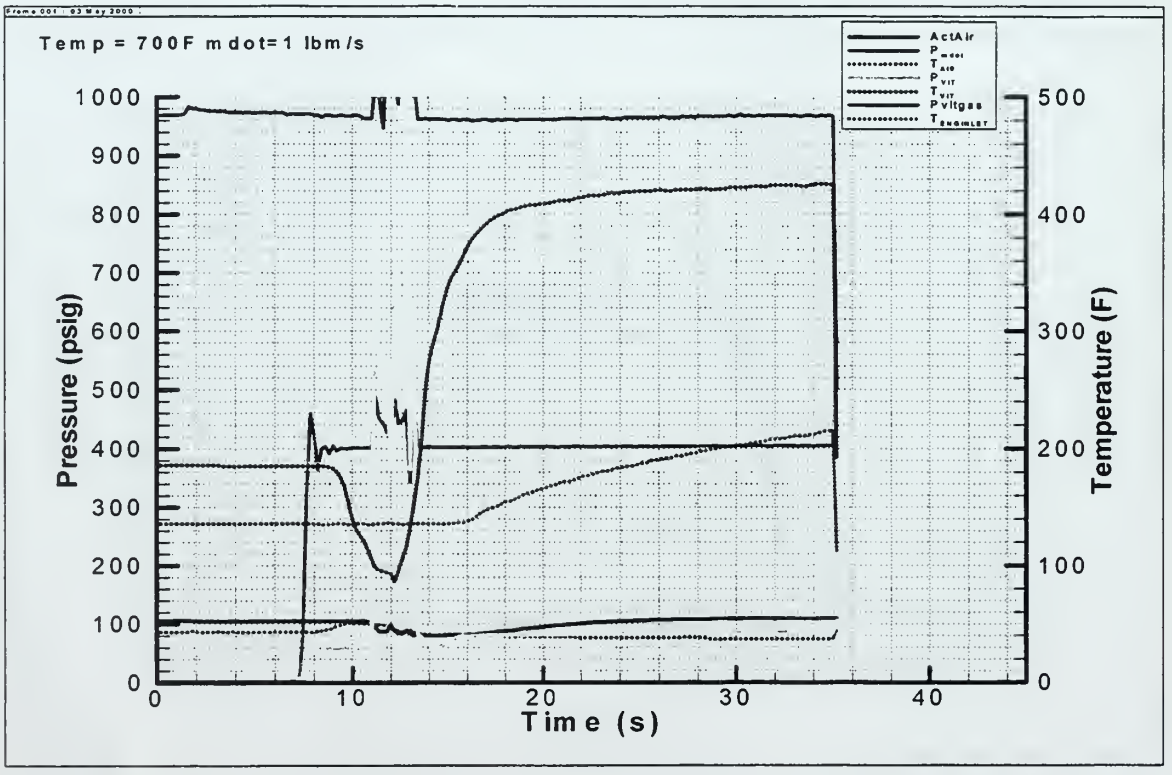


Figure B-6.

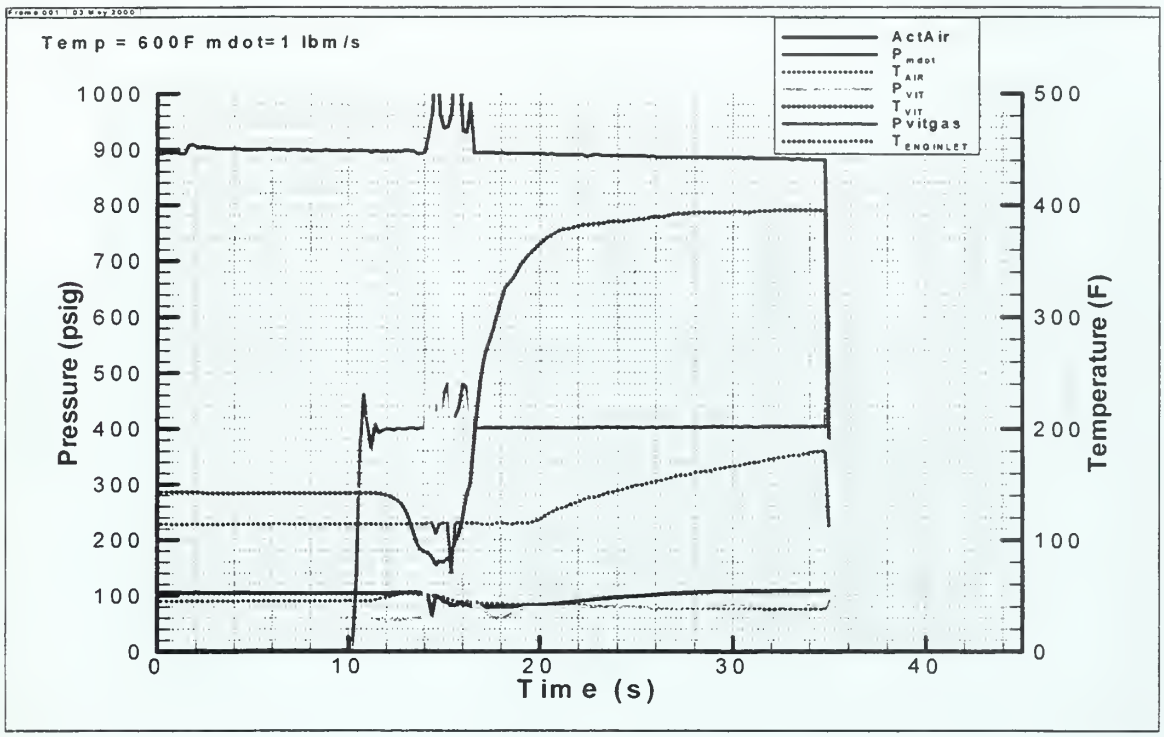


Figure B-7.

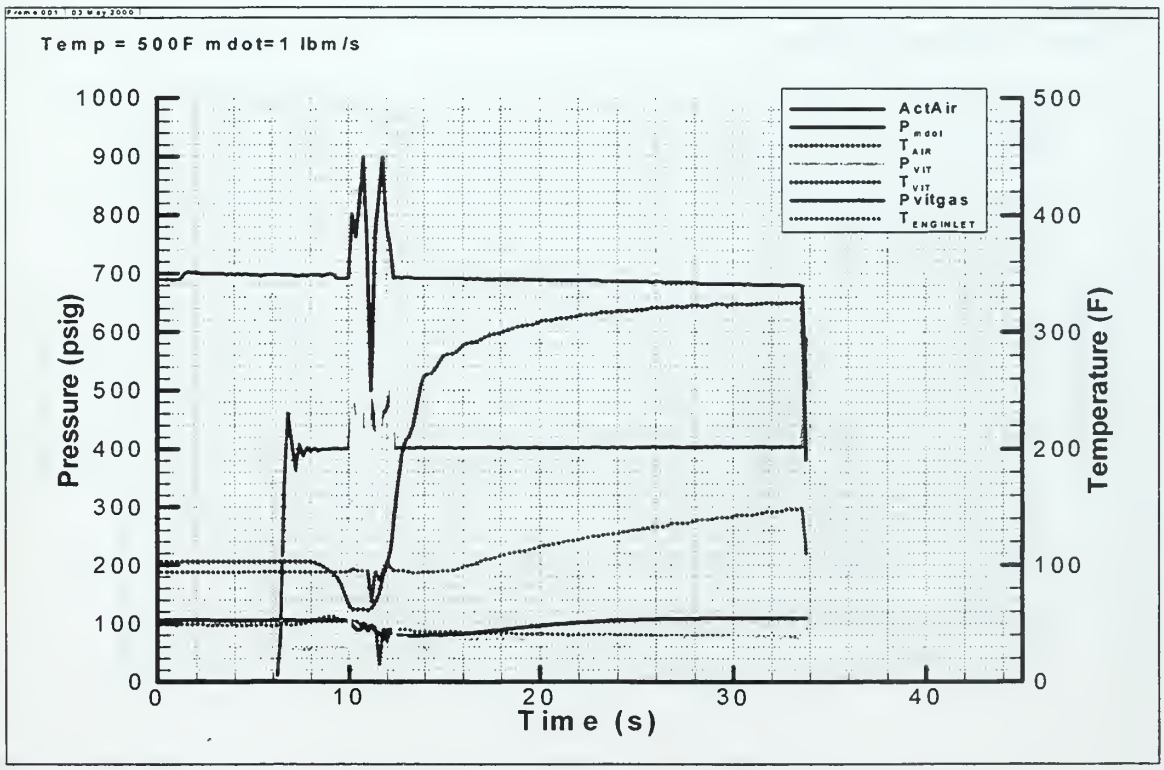


Figure B-8.

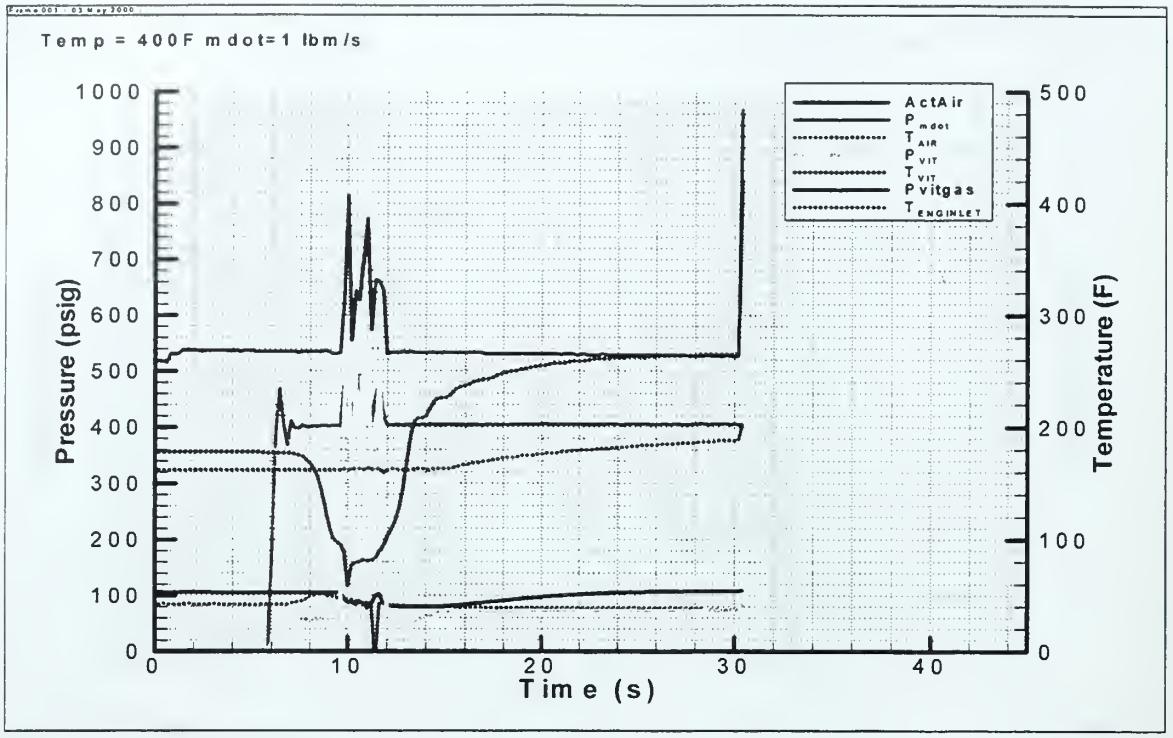


Figure B-9.

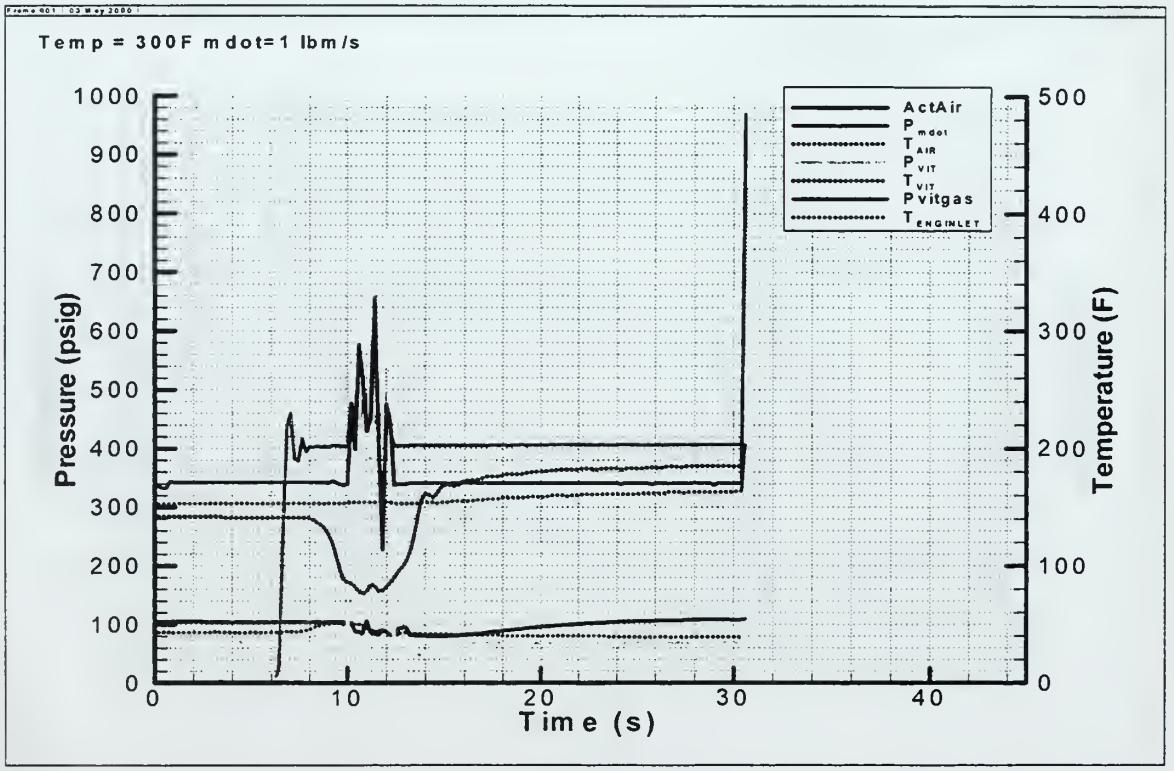


Figure B-10.

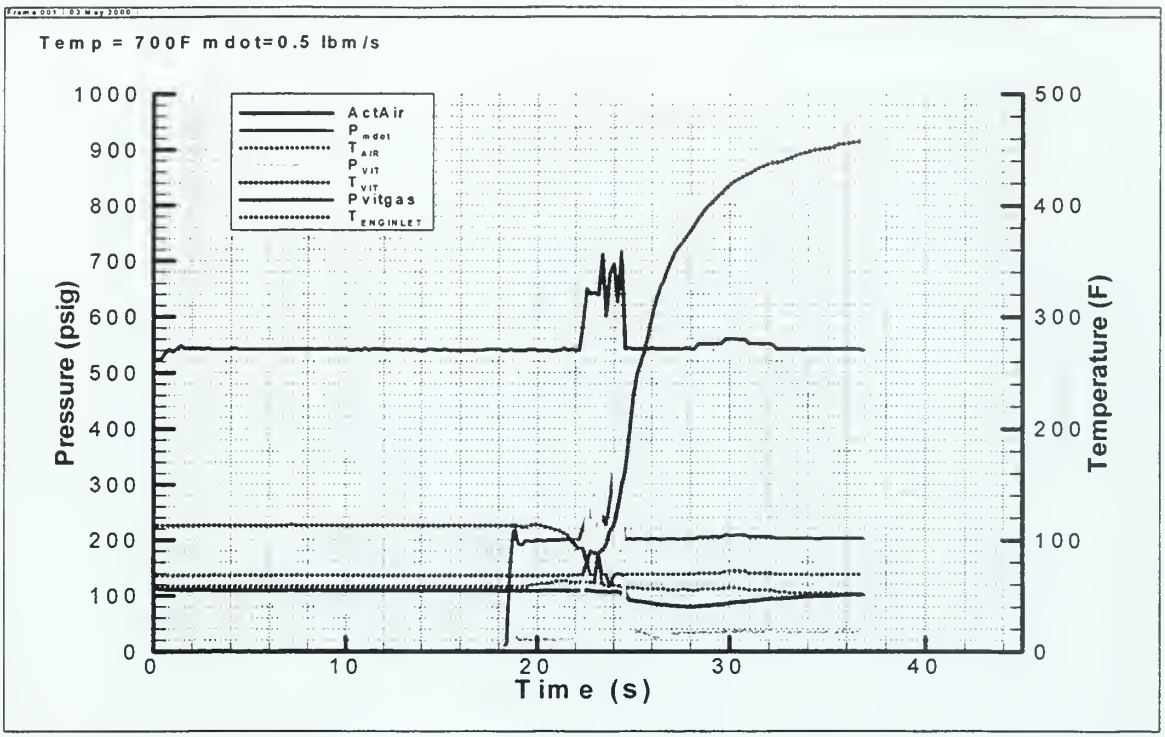


Figure B-11.

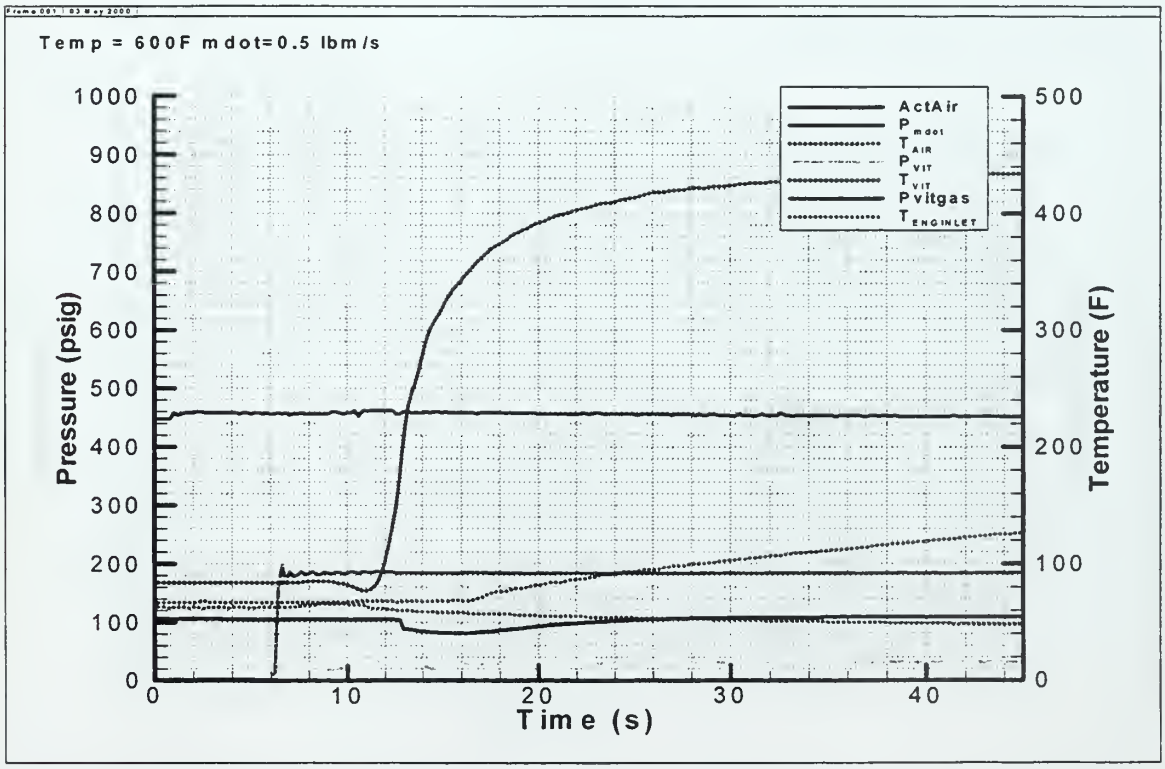


Figure B-12.

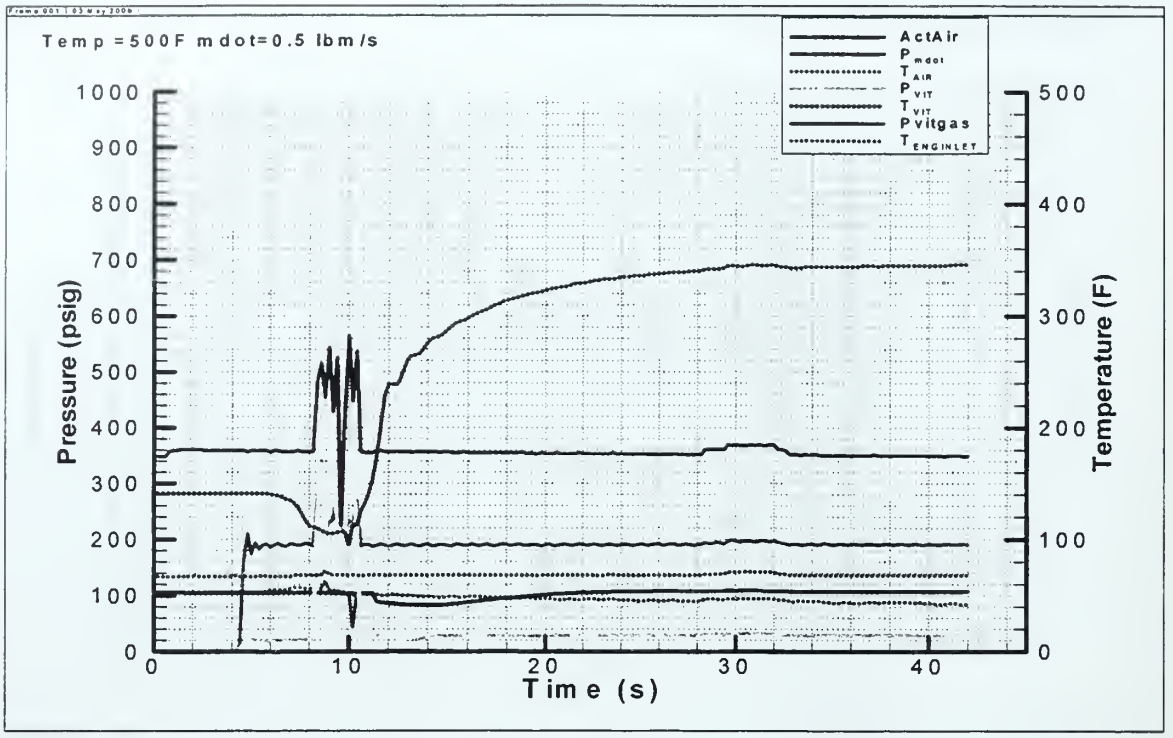


Figure B-13.

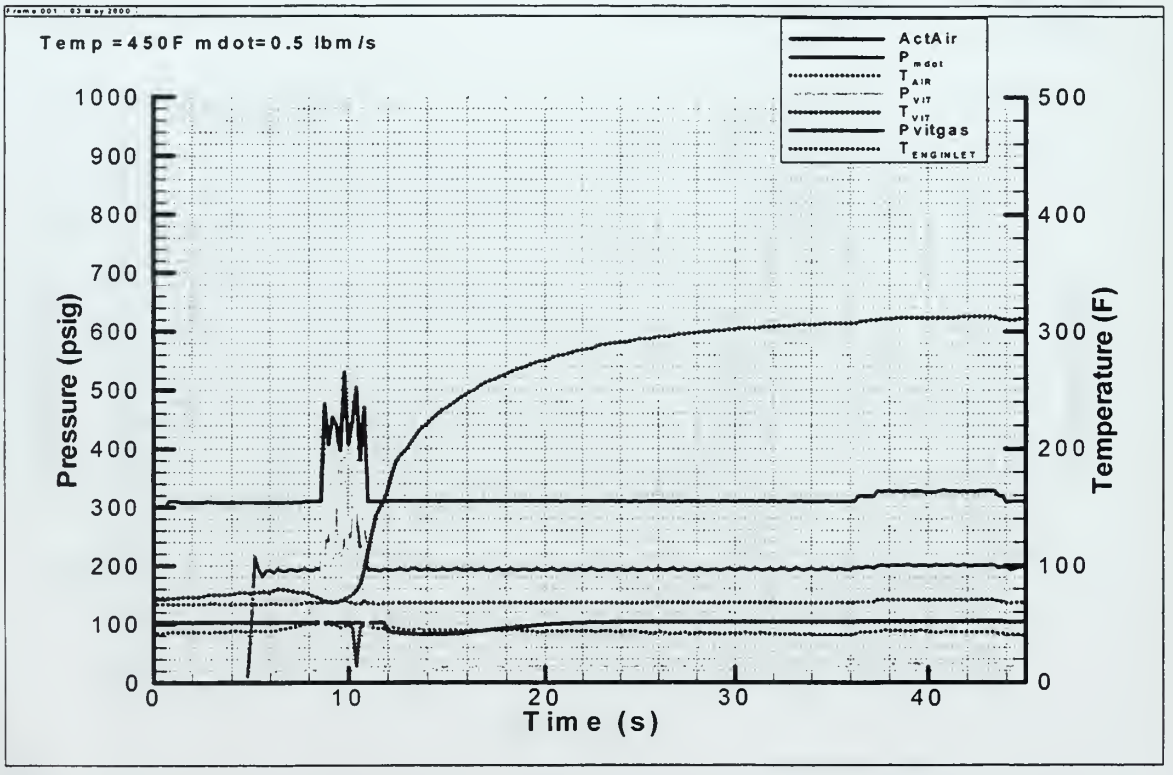


Figure B-14.

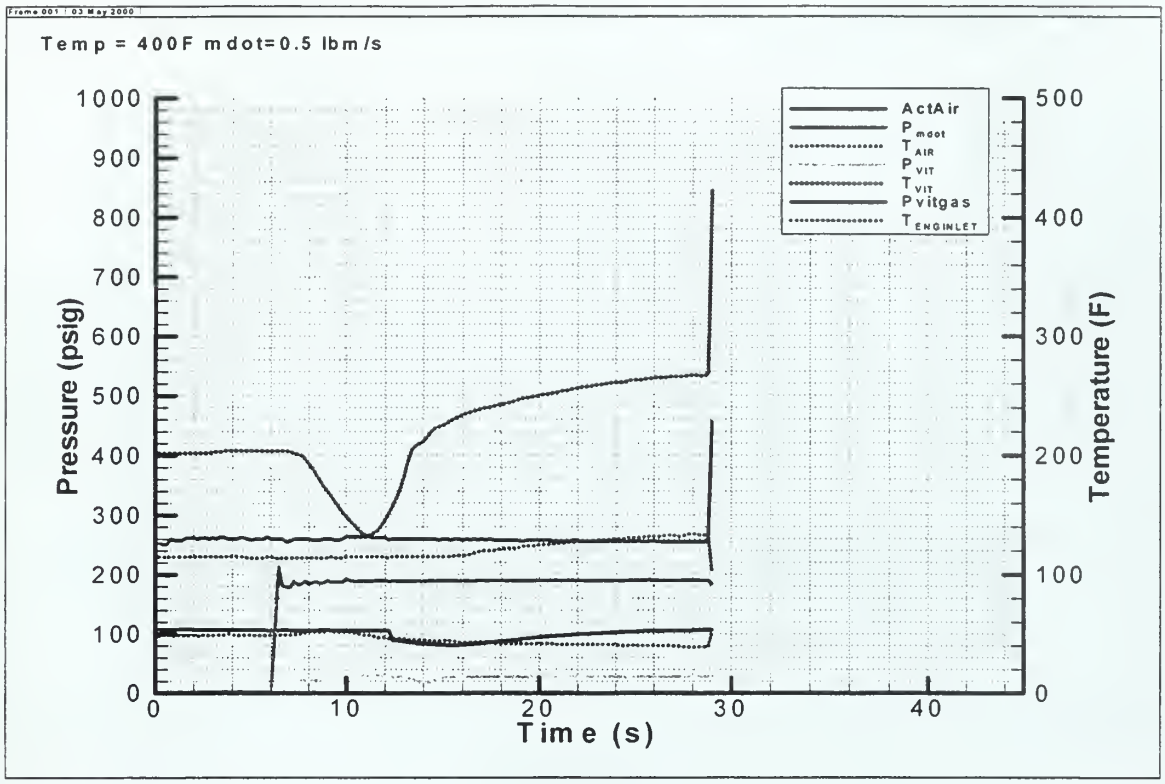


Figure B-15.

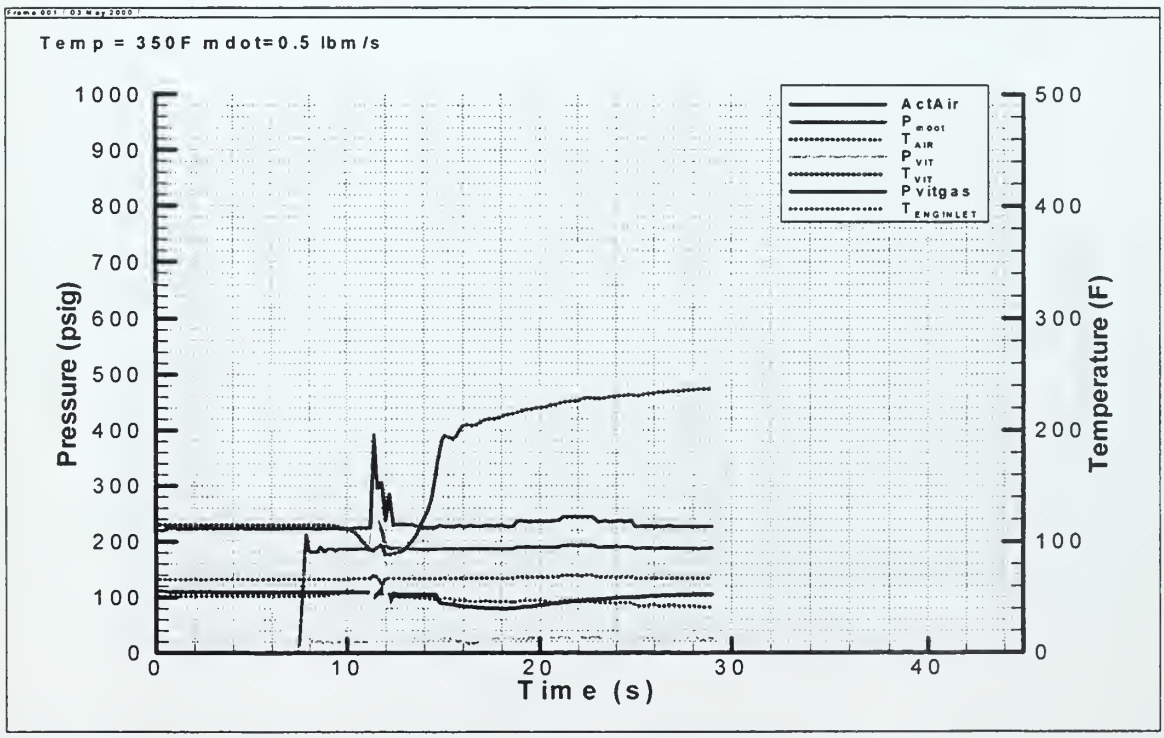


Figure B-16.

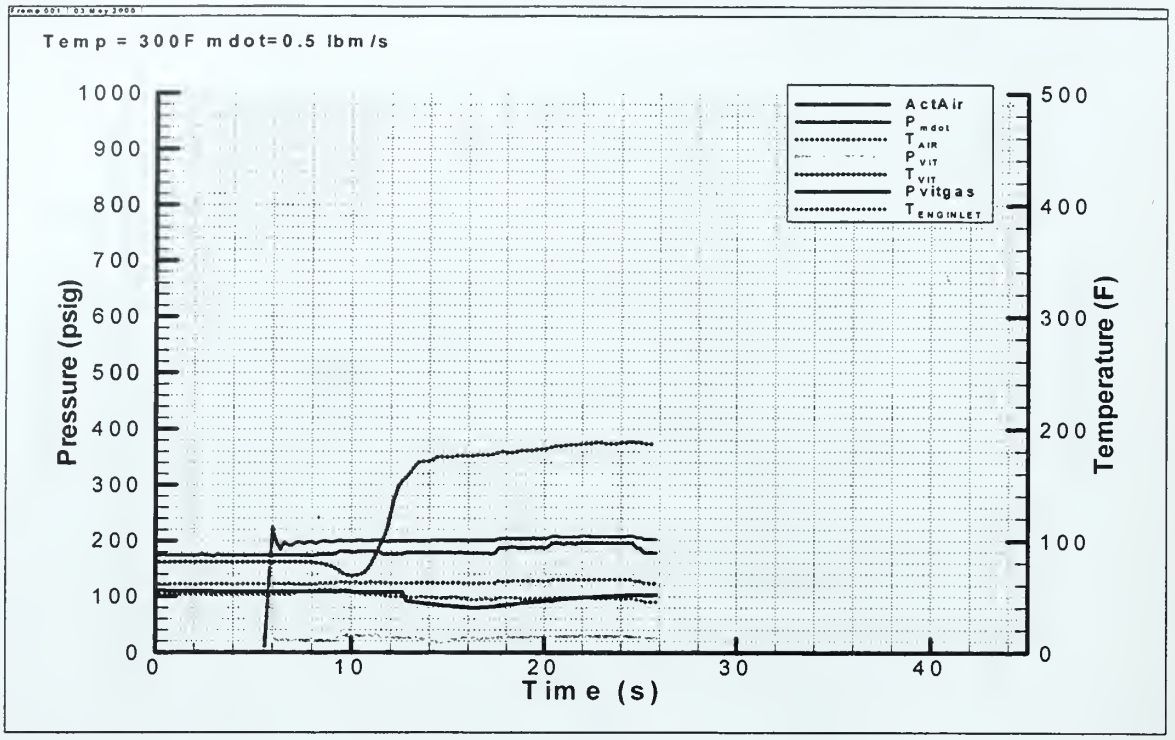


Figure B-17.

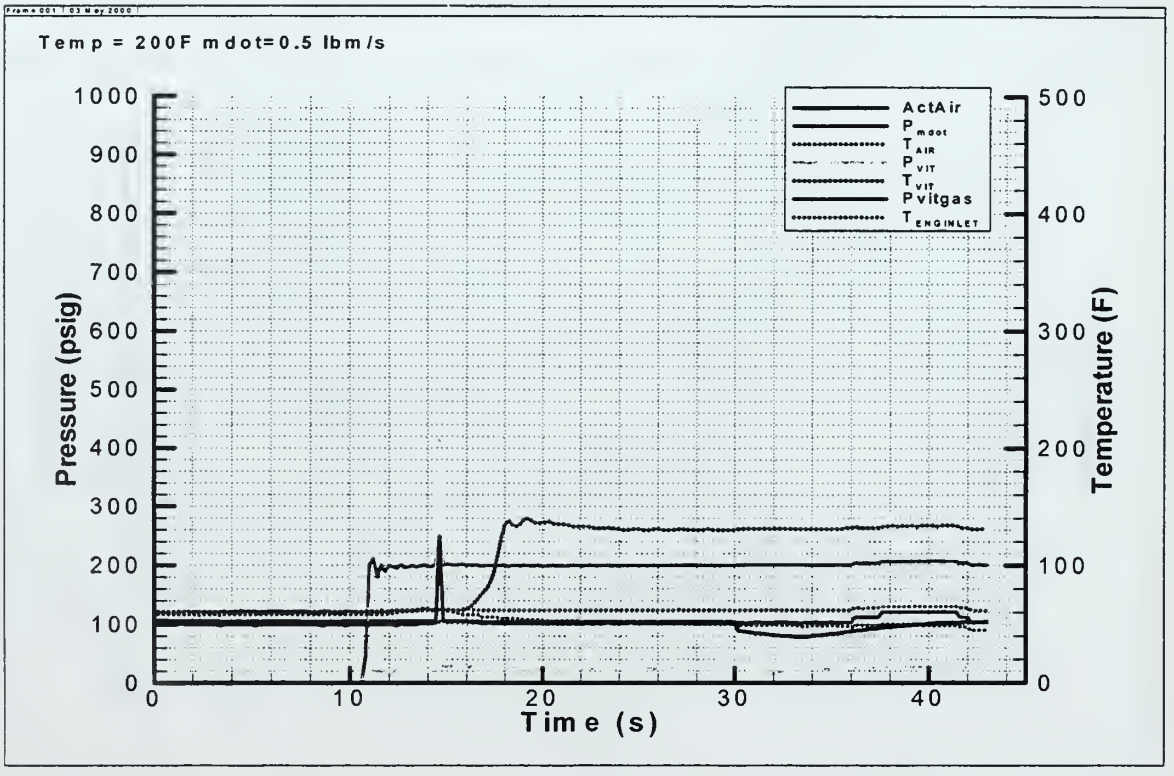


Figure B-18.

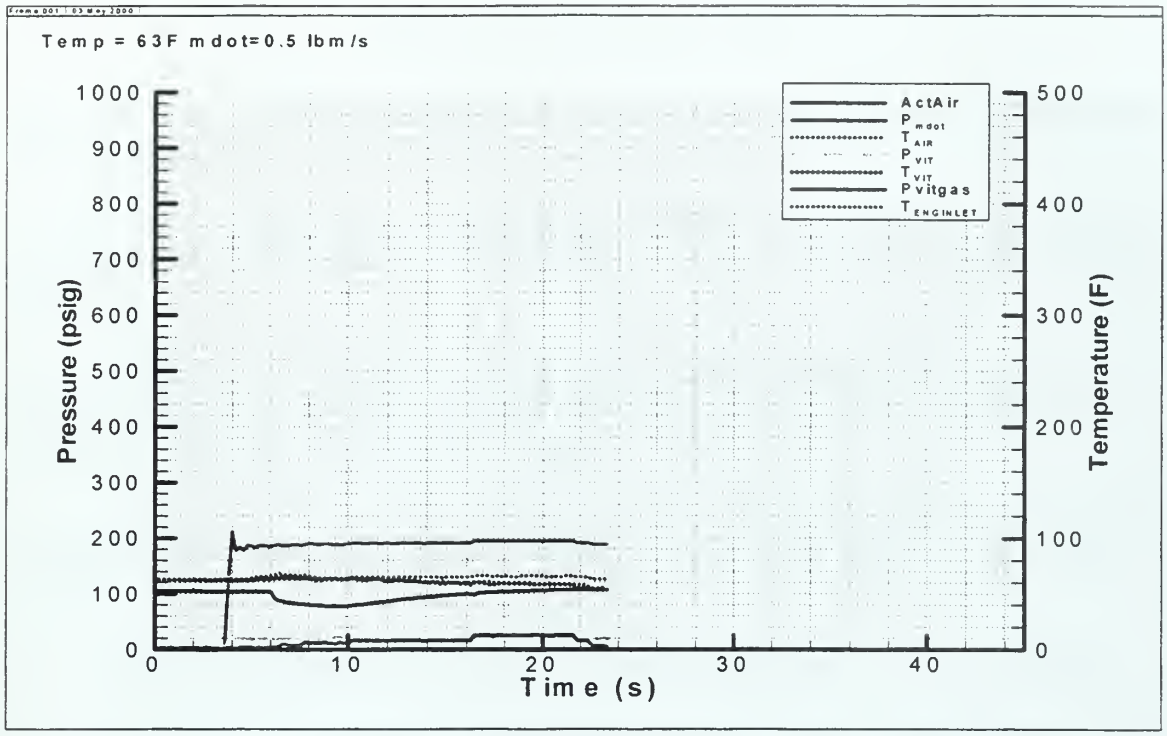
Temp = 63F mdot=0.5 lbm/s
Pressure (psig)
Temperature (F)
Time (s)
ActAir
P mdot
T AIR
P VIT
T VIT
Pvitgas
T ENGINLET
0
100
200
300
400
500
600
700
800
900
1000
0
10
20
30
40

Figure B-19.

THIS PAGE INTENTIONALLY LEFT BLANK

# LIST OF REFERENCES


1. Sutton, G. P. Rocket Propulsion Elements: An Introduction to the Engineering of Rockets, Sixth Edition. John Wiley & Sons, 1992. pp. 17, 539.

2. Kailas, K. "Applications of Detonations to Propulsion: A Review", 37th AIAA Aerospace Sciences Meeting & Exhibit, Reno NV, January 11-14 1999. Paper No. AIAA 99-1067.

3. Eidelman, S. & Grossmann, W. "Pulsed Detonation Engine Experimental & Theoretical Review", AIAA/SAE/ASME/ASEE 28th Joint Propulsion Conference & Exhibit, Nashville TN, July 6-8 1992. Paper No. AIAA 92-3168.

4. Brophy, C. & Netzer, D. & Forster, D. "Detonation Studies of JP-10 with Air and Oxygen for Pulse Detonation Engine Development", July 1998, Paper No. AIAA 98-4003.

5. Kuo, K., Principles of Combustion. John Wiley and Sons, 1986, pp. 230-282.

6. Zucrow, M. & Hoffman, J. Gas Dynamics Volume 1. John Wiley & Sons, 1976, pp. 462-507.

7. Forster, D. "Evaluation of a Liquid-Fueled Pulse Detonation Engine Combustor", Master's Thesis, U. S. Naval Postgraduate School, Monterey CA, December 1998.

8. Glassman, I. Combustion. Academic Press, Inc. 1987.

9. Knystautas, R., Guirao, C., Lee, J. H., Sulmistras, A. "Measurements of Cell Size in Hydrocarbon-Air Mixtures and Predictions of Critical Tube Diameter, Critical Initiation Energy, and Detonability Limits," Dynamics of Shock Waves, Explosions, and Detonations. Progress in Astronautics and Aeronautics Volume 94, American Institute of Aeronautics and Astronautics (AIAA), Inc., 1984.

10. Bete Fog Nozzle, Incorporated.

11. Tulis, A., & Selman, R., "Unconfined Aluminum Particle Two-Phase Detonation in Air", Dynamics of Shock Waves, Explosions, and Detonations Volume 94, AIAA Inc., 1984, pp. 227-292.

THIS PAGE INTENTIONALLY LEFT BLANK

# INITIAL DISTRIBUTION LIST

1. Defense Technical Information Center ..... 2
   8725 John J. Kingman Rd., STE 0944
   Ft. Belvoir, VA 22060-6218

2. Dudley Knox Library ..... 2
   Naval Postgraduate School
   411 Dyer Rd.
   Monterey, CA 93943-5101

3. Dr. Christopher M. Brophy, Code AA/Br ..... 3
   Department of Aeronautics and Astronautics
   United States Naval Postgraduate School
   Monterey, CA 93943-5000

4. Dr. David W. Netzer, Code AA/Nt ..... 1
   Department of Aeronautics and Astronautics
   United States Naval Postgraduate School
   Monterey, CA 93943-5000

5. LT. Robert G. Johnson ..... 3
   14174 Chicarita Creek Road
   San Diego, CA 92128

6. Dr. Gabriel Roy ..... 1
   Office of Naval Research
   Mechanics Division, Office 333
   Ballston Tower One
   800 N. Quincy Street
   Arlington, VA 22217-5660

7. Department of Aeronautics and Astronautics ..... 1
   Code AA
   Naval Postgraduate School
   699 Dyer Rd. Rm. 137
   Monterey, CA 93943-5106